1993

ATLSS connections with moment capacity

Richard B. Garlock
Lehigh University

AUTHOR:

Garlock, Richard B.

TITLE:

ATLSS Connections with Moment Capacity

DATE: October 10, 1993

ATLSS CONNECTIONS WITH MOMENT CAPACITY

by

Richard B. Garlock

A Thesis

Presented to the Graduate and Research Committee

of Lehigh University

in Candidacy for the Degree of

Master of Science

in

Civil Engineering

Lehigh University

October 1993

CERTIFICATE OF APPROVAL

This thesis is accepted and approved in partial fulfillment of the requirements for the degree of Master of Science in Civil Engineering.

August 26, 1993
Date

Le-Wu Lu
Thesis Advisor

Irwin J. Kugelman
Department Chairman

Dedicated to the memory of my mother and father.

ACKNOWLEDGEMENTS

This research was conducted at Lehigh University's Research Center for Advanced Technology of Large Structural Systems (ATLSS). Dr. Irwin J. Kugelman is the chairman of the Civil Engineering Department and Dr. John W. Fisher is the director of the ATLSS Research Center.

The author would like to express his appreciation to Dr. Le-Wu Lu and Dr. B. Vincent Viscomi for their assistance and direction in the preparation of this thesis. It has been an privilege to work with them.

Appreciation is extended to the following graduate students for their contributions to my work; Alan Rosa, Robert Fleischman, John Abruzzo, Nazzal Armouti, Wayne Lawrence, and Christopher Higgins.

Many thanks to Catalina Marulanda, undergraduate assistant with the project for her excellent work. The author would also like to thank Daniel O'Connor and Sean Jensen for their contributions.

The author would also like to acknowledge the staff of the ATLSS and Fritz Laboratories for their assistance, especially Robert Dales, Mark Kaczinski, Ed Tomlinson, Peter Bryan, Dick Sopko, and Bert Wescott. The practical contributions of John Hoffner and his dependable fabrication were a credit to this project.

Special thank you to my aunt and uncle; Mary Lou and Jack Garlock, and to my brothers; John and Gary Garlock for their encouragement and support. My thanks go out to the many friends who each assisted in their own way.

TABLE OF CONTENTS

LIST OF TABLES

LIST OF FIGURES

ABSTRACT

ATLSS Connections are a family of beam-to-column connections which utilize the self-aligning feature of a specially developed connector and are developed for possible use in an automated construction process. Work previously reported describes the design, erection, and structural characteristics of a connector acting as a mid-web shear attachment. These studies show encouraging results for its shear resistance and rotational capacity.

The work has now been expanded to develop connections, using the ATLSS connectors, to achieve moment resisting capacity. Three different connection configurations, involving the use of shop welded and field bolted details and having varying degrees of restraint, were studied experimentally and analytically. Five tests were conducted on exterior connections, scaled from a prototype frame, which had been designed based on the current practice. Erection of the test connections in the laboratory was performed with ease. Loading programs were both monotonic and cyclic, thus allowing for the assessment of static strength and stiffness as well as energy dissipation of the connections. Two types of finite element analyses were performed to predict the behavior of the test connections. The ATLSS Connector aided conventional fully restrained connection achieved 1.11 M_P (plastic moment of the beam) in negative bending and 1.12 M_P in positive bending. The partially restrained connection aided by an ATLSS Connector achieved 0.97 M_P in negative bending and 0.59 M_P in positive bending. While acting as a mid-web shear attachment, the ATLSS Connector contributed up to 16% of the moment capacity. Comparison between the experimental results and the finite element

analyses showed that the analytical models with detailed connection representations offer reasonable predictions of the yield load, yield deflection, and initial stiffness of the connections. Recommendations regarding the ATLSS Connector design are given.

CHAPTER 1 - INTRODUCTION

1.1 General

The Engineering Research Center for Advanced Technology for Large Structural Systems (ATLSS) was created with a goal to increase the competitiveness of the U.S. construction industry. The program of the center is divided among clusters, each dealing with an area of common concern and organizing the individual research projects in that area. One research cluster, called ATLSS Integrated Building Systems (AIBS), was established to develop, design, fabricate, erect, and evaluate cost-competitive building systems with a focus on providing an integrated system approach to construction (ATLSS V.1, 92).

The systems approach calls for building construction utilizing modular elements that could be assembled easily and rapidly on site, and provide a durable and stable structure. The need for a new connection with enhanced fabrication and erection characteristics was recognized early in the planning of the cluster's research. The complete systems approach would require implementation of a specialized crane, as well as computer integrated design, fabrication, and erection. A crane with a high degree of maneuverability for placement of payload would be effective in conjunction with a connection which could easily slip into position. Simplification of the many complex and different arrangements of connections would provide for a degree of regularity, and aid in the creation of an integrated structural system.

With these ideas in mind, a family of connections known as the ATLSS Connections have been developed. Utilizing the input of interdisciplinary specialists,

from both research and industry, an initial prototype connector was formulated. Referred to as the ATLSS Connector (AC), it was developed to provide ease and speed of erection. The connector was initially designed to carry only the resultant shear force at the beam ends. However steel structures utilize many types of connections throughout a building including those required to resist moment as well as shear. The initial research performed on the connector suggested that it could provide superior rotational stiffness and qualities of erection to steel and composite joints in modern steel framed structures.

This report discusses the effect of implementing the AC on connections which resist moment as well as shear. The cast structural steel prototype AC utilized in this research is illustrated in Fig. 1.1. The configurations which utilize the AC are discussed after review of the present practices of the construction industry and discussion of previous research on the AC.

1.2 Background

1.2.1 Conventional Design

Current steel construction practice utilizes traditional connections to join horizontal and vertical structural elements. The requirements of these connections depends on the type of design chosen for the structure. The author realizes conventional design practices vary depending on the design situation. Therefore, the following scenario is a general case of what typically happens in today's construction industry. The design engineer selects the structural members, and specifies what loads the connections are to resist. Connection design is generally performed by the structural fabricator, not by the engineer. Connection designs are submitted to the engineer for approval. The current

practice permits the fabricator to use any configuration which will perform as the engineer requires. As a result, many different connection configurations have been developed. This increased variability leaves room for discrepancies in design and construction.

The American Institute of Steel Construction (AISC) separates beam-to-column connections into three categories, as shown in Table 1.1 (AISC, Manual, 91). The divisions are made based on the restraint characteristics of the connections (Blodgett, 91). Type 2 is the most flexible and is referred to as simple or shear connection, while Types 1 (fully rigid) and 3 (semi-rigid) are both moment connections. The difference between the two is related to the rotational stiffness and the amount of bending moment that can develop at the connection. The type of connection utilized depends on the frame design. Typically, frames are designed with either simple, fully rigid, or semi-rigid constraints. A beam-to-column connection used to transfer shear load would typically fasten the beam web to the column face. If moment capacity is required, the connection would fasten the beam flanges to the column as well. The degree of restraint provided by the moment connection would then depend upon the stiffness of the flange attachments.

1.2.2 ATLSS Connector

The ATLSS Connector was initially designed as a shear connection. The connector was developed to provide safer and easier erection, and ultimately less expensive steel connections. Review of the connector and familiarization with its idioms are necessary for further discussion of the research. The connector is made up of two components, the mortise and tenon (see Fig. 1.1(b)). Typically the mortise is shop-welded to the column while the tenon is shop-bolted to the beam web. The base of the

tenon is first introduced into the larger mouth of the mortise and then allowed to lower into place. The passage of the tenon into the mortise is arrested when the two are in contact along the sides and back. The original mortise design for the AC consisted of only two sides, referred to as arms. Later designs included a seat at the base of the mortise, and a pair of flutes on each arm of the mortise. The flutes and seat provide stiffness for the mortise arms to prevent them from opening out; because when the mortise opens, the tenon is allowed to slip downward, or pull outward. A bolt at the base of the connector, referred to as the seating bolt, is placed at the erector's convenience to preload the connector and alleviate initial settlement. The overall configuration of the connection allows for the tolerances or misfits to be resolved in the final erection adjustment of the building.

The ATLSS Connector has undergone rigorous experimental testing and analytical evaluation, followed by a series of reports (Fleischman, et al, 91,93). The testing program consisted of both short and long simple beam tests, pullout tests, rotational tests, tension tests, erection feasibility tests, and push-through tests. The connector underwent design changes following each major phase of completion. The latest connector developed is called a Phase II AC and is the design used in this research program. Results show that a Phase II connector without the flutes exhibited moment capacity of 13.4 kip-ft. at an end rotation of 0.197 radians, shear capacity of 92 kips, and 82 kips in tension (Fleischman, et al, 93)[1]. The Phase II AC used had flutes on the mortise sides and thus

[1]The dimensions and material properties of these Phase II connectors will be given later in this report.

an increase in its strength was expected.

With the understanding of the shear capabilities of the connector, the next phase of experimentation for this connector moved forward. The test program discussed in this report deals with one of the two moment connection studies recently undertaken at Lehigh. A semi-rigid composite system utilizing the ATLSS Connector has been tested and reported (Rosa, 93).

1.2.3 AIBS System

The AIBS structural system can place single beams as well as assemblages of beams and girders. The latter is presently based on the erection of two groups of structural members, one being the columns, and the other the girder and beam assemblages, referred to as bays. Erection of the building would begin with placement of the columns. A bay would be assembled on the ground, and then raised by a crane, maneuvered into place, and connected to the columns. Conventional connections would be used to join the connections on the ground. Connections which would be completed above ground would be constructed with the aid of the AC's. Therefore, these connections used to attach bays to the columns would require ATLSS Connectors.

Construction industry input has played an important role in the creation of the connector, which would be transferable from the research lab to the construction site. The connector has been implemented in a temporary factory roof which required a connection that could be, easily and quickly, removed. The results from this field test were very encouraging (Fleischman, et al, 93).

Research of the AIBS structural system erectibility and the effect that the AC has

upon it is underway at ATLSS (Kaczinski, et al, 92). Construction of a small scale, fully operational, six degree of motion control crane, referred to as the Stewart Platform (SP), has been completed at ATLSS. Testing included placing a set of beams equipped with the ATLSS Connector by the SP. Results for these tests were again very encouraging. The SP was able to maneuver the beam, as well as the bay, into various positions and achieve proper alignments. Therefore, the increased maneuverability of the crane, with the relaxed erection tolerances of the connector can provide for a building which can be assembled by the SP operator.

1.3 Statement of Problem

Research has focused thus far on the shear connections used throughout a simply connected frame design. As discussed earlier, however, connection design often requires more than shear transfer. Connections may need to develop some degree of restraint or moment capacity for the beam. In the case of the AIBS system for rigid frame design, the connections, which connect the bays to the columns, would need to be fully restrained connections.

There are many different configurations of conventional steel connections which can produce nominally the same rotational capacity. There may be welded end-plates, or bolted tee stubs, or numerous other combinations. However, these methods may or may not be applicable to the family of ATLSS Connections.

Design of the actual AC itself is an ongoing task. Evaluation of the connector in a rigid joint may show ways in which the present design can be enhanced. Frame tests will be an integral part of the overall evaluation of the connector, and connector assisted

joints. Before tests of such magnitude can be undertaken, pilot tests on the joints must be performed in order to learn about how the frame will likely respond.

1.4 Objective and Scope of Research

The objective of the research presented herein is the design, analysis, and experimentation of pilot tests to explore the adaptation of the ATLSS Connector to achieve moment capacity of steel beam-to-column joints. The emphasis of the beam-to-column connections was on shop-welded fabrication and field-bolted erection. A low-rise prototype steel frame was chosen to establish a baseline for comparison of the results achieved in the various types of connections studied. A scaled-down beam-to-column joint was selected from the frame beam to a size suitable for testing.

Modifications to the connectors tested were limited, since changes could only be made after weighing advantages gained with the other research being performed on the connector. Slight change of the mortise bevel was the only geometrical alteration the experimental connectors underwent. The material properties were modified during the test program. The strength of the cast material was increased in an attempt to achieve greater rotational and shear capacity of the joint.

1.4.1 Joint Description

After consideration of many types of joint configurations, three arrangements were chosen for investigation (Fig. 1.2). The joints consisted of flange attachments and an ATLSS Connector bolted to the beam web. Type A is a conventional moment connection where the shear transfer is performed by the ATLSS Connector instead of a double angle web connector, which is often used in a conventional connection. Type B is a Type A

connection minus the AC and is used as an benchmark for comparison and is not intended to be used in actual construction. The last configuration, Type C is one which eliminates the bottom flange plate, places the AC at the bottom of the web, and retains the tee stub at the top flange. The study focused mainly on the behavior of the Type A and Type C connections. It was anticipated that the Type A connection would demonstrate full shear and partial moment capacity of the AC. However, it was felt that this configuration does not utilize the AC to its full capacity. Therefore, the Type C connection will demonstrate the connector's negative and positive bending resistance as well as its shear resistance.

CHAPTER 2 - PROTOTYPE STRUCTURE

2.1 Development

The AIBS cluster is currently conducting several studies to develop and assess the performance of several different types of beam-to-column connections utilizing the ATLSS Connector. To provide a systematic comparison of results from the different studies, a prototype structure is required. This structure would establish a baseline for the initial study of AC effects. The frames were constant in dimensions, but varied connection stiffness resulted in different member sizes for the frame members. Recognizing that there are many methods used to construct a building, discussions were held among the ATLSS researchers as well as government and industry partners to determine which types of structure would be best suited for the initial application of the AC. The goal for the connector is that eventually the connection will impact all areas of construction from low to high rise buildings. Based on the tonnage of buildings erected each year, the decision was made to assess the connectors performance in a low-rise steel structure. The detailed origin and design of the frame for the cluster structure has been reviewed by another ATLSS researcher (Rosa, 93).

The prototype building used in this project was a five story, two by six bay, rigid steel frame with story heights of 13 ft. 0 in. and square bays of 25 ft. 8 in. by 25 ft. 8 in. (see Fig. 2.1). Total building elevation was 65 ft. 0 in., with an overall width of 51 ft. 4 in., and length of 154 ft. 0 in. The structural members selected by Rosa used A36 steel. However, with the current improvements on the AC, a more balanced joint design was achieved by using high strength steel for the members of the rigid frame adopted for this

study. The high strength steel used was A572 Grade 50, having a nominal yield stress of 50 ksi.

The design parameters and methods for the fully rigid prototype frame pertinent to this study are reviewed in the following sections. This review includes the prescribed code specified loadings, the methods used in design, and selection of the critical connection location.

2.2 Loadings

Loadings applied to the prototype steel frame include live, dead, lateral, and roof loads, as prescribed by the Standard Minimum Design Loads (ASCE, 88). The geographic location of the building was considered to be the northeastern section of the United States. The design loads were taken for an office structure and are described below:

Full Live Load (L)	= 100 psf	(before the allowed reduction)
Dead Load (D)	= 55 psf	
Roof Dead Load (L_r)	= 30 psf	
Snow Load (S)	= 20 psf	
Curtain Wall (C)	= 15 psf	
Partition Load (P)	= 20 psf	

A live load reduction of 33% was applied to the girders and calculated based on the tributary area as permitted (ASCE, 88). Wind load (W) was calculated from the design pressure, Eq. 2.1, using an importance factor of 1.0, and basic wind speed of 80 mph.

$$p = \underbrace{(q_z)(C_p)(G_h)}_{windward} + \underbrace{(q_h)(C_p)(G_h)}_{leeward} \qquad (2.1)$$

where p = design wind pressure at height z
q_z = velocity pressure at height z
C_p = external pressure coefficient (windward or leeward)
G_h = gust response factor at height z = h (h is the overall height)
q_h = velocity pressure at height z = h

Earthquake load (E) was calculated based on the NEHRP Equivalent Lateral Force Procedure (NEHRP, 91). Design criteria include Seismic Hazard Exposure Group I, Seismic Performance Category C, effective peak acceleration coefficient 0.1, effective peak velocity coefficient of 0.1, and the soil profile type S_1. The parameters were selected based on an ordinary moment frame, as defined by NEHRP.

The AISC and NEHRP load combinations used are listed below (AISC, Load, 86 and NEHRP, 91). Individual members were designed based on which load combination induced the largest strength and serviceability values. The NEHRP load combinations were used only for the verification of the design to insure the lateral load requirements were governed by wind loading.

AISC

[A4-2] $1.2\ D + 1.6\ L + 0.5\ L_r$
[A4-3] $1.2\ D + 1.6\ L + 0.8\ W$
[A4-4] $1.2\ D + 0.5\ L + 1.3\ W + 0.5\ L_r$
[A4-6] $0.9\ D + 1.3\ W$

NEHRP

[3-2] $1.15\ D + L + 0.7\ L_r + E$
[3-3] $0.85\ D + E$

2.3 Frame Analysis and Results

The steel frame analysis and design were assisted by the structural design package,

SODA[2]. A second-order elastic analysis considering the P-Delta effect was used in calculating the optimum member sizes based on the loads and load combinations previously presented. The plan layout of the building is illustrated in Fig. 2.1(a). The building elevation, as well as the resulting sizes of the girders and columns from the analysis and design are presented in Fig. 2.1(b). Additionally, there are two infill beams, spanning from girder to girder, in three equal spaces throughout each bay. These beams utilize simple connections as they transfer only shear. Girders are attached to the strong axis of the column. The girder-to-column connections are fully rigid.

The frame analysis and design calculated the deflections, forces, and the resultant member sizes. The highest connection moment was realized on the leeward side of the first level resulting from AISC combination A4-2. This exterior girder to column joint was chosen as the focus of this research (Fig. 3.1).

2.4 Connection Design

Design of a moment resisting connection using the ATLSS Connector required adherence to several key precepts to establish the optimum moment resisting configuration. These precepts include criteria specific to the ATLSS Connector, as well as preferred techniques for fabrication and erection. Before development of an AC, specific criteria were established to guide the design of the AC (Fleischman, et al, 91). The five criteria defined originally have been modified to encompass both the connector and flange attachments.

---

[2]Structural Optimization Design and Analysis, Copyright 1991 by Acronym Software, Waterloo Engineering Software, and Microsoft Corp.

The modified precepts include:

- **Self-alignment** - The attachments located either on the column face or beam flange must not impede the placement of the tenon into the mortise. Once introduced the vertical surfaces tenon must come to full contact with the mortise, using only the assistance of gravity.

- **Tolerances** - The connection can not be so complex as to increase the difficulty of erection. It must handle the material tolerances of the building components and/or connection.

- **Adjustment** - Given the tolerances provided throughout the fabrication process, the connection must be able to accommodate minimum alignment corrections.

- **Strength and Stability** - The connection must fulfill the strength requirements of the structure during erection as well as during its service life. The connector must be positioned to keep the structure stable until the final tightening.

- **Modularity** - Allow for the mass production, and simple design procedure for the connections.

Additionally, the industry partner participants recommended shop-welded, field-bolted fabrication and erection methods became the design bases adopted in this study. These individual criteria ensure ease and speed of construction.

The connections tested are a scaled down version of those which would be used in the full-scale prototype frame. The dimensions and geometric configuration of the ATLSS Connector is illustrated in Fig. 2.2. The method used to scale down the connections for the tests is described in Section 3.2.2 (Specimens). The design methods presented below are based on parameters, not on the actual values for either the prototype frame members, or the specimen members. Refer again to Fig. 1.2 for illustration of the presented configurations.

2.4.1 Type A Configuration

The design of the conventional full-moment connection, with the ATLSS connector in the place of a standard shear connector, was performed utilizing LRFD design provisions. The plastic moment of the beam (M_P) must be developed for the full-moment connection. An assumption was then made that an AC with flutes and higher strength material than tested previously could carry approximately 20% M_P. The remaining 80% M_P must be transferred from the flanges of the beam to the column. If material properties are the same, the area of the flange attachment should be equal to the area of the beam flange. For conventional welded moment connection design, flange plates are usually welded to the column and field bolted or welded to the beam. For conventional bolted design, tee stubs are usually bolted to the beam and column. Neither of these configurations alone satisfied the criteria, but in conjunction would achieve the precepts set earlier. Therefore, the design was established to use a top flange tee stub and a bottom flange plate; the tee stub shop welded to the beam and the plate shop welded to the column. With no obstacles to inhibit the erection, the beam could be placed by aligning the mortise and tenon of the connector and dropping the beam into place. Bolts would be field placed from tee stub to column and plate to beam to complete the connection. The use of the ATLSS Connector would support the erection procedure alone, until the bolts needed to complete and align the joint are placed. The tee stub was designed as a structural hanger section (AISC, Load, 86), where the horizontal distance between the bolts is minimized to limit the prying forces on the tee bolts.

With the ATLSS Connector attached to the beam the clear distance from the beam

to column must be greater than 1-11/16 in. (see Fig. 2.2). This extends the length required for the tee stub and plate to reach the flange. This increase in length contributes to a more flexible response.

2.4.2 Type B Configuration

This connection removes the AC but everything else remains identical to the Type A configuration. This configuration is not a plausible structural connection, and it was used for comparison purposes for these tests alone. This configuration is used to isolate the AC behavior and to assist in the verification of the analytical model. The shear component normally carried by the AC is carried by the tee stub and plate.

2.4.3 Type C Configuration

This moment connection utilizes the limited contribution to moment capacity of the AC. The tee stub remained at its top-flange location, while the bottom flange plate is eliminated, and the AC is lowered from middle web to bottom web. In this case the tensile axial force in negative bending relied upon the tee stub, and in positive bending relies on the ATLSS Connector. A full-moment connection in a steel frame design for combined gravity and lateral loadings reaches the maximum moment under negative bending, while only reaching a fraction of that under positive bending.

2.4.4 Tolerances

Moment connections inherently possess greater tolerance problems than simple connections. Overall connection design had to accommodate the idea of shop welding the attachments to the beam and column. This further hampered the adjustment ability when coupled with the AC. The ATLSS Connector is designed to accommodate ± 1/16

in. vertical tolerance, and ± 3/32 in. horizontal tolerance. Horizontal tolerances for the flange plate attachment are obtained by using oversized holes. Oversized holes provide a hole diameter equal to a bolt diameter plus 3/16 in. (AISC, Load, 86). To assist the vertical tolerances, the bolt holes in the beam web, and those in the column, were also designed as oversized.

CHAPTER 3 - EXPERIMENTAL PROGRAM

3.1 General

The experimental approach consisted of five cantilever tests simulating three different exterior joint configurations, as described in Chapter 2. Two tests were performed on the Type A configuration, one on the Type B configuration, and two on the Type C configuration. The loading programs were generally monotonic, but one cycle of reverse loading was added to obtain additional information. The second of the Type A tests was subjected to cyclic loading to evaluate the seismic behavior of the configuration.

The experiments were performed in the ATLSS Multidirectional Testing Laboratory at Lehigh University's Mountaintop Campus. Fabrication of the test fixtures and specimens was performed by ATLSS technicians.

3.2 Specimens

This project is one phase of the larger research program pursued by AIBS, as described in Chapter 1. It is anticipated that a scaled down frame will be tested in the future, which will utilize connections chosen from among the series of pilot tests. Therefore, in the scale down from the prototype frame to the specimen, consideration was given so that direct correlation can be made between these tests and those to be done on a frame. The size of the test frame specimen depended upon the size of the prototype ATLSS Connector and the anchor bolt layout of the lab floor (which are spaced at 5 ft. increments). It was decided that a 15 ft. length would equate to the 25 ft. 8 in. prototype frame bay width.

The scale factor ξ is calculated as:

$$\xi = \frac{3 \textit{ lab floor divisions}}{\textit{Prototype frame bay dimension}} = \frac{15'}{25'-8''} = 0.58$$

The beam dimensions from the prototype frame were scaled down by ξ, and the nearest available section was chosen: the W12x22. The column was also scaled down, but in order to better assess the connection performance, a larger section, W8x58, was selected to limit the inelastic column effects. The column effects would be an added degree of complexity in the evaluation of the connection behavior. The steel selected was A572 (50).

The design of the flange attachments for the connection followed the methods described in Section 2.3. The top attachment was a tee stub and the bottom attachment was a plate. The tee stub was cut from an A572 (50) W30x99 and was bolted to the column using 2-3/4 in. x 3/4 in. dia. A325 bolts and clipped washers. The tapered stub was welded to the beam flange by a 3/8 in. weld 13-5/16 in. in length. The bottom flange plate was cut from A572 (50) 1/2 in. thick plate and was welded to the column using a full penetration weld with a 1/4 in. root opening and a 45° bevel. It was bolted to the flange by eight 2-1/4 in. x 3/4 in. dia. A325 bolts with standard washers. The details of these attachments allowed sufficient space for bolt tightening, satisfied the code specified edge distances, allowed sufficient room for welding of the tee stub to the beam flange, and kept the prying forces in the bolts of the stub low.

Recent modifications to the ATLSS Connector include casting a bevel around the back edge of the mortise. The 45° bevel facilitates welding of the mortise to the column.

This bevel extends all the way around the perimeter of the mortise, including the flutes (the set of braces protruding from either side of the mortise). Throughout the tests, variations of the bevels on the individual connectors were specified and evaluated.

The basic configuration of the specimens is an exterior beam-to-column subassemblage shown in Fig. 3.1. Based on analysis of the prototype frame, the inflection points of the beam and columns for given loadings were determined. The end of the cantilever was designated as the length from the centerline of the column to the inflection point of the beam under gravity loads with a rigid joint condition. This distance is referred to as B. The height L denotes the distance between inflection points of the column. Hinges were utilized as support for the column at these inflection points. The hinges allow for rotation but not translation of the end of the column specimens. The subassemblage models the typical behavior for a column with mid-story height inflection points and allows for the overall test specimen configuration to remain statically determinate globally. A typical test specimen is pictured in Fig. 3.2.

The column used in this test was checked for excessive panel zone and bending deformations during design. As a further precaution to large column deformations, stiffeners were placed in the column at flange attachment locations. Stiffeners were also added to the beam at the point of load application to prevent localized yielding of the member. The specimens were designed so that each beam end and column face could be used for a test. Therefore, it was possible to perform two tests on each column and beam. The beam was extended beyond the point of load application to permit lateral bracing of the beam. Lateral bracing was carefully checked to permit the unrestricted vertical

displacement of the free end of the beam, while preventing the beam from twisting. Grease was applied generously where the beam and bracing contacted to minimize friction effects.

3.3 Test Setup

The Multidirectional Testing Laboratory has 102 ft. x 40 ft. of test space. The laboratory has anchor bolt sets placed in a 5 ft. grid across the floor. The anchor bolts used to connect the test fixtures to the floor were 3-3/16 in. diameter. The experiments were performed in a frame erected on the test floor and located in the east side of the laboratory. The frame was capable of resisting the loads necessary to test all the specimens.

3.3.1 Test Frame

The test frame was constructed of W12x87 columns and each was reinforced in the weak axis by a W18x71 column as shown in Fig. 3.3. A main beam was constructed of two side by side W36x210 beams. The top hinge support for the specimen was attached to the main beam. The bottom hinge was bolted to a steel pad which was anchored to the laboratory floor. The top hinge arrangement was longitudinally braced back to the frame corner. The test frame columns were braced in the longitudinal and lateral direction. The load application device, or servo-actuator, was suspended from the main beam.

The hydraulic servo-actuator was a Hanna model 2H-LINE with a 4.5 in. diameter cylinder. The Pegasus hydraulic pump maintained a pressure output of 3000 psi. Actuator load was monitored by a LEBOW model 3156-120K load cell with a capacity

of 120 kips. The actuator required a special loading fixture which permitted reversal of the load direction, and maintained vertical application of the load as the specimen deflected. The loading fixture was welded to the specimen, and pin connected to the actuator. The pin allowed the beam to rotate freely relative to the actuator cylinder. The actuator was controlled by a Vickers Control software package, which utilized a TS&S Hydraulic Service Manifold, located between the pump and the actuator. The software was operated in displacement control in user specified increments. Each increment of displacement had a haversine shape. These haversine displacement increments were 0.01 in. over a period of 2 seconds. In this manner the specimen experienced an essentially static loading.

3.3.2 Instrumentation

A wide variety of electronics were used to obtain the relevant data from each test (see Fig. 3.4). Joint rotation was measured by placing Applied Geomechanics model 800W tiltmeters on the beam and column. Trans-Tek Linear Variable Displacement Transducers (LVDT) of various sizes were used to measure displacements throughout the specimen (see Table 3.1). Table 3.1 has a reference column which describes the point at which the LVDT is based. Strain gauges of 1/16 in., 1/8 in., 1/4 in., and 6 mm. gauge lengths manufactured by Micro-Measurements and Kenkyujo were used.

The joints constructed with three attachments, the tee stub, ATLSS Connector, and flange plate, were locally indeterminate by a degree of one, based on equilibrium. Clip gauges were used in the second test in an attempt to eliminate the degree of indeterminacy and directly calculate the force in the plate and tee stub in both the elastic

and plastic regions of response. Results were obtained with some difficulty due to the limited area on the flange attachments for which to place instrumentation. The remaining three tests were statically determinant since there were only two attachments, and so it was no longer necessary to continue the use of the clip gauges.

A Temposonic 24 in. stroke LVDT was used to control and monitor the actuator, during the tests. To provide more accurate deflection data for the tests an additional LVDT was aligned under the actuator (LVDT #1 in Table 3.1).

3.3.3 Data Acquisition

The data acquisition system utilized was OPTIM Electronics MEGADAC A2300 hardware, in combination with their OPUS2000 operating software. This system was used to monitor and record the results at each load step. Ten instantaneous readings were stored at each step from every transducer. Upon completion of the test, the raw data was averaged by OPUS2000 and then transferred to a SUN Station with UNIX operating system for processing and storage. QuickBasic computer programs were used to reduce each string of binary data into data that commercial software was able to read. QuattroPro and Gnuplot were used for reducing, calculating, and plotting of the results.

3.4 Material Properties

The material properties reported include those of the column, beam, plate, and tee stub material. The parameters reported are calculated based on the guidelines set forth in (Davis, et al., 86). The ATLSS connector material composition was altered several times, and therefore the material composition of the connector in each test is reported.

3.4.1 Hot-Rolled Structural Steel, ASTM-A572

Material properties for the rolled steel are given in Table 3.2. For tests #1 through #4, the material properties are the same, but for test #5, new material was used and new property data are reported. Each of the material types had two tensile coupons machined and tested to produce plots for static yield as well as strain hardening properties. The strain hardening properties assisted in more accurately representing experimental behavior in the finite element models. Two bolts from every batch received were tested for load-strain relationships. Using the Rockwell hardness values and the load-strain relationships of these bolts and comparing them to the Rockwell values from those tested previously, a parameter was calculated for determining the load-strain relationship for each bolt. This was then used in the test to assist in following the failure of the test joint.

3.4.2 Cast Structural Steel, ASTM-A27, A148, and Experimental HSLA

ASTM specifications were used to provide the guidelines for fabrication of the first set of structural cast steel AC's. The ASTM-A27, and A148 connections were cast at Effort Foundry in Bath, Pennsylvania. After casting, the connectors were heat treated, sand blasted, and then transported to ATLSS.

At the same time this study was being conducted, new material compositions were being investigated to further improve the strength and weldability of the AC. As part of the investigation into new material compositions, trial castings were made from an experimental high strength low alloy (HSLA) steel. One of the connectors from the trial castings was used in the test program.

The individual chemical compositions were of importance in evaluation of the

performance of the ATLSS Connectors in the connections. Specimens were sent out to Laboratory Testing, Inc., (LTI), in Dublin, PA. for spectral analysis. Evaluations on weldability were made with the carbon equivalence (C_{eq}) ratings, and were based on the following equation (AWS, 90):

$$C_{eq} = C + \frac{Mn}{6} + \frac{Cr+Mo+V}{5} + \frac{Ni+Cu}{15} \qquad (3.1)$$

The C_{eq} rating is a percentage of carbon equivalent present in the material from which weldability of the material can be estimated. Usually C_{eq} values between 0.2 and 0.5 are acceptable for welding without preheat. The C_{eq} values are included with the mechanical property data from tensile tests in Table 3.3.

Connections were randomly selected for evaluation by radiography, also performed at LTI, and consistently met ASTM standards for structural casting soundness.

3.5 Test Procedures

The following sections discuss the specific procedures utilized for the assembly and testing for each test. Table 3.4 shows a summary of the experiments, dates and types of loading programs.

3.5.1 TPA-1

Test #1 was the first of two tests performed on Type A connections, which consisted of a (T)ee-stub, (P)late, and (A)TLSS Connector. The ATLSS Connector implemented in this test had material composition of cast A27 steel, and did not have the 45° bevel on the mortise (see Fig. 3.5).

The erection procedure is detailed here but performed with more ease than a

conventional connection. The shop-welded mortise and bottom flange plate awaited the beam (see Fig. 3.6). The shop fabricated holes in the column and in the plate were oversized. The beam with the shop-welded tee stub and shop-bolted ATLSS Connector was lowered into position (see Fig. 3.7). The tenon was placed in the mortise and aligned itself as it was allowed to drop into place.

The overview of the ATLSS Connector given in Chapter 2 showed the use of the seating bolt (Fig. 2.2). However, in this configuration the seating bolt was not needed. The flange bolts performed the same function. Therefore, once the AC was in place, and there was a sufficient gap between the bottom flange and the flange plate (1/16"-1/8"), the AC web bolts were fully pretensioned. By placing and pretensioning the two bolts on the flange plate directly below the AC, the AC is seated (see Fig. 3.8). The remaining bolts are then placed and pretensioned on the flange plate and tee stub (see Fig. 3.9). The entire bolting procedure was performed as recommended in the LRFD Steel Design Manual.

A typical loading program is shown in Fig. 3.10, and is described here as large-amplitude post-yielding reversal. The actuator started displacing the beam downward (positive deflection), imposing negative bending. At a pre-selected inelastic range tip-deflection, the actuator was reversed and loaded the beam in the opposite direction, until approximately the same amplitude was reached in positive bending. The load was again reversed and the connection failed in negative bending. The connection was then repaired, and reversed once more to induce failure in the positive bending direction.

3.5.2 TPA-CY2

Test #2 was the second test on a Type A connection, and the specimen was essentially a duplicate of TPA-1. However, the cantilever loading was (CY)clic. The ATLSS Connector implemented in this test had a material composition of cast A148 steel, and had the 45° bevel all the way around the perimeter of the mortise. Erection took place as it did in the previous test.

The test was conducted by applying a series of controlled displacement cycles at the cantilever tip. The selection of displacement program followed a recommended seismic testing procedure developed in Europe (Plumier, 83); it was based on an estimated yield deflection, Δ_{YE}, taken as the yield deflection found in the monotonic test TPA-1. The procedure for estimating Δ_{YE} is explained in Chapter 4. The groups of cycles had the increasing amplitudes of:

$$\frac{1}{4}\Delta_{YE} \rightarrow \frac{1}{2}\Delta_{YE} \rightarrow \frac{3}{4}\Delta_{YE} \rightarrow \Delta_{YE} \rightarrow 2\Delta_{YE} \rightarrow 3\Delta_{YE} \rightarrow 4\Delta_{YE} \ldots\ldots$$

The initial groups consisted of three cycles each until $3\Delta_{YE}$ where the groups encompassed only two cycles. This pattern was followed until failure occurred in one direction. The specimen was then repaired and the failure load in the opposite direction was attained. The cyclic displacement program used in the test is illustrated in Fig. 3.11.

3.5.3 TP-3

The third test was a control or reference test for the first two. The total elimination of the AC in this configuration allowed for direct evaluation of the contribution of the AC on rotational resistance. The configuration, having only the (T)ee-

stub and (P)late, was a Type B connection (Fig. 3.12). The erection was not as complex as Type A, the bolt holes only needed to line up and the bolts placed and pretensioned. The loading sequence remained as close as possible to the large-amplitude post-yielding program adopted for the first test. This test was important in that the results were easier to compare with the analytical results from the finite element analysis, before the more complex AC model was inserted into the joint. The completed connection is shown in detail before the test in Fig. 3.13.

3.5.4 TA-4

The last two tests were on the Type C configuration. The (T)ee-stub remained at the top flange, but the bottom flange plate was removed and an (A)TLSS Connector was placed at the lowest possible elevation on the beam web (see Fig. 3.14). It was anticipated this configuration would achieve full negative bending, shear, and a considerable amount of positive bending resistance. Test TA-4 utilized a connector made of A148 cast steel and with the bevel limited to the sloping sides of the mortise only. This design eliminated the bevel on the top and bottom of the mortise, as well as along the edges of the flutes.

The erection procedure for this connection consisted of depositing the ATLSS Connector into place, tightening the web bolts, placing and tightening the seating bolt, and then placing and tightening the tee stub to column bolts. The only tolerance consideration was to tighten the web bolts after ensuring that the tee stub bolts were able to be placed.

The loadings applied are again of the type described as large-amplitude post-yielding.

3.5.5 TAR-5

Test #5 was a (R)etest of test #4, Type C. The reasons for the retest will be explained in the discussion of the test results for TA-4. The only notable difference between test #4 and #5 was the composition of the cast steel material for the ATLSS Connector. The castings were made from the experimental HSLA steel. This material provided for higher strength than the A27 steel, and yet had low carbon content. The low carbon content allowed for better weldability. The geometry had the limited bevel cast into the connector, but the slight curvature of the bevel from the casting procedure was ground flat. This enabled for the design weld throat penetration into the bevel.

The erection procedure, loading procedure, and other considerations are the same as reviewed above for test #4. The completed connection is shown in Fig. 3.15.

CHAPTER 4 - FINITE ELEMENT ANALYSIS

4.1 Assumptions and Limitations

Finite element analyses were performed to predict the behavior of the test connections and the contribution of the ATLSS Connector. Initial finite element models were used to investigate the influence of varying positions of constraints at the fixed end for a cantilever beam. Further analyses were performed using detailed models of two of the connection configurations which were tested. ANSYS[3] Version 4.4A software was utilized to perform the non-linear finite element analyses. The analytical studies were performed on Sun Workstations at ATLSS mountaintop computing facilities.

The models utilized symmetry about the minor axis of the beam cross section. Strain hardening effects were incorporated in the analysis by defining the stress-strain relationship for each material. Dimensions used for the elements were taken from the actual test specimens. Displacements were introduced at the cantilever end and the finite element analysis program calculated the resulting loads needed to produce those displacements.

Two studies were conducted on the beam portion of the test specimens. The model was of a W12x22 beam, 34 in. long[4]. Finite element models of the beams were automatically generated from user input geometrical divisions which provided a fine mesh adjacent to the connection and permitted larger size elements near the free end. The first study examines the effect of different rigid end constraints on how the beam distributes

---

[3]Swanson Analysis Systems, Inc., (1989), Houston, PA 15342

[4]This is the distance from the face of the column to the point of load application of all the test specimens.

the forces to the column through a connection. Rigid boundary conditions were located at the flanges, the web, or a combination of the two. The second study examined the actual geometrical configuration of the flange attachments as well as the beam portion of the experimental specimen. This study included the tee stub and plate flange connections and simulated the AC using non-linear spring elements.

Based on the assumption that the tested column remained elastic, the models were simplified to isolate the beam and connection. As explained in Chapter 3, the column selected for testing was oversized to insure the column remained elastic throughout the test. The models, therefore, assumed that the applied load was transferred from the beam to the connection and then from connection to a rigid support. To complete the analytical model for prediction of and comparison with the experimental results, two elastic column effects were included in the analysis. These were the elastic rotation due to column bending, Θ_B, given by

$$\Theta_B = \frac{\frac{M_C}{2} \times \frac{L}{2}}{3EI_C} \tag{4.1}$$

where M_C = moment at center of column
L = distance from hinge support to hinge support (Fig. 3.1)
E = modulus of elasticity (29,000 ksi)
I_C = column moment of inertia

and the elastic rotation due to column shear deformation, ϕ_C, which can be calculated as

$$\phi_C = \frac{V_C}{GA'} \tag{4.2}$$

where V_C = shear at hinge support
G = shear modulus (11,200 ksi)
A = area of the column web

The rotations at the center of the column induced additional deflection at the cantilever tip. To calculate these added deflections, the rotations were multiplied by the distance from the center of the column to the end of the cantilever, or the previously defined distance B (see Fig. 3.1).

To analyze the results, a consistent method of evaluating the yield deflection is required. The yield deflection, Δ_Y, was calculated as the intersection of lines defined by the slopes of K_E and 0.1 K_E as illustrated in Fig. 4.1 (Plumier, 83). The load corresponding to this displacement is referred to as the yield load, P_Y, of the beam.

4.2 Study of Beam End Conditions (Simplified Models)

Four three-dimensional non-linear analysis models were studied to predict upper-bound moments, stiffnesses, and deflections due to the beam behavior alone. The beam end boundary conditions were varied in the four models. To model the ideal connection behavior for each configuration, ends of the beam were fixed at locations where the actual connecting elements were attached. The fixed condition is when the displacements and rotations for a specific node are prevented.

The beam was modeled using three dimensional inelastic shell elements (Stif-43[5]). The element mesh for the model is illustrated in Fig. 4.2 with a separation between the elements for clarity. The elements represent the plate components of the beam and have both out-of-plane and in-plane bending stiffness. Bending stresses were allowed to vary through the thickness of the elements. The elements also incorporated plasticity effects through user defined stress-strain relationships.

4.2.1 Descriptions of Boundary Conditions

The location of the boundary conditions imposed on the support end of the cantilever beam are described below and illustrated in Figure 4.3.

Fixed End Total (FTOT)

This model represents the ideal behavior of a fixed cantilever beam. Fixed boundary conditions were imposed along the top flange, bottom flange, and along the entire web. The model predicted the overall distribution of the forces in the flanges and the web when both are completely fixed.

Fixed Flange and Mid-Web (FFMW)

The FFMW examined the difference between a fully engaged web and one fastened by a shear connector. Fixed boundary conditions were imposed along the top flange, bottom flange, and along the center third of the web. This configuration would approximate a Type A connection.

Fixed Flange (FF)

This model eliminated the shear and bending resistance imparted by fastening

[5]ANSYS element code name, (ANSYS, 89).

part or all of the web. Fixed boundary conditions were imposed only along the top and bottom flange. This model represents a Type B connection configuration.

Fixed Top Flange and Bottom Web (FTFBW)

Nodal boundary conditions for this model were released along the bottom flange and were imposed only along the top flange and bottom third of the web. The lowest web node restrained is not a node shared by both the flange and the web, but one which is located in the web only. These boundary conditions were not symmetrical with respect to the centroid of the major axis of the beam. Due to these unsymmetrical boundary conditions, the model was analyzed for both positive and negative vertical loading (displacement) to determine if different responses would be obtained. This model represents a Type C connection configuration.

4.2.2 Results

The elastic distribution of moments and shears in the elastic range calculated from the analysis for each model are reported in Table 4.1. The restraint (R) of each connection was defined earlier as the ratio of the moment developed in the connection to the plastic moment of the beam section. The plastic moment value was calculated from the actual experimental beam material properties, and will be presented in further detail in the following chapter. The elastic response was calculated just prior to the departure of the overall stiffness of the load-deflection curve from linear behavior. The distribution of forces for the models was changed after the model went from elastic response to a plastic response (see Table 4.2). The plastic response was evaluated at four times the yield displacement, Δ_{YA}, determined by the individual finite element analyses.

The response in the elastic range is reviewed first. The fully fixed case, FTOT, shows 76% of the shear was carried by the web and 84% of the moment was carried by the flanges. These were the expected distributions. The force distribution in the FFMW model, where two-thirds of the web nodes were released, showed a 69% drop in the moment carried in the web and a 38% decrease in the shear force carried by the web, when compared to the fully fixed model. In the FTFBW model, the web carried a larger percentage of the moment capacity than any of the other models. This was expected because the web compensated for the bottom flange not being connected.

The high elastic restraint values of the FTOT and FFMW models exemplifies why those configurations are most often utilized for AISC fully fixed connection design. Comparing with the FTOT case, the FF and FTFBW connections provided 20% and 58% less elastic R, respectively. The unsymmetrical geometry of the boundary conditions for FTFBW with respect to the centroid of the beam did not effect the results when the load was reversed. Load-deflection curves were identical when the flange was in tension and the web in compression and vice versa. The degree of restraint provided by the configuration, therefore, was identical in both cases.

As the response of the connection changed from elastic to plastic there was a shift in the distribution of the forces. Also, the percent of moment carried by the flange increased for the three cases which engage the web. The moment capacities found for the FTOT and FFMW cases exceeded the plastic moment of the beam section because of the effect of strain hardening. The FF model showed no redistribution due to plasticity since the full moment was always carried by the flanges. The FTFBW model showed

that the axial force in the flange became equal and opposite to the axial force in the web, and thus the moment was carried equally. An equal distribution of shear forces carried between the flange and the web was experienced during the plastic response.

The load-deflection curves for the various boundary condition cases are shown in Fig. 4.4. Selected parameters of the elastic deformation behavior are reported in Table 4.3.

4.3 Refined Analysis Including Tee Stub and Flange Plate

Three-dimensional inelastic models were used to assess the behavior of the actual connections. These models were also constructed to take advantage of symmetry. Two of the actual test configurations were modeled, Type A and Type B. Both of these configurations utilized a tee stub and a plate flange attachments and the second model (ATPA) also incorporated an AC located at mid-web.

4.3.1 Description of Models

The tee stub and plate were constructed of the same type of element as the beam elements but the material properties were based on the actual tensile test values. The tee stub to flange weld was modeled by joining the edge nodes of the tee stub with the beam flange. The plate-to-flange bolting was modeled by joining the nodes of the flange and connecting plate where the actual bolts were located.

Analytical Tee Stub and Plate Connected Beam (ATP)

The model is shown in Fig. 4.5. Boundary conditions were imposed on this model at each node along the connected tee stub and plate. Deformations in the negative bending direction were imposed at the free end of the cantilever beam. The program then

calculated the loads which would induce the specified deformations.

Analytical Tee Stub, Plate, and ATLSS Connector (ATPA)

This model was the same as the model described above, but included non-linear spring elements to model the ATLSS Connector. The AC was modeled using a non-linear force-deflection element (Stif-39[6]). The stiffnesses were calculated based on the previous analytical work which predicted the displacement response of varying sections of an ATLSS Connector (Fleischman, et al., 93). The finite element study consisted of sectioning the connector into slices of unit thickness, applying tensile loads to the slices, and calculating the response of the slice. The non-linear responses are shown in Fig. 4.6. Symmetry was used for the slice model, but the results presented were scaled to represent the full model width.

For the ATPA model, the connector was modeled using six non-linear springs as illustrated in Fig. 4.7. Five horizontal non-linear springs were set equal to the stiffness based on the previously calculated slice data. The non-linear springs corresponded to their location and contributing length. The values are then scaled to account for the symmetry used throughout the model. The seat spring stiffness was based on the actual load-deflection response of the tenon displacement from the first test (TPA-1). The resulting non-linear spring response curves for a full AC are shown in Fig. 4.8. The fixed boundary conditions imposed on this model were the same as reported for the ATP model but the ends of the springs were fixed.

[6]ANSYS element code name, (ANSYS, 89).

4.3.2 Results

The load-deflection response for the ATP and ATPA models are shown in Fig. 4.9. Individual parameters defining the elastic response are shown in Table 4.3. Comparisons of these two models with the simplified models discussed previously are illustrated in Fig. 4.10. Model FFMW provides an the upper bound of response for ATPA and model FF is the upper bound response for ATP. The connection stiffness of model ATP is close to that of the other models with flange attachments, but when compared to FF it carried 27% less load at the yield limit. Model ATPA had a drop of only 7% in the load at yield as compared to the upper limit of model FFMW.

The moment-rotation response for the ATPA and ATP models is shown in Fig. 4.11. This difference between these two models was used to predict the contribution of the ATLSS Connector to the moment resistance of the tee stub and plate connection. The difference is plotted in Fig. 4.12. The method used to measure the contribution of the spring model ATLSS Connector is unable to calculate the resistance at very small values. As the load increased to the later portion of the elastic range, the moment resistance contributed by the AC also increased. At the elastic limit, the moment resistance contributed by the AC Connector was approximately 15% of the plastic moment of the beam section. This contribution increased until leveling off at about 27%.

CHAPTER 5 - EXPERIMENTAL RESULTS

5.1 General

Results from the five exterior connection specimens are presented in this chapter. The response characteristics reported for the tests and the methods used to determine them are reviewed. Information on the strength, displacement, stiffness, ductility, and energy dissipation of the connections is presented. The mode of failure and the behavior of the ATLSS Connector of each test are also reported.

5.2 Methods of Analysis

The response of each test specimen and the results obtained are described in terms of the following structural characteristics; the definition and method of determination for each are given below.

5.2.1 Strength and Displacements

The load history for each specimen is displayed in a load-deflection plot. The load was determined directly from a load cell and verified by strain gauges placed on the beam. The strength of the connection is reported as a percentage of the plastic moment capacity of the beam section. A simplified force system, as shown in Fig. 5.1, is used to describe the distribution of moment and shear resisted by the connection components. The moment applied to the connection is equal to the applied load multiplied by the distance from the load point to the column face. The plastic moment capacity of the section, M_p, has been calculated using the actual specimen dimensions and the average measured yield stresses of both the flange and the web. The actual M_p for tests #1 through #4 is 128.2 kip-ft, and for test #5 it is 119.1 kip-ft. Both values are close to the

nominal value calculated based on the listed properties (AISC, Load, 86).

Deflection of the cantilever beam was measured directly under the load point by an LVDT referenced from the floor. The deformations recorded at this location include several components in addition to the connection response. Displacement of the specimen column within the test fixtures occurred at two separate locations. First, slip of the specimen column occurred at the bolted hinge supports. Second, the stub column which supported the top hinge[7] deformed due to the shear load. Deflection at the cantilever end due to the displacement of the specimen within the test frame was monitored by LVDT's at the base plates and subtracted from the measured values to produce the presented values for deflection.

The yield displacement, Δ_Y, is calculated as the intersection of lines defined by the slopes of K_E and 0.1 K_E as illustrated previously in Fig. 4.1. The corresponding load, P_Y, is referred to as the yield load. The failure displacement, Δ_F, was the displacement of the beam at which failure, due to fracture, has occurred.

The absolute rotation of the connection was determined by taking the difference between the rotation of the tiltmeter located on the column and the tiltmeter located on the beam. This accounted for both the bending of the column as well as the slip of the column relative to the hinge supports. The tiltmeters were not sensitive to the small values of rotation. The plots, therefore, have been averaged at each data point based on two points ahead and two points behind the point being considered. The tabulated values reported for the maximum negative moment and corresponding rotation are not averaged,

[7]Refer to Fig. 3.3

however. The maximum positive bending moment achieved and the moment at failure are given, but the values of rotation are not, because the rotation readings become inaccurate after the occurrence of the first fracture. Therefore, the moment-rotation curves stop at the first fracture which required repair for testing to continue.

5.2.2 Stiffness and Ductility

The initial tangent stiffness of the connection is the slope of the elastic portion of the load-deflection curve. The tangent stiffness, K_E, is taken from the negative bending direction of the test unless otherwise stated.

$$K_E = \frac{P_Y}{\Delta_Y} \tag{5.1}$$

The ductility capacity, μ, is the ratio of deflection at failure to the yield deflection.

$$\mu = \frac{\Delta_F}{\Delta_Y} \tag{5.2}$$

The cyclic ductility ratio, μ_C, is determined by summation of the peak deflections per excursion divided by the experimental yield deflection.

$$\mu_C = \frac{\Sigma \Delta_{PE}}{\Delta_Y} \tag{5.3}$$

where Δ_{PE} = peak deflection of an excursion.

5.2.3 Energy Dissipation

As explained in Section 3.5, the direction of the applied load was reversed two or

three times in each test and in the case of TPA-CY2 many cycles of repeated and reversed loads were applied. This was done in order to obtain information on the energy dissipation characteristics of the connection for possible use in earthquake-resistant design. The energy dissipation capacity is evaluated as the work done by the applied load and is equal to the area enclosed by the cycle's load-deflection loop (Wakabayashi, 86). The work done by each of the tested connections has been calculated using the parameters illustrated in Fig. 5.2.

Two methods are used to present the energy dissipation data. First, the cumulative energy dissipation for a cycle is the work for that particular cycle added to the work of all previous cycles to provide the total energy dissipated during the test. Second, the energy dissipation value of each cycle is plotted with its corresponding deflection. This method is useful for the comparison of the energy dissipation between cycles and data for similar connections from previous research. The normalized work or the energy dissipation ratio, E, is equal to the work performed for a cycle divided by the work done up to the yield point.

$$E = \frac{W}{\frac{1}{2} P_Y \Delta_Y} \tag{5.4}$$

where W = work done per cycle.

The value of energy dissipation for a cycle is dependant upon the amplitude of displacement during the cycle. For convenience of reference the displacement is normalized with respect to the yield deflection, Δ_Y. In the plastic range, the plastic ratio,

π_d, is used, which is defined as

$$\pi_d = \frac{\Delta'}{\Delta_Y} \tag{5.5}$$

where Δ = plastic deformation for a cycle (Fig. 5.2).

The data are normalized in order to create dimensionless values of energy dissipation and displacement, which would permit direct comparisons between the cycles and other tests.

5.2.4 ATLSS Connector

The behavior of the ATLSS Connector can be evaluated using the recorded readings from the strain gauges and displacement transducers. Three strain gauges on one of the mortise arms provided information from which a stress gradient can be calculated. Both sides of the mortise are assumed to deform equally because of the symmetrical geometry about the minor axis of the beam. Three strain gauges were also located on the tenon along one side of the beam web attachment plate. These were used to assess the axial load and bending moment carried by the AC during its elastic response.

Displacement transducers (LDVTs) were used to measure the relative displacements of the tenon. The vertical deformation of the tenon into and out from the mortise was measured by an LVDT located at the top of the tenon and mounted to the column. Horizontal displacement of the tenon in the longitudinal direction of the beam was measured by an LVDT located at the top of the connector and mounted on the column.

5.2.5 Failure Modes

In all the tests, failure was associated with fracture of the flange attachments or the AC. After reaching the failure load in one direction, the connection was repaired and testing resumed to determine the strength and failure load in the opposite direction. If the connector did not fracture before the flange attachments failed, then testing usually continued until failure of the connector occurred. The physical nature of the fracture and observations made of the attachments as well as the beam during testing are described. Whitewash was used during testing to help identify areas of localized yielding in the specimens.

5.3 Results of TPA-1

Test TPA-1 examines the behavior of the connection through large amplitude cycles before failure. This test utilized an AC made of A27 cast material. A statically applied initial loading of 7 kips provided a shakedown of the test specimen and setup. The specimen was then brought back to the start point and loading was reinstated. The load-deflection curve is shown in Fig. 5.3. The test started under negative bending until first reversal at point A. After passing the elastic response under positive bending the connection experienced bolt slip in the flange plate bolts at [B]. The test was reversed at [C]. Bolt slip occurred again in the flange plate bolts near [D], but this time at smaller amounts. The response was slightly stiffer and stronger than the first cycle. The connection reached its maximum negative bending load at [E]. At [F] fracture occurred at the tee stub after considerable necking at the termination of the weld, which attached the stub to the beam top flange (see Fig. 5.4). At [G] the beam was brought back to zero

deflection [point H]. The tee stub was repaired while the load was maintained by the actuator. The drop in load just after [H] was where the shrinkage of the tee stub repair weld lowered the load necessary for the actuator to maintain the prescribed displacement. The test resumed and the specimen again experienced bolt slip at [I]. Fracture occurred in the net section of the first line of bolts of the flange plate [point J] and was followed by a significant drop in load. The test continued with only the repaired tee stub and the AC. At [L] the AC tenon plate fractured at the net section of the first bolt line (see Fig. 5.6). The characteristic displacement and load values are given in Table 5.1.

The moment-rotation behavior of the connection is shown in Fig. 5.7 with the same reference markers as the load-deflection curve. The maximum negative bending moment is 1.17 M_p at a rotation of 0.0340 radians, while the maximum positive bending moment is 1.19 M_p. The initial tangent stiffness in negative bending is 170 kip/in. The ductility ratio, μ, for negative bending is 8.3.

5.3.1 Energy Dissipation

The single cycle of the test is used to assess energy dissipation. The resulting normalized energy dissipation value, E, is 25.9. The energy values for this test are shown in Table 5.2.

5.3.2 ATLSS Connector

The mortise gauges indicated minimal strain readings. The readings are a small percentage of the yield strain because the yielding is most likely occurring closer to the column end of the mortise arm. The moment developed in the AC tenon calculated from the tenon strain gauges was a value equal to about 2% of the total developed moment.

This value is rather low compared to previous research and data collected from subsequent tests and may indicate incorrect readings from the strain gauges.

The measured displacement of the tenon down into the mortise was 0.047 inches at the first reversal. The measured displacement of the tenon up out of the mortise was 0.073 inches at the second reversal. This displacement was not measured after the specimen continued past point [D] on the load-deflection curve. The maximum longitudinal (in the plane of the beam web) displacement of the tenon inward, or toward the column was 0.010 inches at the first reversal. The maximum longitudinal displacement of the tenon was 0.064 inches outward at the negative bending failure.

5.3.3 Failure

The negative bending failure load was 1.07 M_p. The positive bending failure occurred in the bottom flange plate at a positive bending of 1.04 M_p. The test was continued in positive bending with the connection consisting of only the tee stub and the AC. Based on the assumption that the tee stub and AC formed a couple to resist the applied moment, the calculated tensile failure load in the AC was 97 kips. All the fractures occurred at the anticipated locations.

5.4 Results of TPA-CY2

Test TPA-CY2 was conducted with repeated and reversed displacement cycles. The ATLSS Connector used was cast from material complying to the ASTM A148 Specification. The load-deflection loops are shown in Fig. 5.8. The first fracture occurred at the peak of the positive bending during cycle 18, marked as point A. The fracture was along the connector weld which attached the mortise of the ATLSS

Connector to the column (see Fig. 5.9). The test continued and the crack did not affect the negative bending results during the following excursion. At point [B] the maximum load was reached. The specimen was unloaded and an attempt was made to reach the same cycle amplitude in positive bending. The load reached in this cycle was less than the maximum load obtained in the previous positive bending cycle [C]. This was believed to be due to the continued propagation of the weld crack in the mortise. When the load was again reversed, the negative bending strength was depleted. Cracking occurred throughout the rest of the cycle and was evident with the degradation in strength and stiffness, as shown from the load-deflection and moment-rotation plots. The tee stub failed due to fracture at the end of this excursion [D]. The tee stub was repaired at [E] and the load was reversed until failure of the plate at [F]. The tee stub and flange plate fractured in the same manner and location as in test TPA-1. After the plate fractured, the photograph of Fig. 5.9 was taken.

The consecutive cycles for a given amplitude fall essentially on top of the original cycle. The load-deflection relationships of the first 12 cycles are shown in Fig. 5.10. These cycles show small amounts of stiffness degradation in the negative bending direction of the connection. The moment-rotation behavior for the entire test is shown in Fig. 5.11. The maximum moment capacity is 1.05 M_p in both directions. The rotations corresponding to these moments are 0.0256 radians in negative bending and 0.0221 radians in positive bending. These values were recorded before the first significant failure occurred. Therefore, reliable negative and positive displacement values are available.

The initial tangent stiffness for the tests is taken from the second cycle under negative bending. The first cycle is used to relieve the connection of the residual stresses in the same manner as was done in test TPA-1. The resulting tangent stiffness is 187 kip/in.

5.4.1 Energy Dissipation

The results of the cyclic test pertaining to the energy dissipation and ductility is shown are Table 5.2. The energy dissipation accumulated over the entire test is plotted for each cycle in Fig. 5.12. The energy dissipation ratio, E, is plotted against the plasticity ratio, π_d in Fig. 5.13. The points displayed near the origin are occasionally overlapped. The data points have a linear best-fit line through them with an equation of:

$$E = 3.19\pi_d$$

5.4.2 ATLSS Connector

As in the TPA-1 test, mortise strain gauges indicated very small strain readings, amounting to small percentage of the yield strain. The moment developed in the AC tenon during the tenon's elastic response calculated from the tenon strain gauges was approximately 8% of the total developed moment. After the first excursion the moment could not be calculated because the top tenon gauge was faulty.

The maximum measured displacement of the tenon up out of the mortise was 0.090 inches just after AC mortise weld began to crack. The maximum measured displacement of the tenon down into the mortise was 0.068 inches when the tee stub failed. The longitudinal (in the plane of the beam web) range of displacements of the tenon was between 0.012 inches inward, or toward the column, just after AC mortise weld

failure and 0.018 inches outward at the tee stub failure.

5.4.3 Failure

The connection was under positive bending when the first significant fracture occurred. The test was reaching the first excursion of positive bending at the maximum amplitude of 1.2 in. When the mortise weld fractured, the load dropped from 48 to 39 kips. The fracture occurred within the heat affected zone of the mortise base material. With the effectiveness of the AC as a shear connector depleted, the failure of the flange components progressed sooner than in test TPA-1.

5.5 Results of TP-3

This was the only test performed on the Type B connection. A statically applied initial load of 7 kips provided a shakedown of the test specimen and setup and allowed for a check on the measuring instruments. The test was then brought back to the starting point and loading proceeded. The load-deflection curve is shown in Fig. 5.14. The connection experienced bolt slip prior to the first reversal at [A], shown by the erratic spikes on the curve. The load was reversed under positive bending at [B]. After the cycle returned to negative bending, the response exhibited less strength than the initial post yielding response. This is believed to be a result of the bolt slip which occurred when the specimen was loaded previously in negative bending. The previous slips were observed as spikes on the curve, whereas in the second excursion the movements due to the slips were occurring continuously. Maximum load was attained at [C]. The tee stub fractured at [D] after necking was observed at the termination of the weld attaching the stub to the top flange (Fig. 5.15). At [E] the connection was repaired and testing resumed

under positive bending. Bolt slip occurred at [F] and then fracture of the flange plate followed at [G]. The fracture observed was attributed to low cycle fatigue of the metal of the bottom flange plate at the gross section between the column and the first bolt line (see Fig. 5.16). The backing bar was left in place behind the full penetration weld of the flange plate. This provided for localized bending to occur through a shortened distance, causing large localized displacements, and thus the low cycle fatigue. Important displacement and load values obtained from the test are given in Table 5.3.

The moment-rotation behavior of the connection is shown in Fig. 5.17. The maximum negative bending moment is 1.05 M_p at a rotation of 0.0393 radians, while the maximum positive bending moment is 0.80 M_p. The initial stiffness of the connection is 171 kip/in. The ductility ratio, μ, is 12.7.

5.5.1 Energy Dissipation

The single cycle of the test is used to assess the energy dissipation capacity. The resulting normalized energy dissipation ratio, E, is 22.8, as shown in Table 5.2.

5.5.2 Failure

The failure moment for negative bending was 0.65 M_p at a rotation of 0.0522 radians. The large shear force caused the premature fracture of the flange plate, which resulted in a positive bending failure moment of 0.80 M_p.

5.6 Results of TA-4

This test was the first experiment performed on the Type C configuration, and was the last to utilize the A148 ATLSS Connector. Difficulties had been encountered during testing of TPA-CY2 which indicated problems with the strength of the AC. It was

perceived to be a problem with the inability to fully apply weld to the mortise bevel. For this test, extra weld was added to the fillet weld around the perimeter of the mortise, and a plug weld was applied to the back of the mortise. The load history of the test is shown in Fig. 5.18. As the applied downward load exceeded 18.5 kips, the first small drops in load began occurring, which were accompanied by sharp "cricking" sounds not indicative of bolt slip. This sound continued until a load drop of 7.5 kip occurred at [A], which was believed to be bolt slip. The load was reversed until the same loss of load occurred twice under positive bending [point B]. This was again believed to be bolt slip, but additional "cricking" was also experienced. The load was reversed, because it was decided that the mortise was failing. At [C] the bolts slipped back in the opposite direction, but the "cricking" was not experienced. Maximum load under negative bending was attained at [D], and the connection reached its failure load at [E]. Early in the test it was realized that there was not a strength problem with the connector, but a problem associated with welding might have existed. After completion of the test, the connection was dismantled and a thorough investigation into the material of the AC was undertaken. The analysis revealed that cold-cracking had occurred within the heat affected zone of the AC mortise. Spectral analysis revealed a chemical composition containing a high carbon content in the AC material. The material properties were modified before further tests were performed. The results of this test are presented here for completeness of this study.

The moment-rotation behavior is shown in Fig. 5.19. The maximum negative bending moment is 1.06 M_p and maximum positive bending moment is 0.34 M_p.

5.6.1 Energy Dissipation

Since it was not possible to complete a single cycle of loading, the energy dissipation values could not be evaluated.

5.6.2 ATLSS Connector

Due to premature welding failure, the test did not provide information which would allow the behavior of the AC components to be separately evaluated.

5.6.3 Failure

The failure of the ATLSS Connector due to cold-cracking distorted the true connection response. After the test the outside of the connector welds showed no visible cracking. However, the composition analysis showed a large carbon equivalent, C_{eq}, value for the connector material. The conclusion was that the large carbon content in the composition of the cast connector caused the internal weld interfaces to crack.

5.7 Results of TAR-5

Material properties of the ATLSS Connector were modified and a second and duplicate of TA-4 was fabricated. Experimental HSLA steel was used for the AC material. The C_{eq} value for this material was 0.32%, a value well within the range for good weldability. The top and bottom bevels on the back of the mortise were eliminated and a normal perimeter weld, up to 5/16 in. throat, was used to weld the mortise to the column flange. The load-deflection relationship of the test is shown in Fig. 5.20. The test proceeded under negative bending until [A] where the load was reversed. The "cricking" sounds evident in test TA-4 were not experienced. Slip of the tenon plate bolts occurred at [B] until each went into bearing. One of the main interests of this test was

the performance of the AC under positive bending, so the load was increased until fracture of the tenon plate at [C]. The load was reversed and at [D] the connection experienced the same slip as [B] but in the opposite direction. The maximum load was attained at [E]. At [F] the tee stub fractured at the same location as discussed in the previous tests (see Fig. 5.21). Key information obtained from the test is shown in Table 5.4.

The initial stiffness of the connection is 98 kip/in. The ductility ratio, μ, is 8.9. The moment-rotation behavior is shown in Fig. 5.22. The maximum moment achieved in negative bending is 0.97 M_p at a rotation of 0.0402 radians, while in positive bending the maximum moment is 0.59 M_p.

5.7.1 Energy Dissipation

The single cycle of the test is again used to assess energy dissipation. The normalized energy dissipation ratio, E, is 14.7, as reported in Table 5.2.

5.7.2 ATLSS Connector

The readings from the strain gauges mounted on the mortise were very small, amounting to a few percentage of the yield strain. The tensile load in the tenon calculated from the tenon strains showed consistently a value of approximately four times the applied load. From equilibrium it can be seen that the axial force in the tee stub and AC should be four times the applied load to resist the resulting beam end moment.

The maximum measured displacement of the tenon into the mortise was 0.012 inches at tee stub failure and did not move out past its starting position. The maximum measured longitudinal (in the plane of the beam web) displacement of the tenon in

towards the column was 0.001 inches at the second reversal. The maximum measured longitudinal displacement of the tenon outward was 0.013 inches at the tee stub failure.

5.7.3 Failure

The connection failed in positive bending at a moment of 0.59 M_p. The failure was due to AC fracture, which was similar to that in test TPA-1, where the AC tenon fractured along the first bolt line. The nature of the fracture was such that it did not affect the negative bending performance, because the crack would close under the compressive force. The resulting fracture of the tee stub was at a negative bending moment of 0.69 M_p .

CHAPTER 6 - DISCUSSION OF RESULTS

6.1 General

In this chapter the previously presented results are reviewed and discussed. Comparison of the erection behavior of the different configurations is followed by a summary of performances of the three types of configurations tested. The predictions from the finite element study are compared to the experimental values. Energy dissipation data for the large amplitude tests are presented and compared to TPA-CY2 results. Different joints types are then compared to quantify the performance of the ATLSS Connector in the individual tests.

6.2 Erection

The installation of the Type A configuration was performed with few difficulties. In both tests, TPA-1, and TPA-CY2, the tenon was placed into the mortise and the gap required to seat the AC was achieved. The AC held the beam in place throughout the bolt placement and tightening. The AC was seated and the bolt holes aligned with the assistance of a drift pin. Bolt placement in TPA-1 proceeded easily. Bolt placement for TPA-CY2 required more effort to connect the bottom flange. In both cases, placement of the tee stub bolts proceeded easier than the placement of the flange bolts. Also, the fully fastened connection required no shims to insure perpendicular placement of the beam with respect to the column.

For the Type B joint, test TP-3, it was necessary to hold the beam in place while the bolts were placed and then the first few were tightened. No shims were required for this connection to be aligned perpendicular to the column.

The Type C connections, tests TA-4 and TAR-5, were erected simply. Both specimens were fully tightened easily and without shims. The use of the seating bolt located at the base of the mortise produced the same seating displacement to the connection as the flange seated connection. As a result of the proper seating displacement, the tee stub bolts were placed with ease.

6.3 Joint Performance

Experimental results gathered from the three types of configurations tested are summarized in this section. Each type is discussed separately.

6.3.1 Joint Type A

The maximum moment capacity achieved in TPA-1 and TPA-CY2 was an average of 1.11 M_P in negative bending, and 1.12 M_P in positive bending. Higher values of maximum moment would have been achieved if not for premature fracture of the AC mortise weld in TPA-CY2. The response of the connections departed from linear-elastic response rather early. This may be due to the presence of residual stresses in the beam from cooling (after rolling and welding operations) and cold straightening. Yield lines were evident on the flanges of all the beam sections before testing.

Results from the full closed cycles of the cyclic tests show a respectable energy dissipation capacity. Some stiffness degradation was perceptible for successive amplitude increases. Each cycle exhibited a positive post-yielding slope. The Bauschinger effect was evident on the load-deflection curves (Wakabayashi, 86).

Cyclic tests performed at the University of California, Berkeley provided energy dissipation data for different types of conventional connections (Popov and Pinkney, 67).

The results and methods of evaluation which were utilized in that study are also used to describe, compare, and evaluate the results of this study. Their results are presented as non-dimensional quantities and can, therefore, be compared to those reported here. The values from cyclic test TPA-CY2 are compared to their specimen F3B-C7, a full moment connection with bolted beam flange plates, which were welded to the column flange, and a double angle web shear connector. The connection was designed to allow failure to occur in the plates before occurring in the flanges. A comparison of the energy dissipation ratios of the two specimens are shown in Fig. 6.1. A linear regression has been performed through the data points of TPA-CY2 and the following equation was obtained:

$$E = 3.19\pi_d$$

Popov and Pinkney gave the expression $E = 1.77\pi_d$ as the best fit linear equation through all the data points of the connections they tested. The individual data points plotted in Fig. 6.1 are those pertaining only to the F3B-C7 connection. This comparison of values show that AC-aided connection dissipated more energy than the conventional moment connections of approximately the same design. The Type A connection is more flexible than its conventional counterpart because it has a bolted tee stub, and the beam has a clear distance of 1.625 inches to the column flange. Both most likely contributed to the greater energy dissipation observed from the tests.

The AC aided Type A connection performed similarly to a full moment connection, and provided ample energy dissipation capacities.

6.3.2 Joint Type B

Test TP-3 reached 1.05 M_p in negative bending, but only 0.80 M_p in positive bending. This was due to high localized shear deformations in the flange attachments adjacent to the column. The localized shear deformations led to low cycle fatigue failure instead of tensile fracture of the bottom flange plate attachment as would normally be expected. The response of the joint also departed early from the linear-elastic response rather early and assumed to be for the same reason as presented in the previous section.

6.3.3 Joint Type C

Test TA-4 is not discussed because of its premature weld failure. The connection in TAR-5 reached a maximum moment of 0.97 M_p in negative bending and 0.59 M_p in positive bending. Bolt-slip occurred at the tenon to beam web connection which shifted the load-deflection and moment-rotation plots. The response of the joint also departed early from the linear-elastic response for the same assumption discussed previously.

6.4 Comparison of Test Results

The relative performance of the three types of connections studied may be evaluated by comparing the results of TPA-1, TP-3, and TAR-5.

6.4.1 Load-Deflection

The load-deflection comparison between test TPA-1 and TP-3 is shown in Fig. 6.2. The strength for the AC aided connection was greater than that of the flange-alone attached connection. However, this added strength was rather small in the elastic range, but became significant through the post-yielding region. The added flexibility of TP-3 was due to the rigid body translation of the connected beam end. This translation was

caused by very high shear forces in its flange attachments.

The load-deflection comparison between test TPA-1 and TAR-5 is shown in Fig. 6.3. The initial tangent stiffness of the Type C connection was 42% less than the Type A configuration.

6.4.2 Moment-Rotation

The moment-rotation comparison between test TPA-1 and TP-3 is shown in Fig. 6.4. The moment capacity was reduced for the connection without the AC. The maximum negative bending moments for TPA-1 and TP-3 were 1.17 M_P and 1.05 M_P, respectively. TPA-1 exhibited greater strength, while TP-3 exhibited larger flexibility. The rotations corresponding to the maximum negative moments for TPA-1 and TP-3 were 0.0340 and 0.0393 radians, respectively.

The moment-rotation comparison between test TPA-1 and TAR-5 is shown in Fig. 6.5. The strength is reduced for the connection without a bottom flange plate. In addition to having an adequate shear strength, the moment resistance of the Type C connection allows for an easily erected connection which developed a maximum moment of 0.97 M_P for negative bending, and 0.59 M_P for positive bending. These values indicate that the connection can be adapted in a semi-rigid frame resisting gravity or combined gravity and lateral loading. The rotations at the maximum negative moment levels for TPA-1 and TAR-5 were 0.0340 and 0.04042 radians, respectively.

6.4.3 Energy Dissipation

The energy dissipation values calculated for the single cycle experienced by TPA-1, TP-3, and TAR-5 are added, in Fig. 6.6, to the energy dissipation data given in Fig.

6.1. These values are again normalized, and can be seen to be slightly larger than those of TPA-CY2, because there were no other cycles before them. Since the cyclic test results show very little strength degradation between cycles, it could, therefore, be assumed that cyclic tests performed on other connection configurations would also degrade insignificantly.

Comparison of the single cycle values for TPA-1, TP-3, TAR-5 show that the energy dissipation value of the Type A configuration is 14% greater than that for the Type B configuration. This difference can be attributed to the presence of the ATLSS Connector. The Type A configuration energy dissipation value is 43% greater than for the Type C configuration.

6.4.4 ATLSS Connector

An estimation of the contribution of the ATLSS Connection to the moment capacity to the Type A configuration can be made from the comparison of the moment-rotation responses of TPA-1 and TP-3. Lines were fit through what would be the monotonic test response. The difference between the responses for a given rotation is then evaluated (see Fig 6.7). This difference becomes significant after the response deviates from the linear-elastic range. The AC began to contribute to the moment capacity at a rotation of 0.0075 radians, when the applied moment was 0.77 M_p. The contribution reached a maximum of 16% M_p at a rotation of 0.0315 radians, when TPA-1 reached its maximum moment capacity.

6.4.5 Failure Mode

The failure mode for all the tests occurred within the connections. For the tests

in which material composition problems with the AC were not prominent, the failures first occurred in the flange attachments. These failures all occurred within the attachments when they were in tension. The failure modes and maximum strengths of all the tests have been summarized in Table 6.1.

Failure modes of the tests in which the AC failed provided very important information and experience regarding the connections. In test TPA-CY2, when the AC fractured along the mortise weld, it was realized that the bevel along the perimeter of the mortise was not a true 45° angle. The welder was unable to fully insert the rod into the bevel because the connector bevel was somewhat rounded. In test TA-4, the cracking of the weld attaching the mortise to the column revealed that the size of the weld was adequate, but that the composition of the AC contributed to cold-cracking of the weld in the heat affected zone.

These unforeseen failures successfully propelled improvements of the geometry and composition of the AC. The problems encountered during the prior tests were largely eliminated when the experimental HSLA material was used to cast the AC.

6.5 Predicted vs. Experimental

In this section comparisons between the load-deflection and moment-rotation relationships from the finite element analysis and those from the experiments are presented. The experimental data plotted in each case is from the first excursion of negative bending. The yield deformation data from the experimental results are given along with the finite element results in Table 6.2. The experimental moment-rotation plots already excluded the contribution due to the rotations about the center of the

column; therefore, the experimental data did not need to be modified to be compared with the FE results.

The load-deflection comparison of TPA-1, model FFMW, and model ATPA is shown in Fig. 6.8. The initial stiffnesses of the three curves are similar. The experimental data departs from the linear response earlier than the analytical models do. The post-yield stiffness of the test connection is greater than that predicted by either model. Comparison of the yield data from Table 6.2 shows the model ATPA overestimates the yield displacement, Δ_Y, by 9% and the yield load, P_Y, by 15%. The initial tangent stiffnesses from the analytical and experimental results are very similar.

The load-deflection curves of TP-3, model FF, and model ATP are compared in Fig. 6.9. The experimental stiffness is initially greater than the analytical stiffness. Model ATP more accurately predicts the experimental departure from linear response. The post-yield stiffness of the experimental connection is again greater than predicted by either model. Comparison of the yield data from Table 6.2 shows model ATP accurately predicted Δ_Y and underestimates P_Y by 14%. The initial tangent stiffness is underestimated by 10%.

The load-deflection comparison of TAR-5 and model FTWBF is shown in Fig. 6.10. The initial stiffness of the analytical model is again very similar to the experimental results. The experimental response departs from linear response before the analytical prediction does. The post-yield stiffness of the experimental results is greater than predicted by the analytical model. Table 6.2 shows that model FTWBF underestimated Δ_Y by 9% and P_Y by 11%. The initial tangent stiffness of the experimental connection

is over estimated by the analytical model by 16%. This was the only configuration where the experimental strength surpassed the predicted upperbound strength.

The moment-rotation comparison of TPA-1 and model ATPA is shown in Fig. 6.11. Conclusions were difficult to make concerning this comparison because of the erratic response measured during testing. The experimental data deviates from the linear response before the analytical model does, but the post-yield slope is greater. The two lines may converge at greater rotations. The moment-rotation comparison of TP-3 and model ATP is shown in Fig. 6.12. Conclusions were again difficult to make concerning this comparison because of the erratic response measured during testing. However, the model seems to predict the general behavior of the connection adequately.

The comparison of the analytical results ATPA and ATP gives an estimate of the moment carried by the connector of 0.28 M_p. Comparison between tests TPA-1 and TP-3 indicated a contribution of 0.16 M_p (see Fig 6.13). The analytical models predicted the rotation required to engage the AC to carry moment was only 0.0004 radians. On the other hand, the experimentally determined rotation required for the AC to carry moment is 0.0075 radians. The analytical model predicted the AC begins to develop moment earlier than that observed during testing. This is perhaps due to very small gaps in the contact surface between the mortise and the tenon which were not modeled analytically.

CHAPTER 7 - SUMMARY AND CONCLUSIONS

7.1 Summary

A total of five exterior connection tests were performed on cantilever beam-and-column assemblages: a monotonically loaded AC aided fully restrained moment connection; a cyclically loaded AC aided fully restrained moment connection; a monotonically loaded moment connection without a web shear connector; and two monotonically loaded AC aided partially restrained connections. Finite element studies were performed on the test connection configurations to investigate the distribution of forces which are transferred to the column from the beam by the connection. Predictions of the yield displacement, yield load, and initial stiffness of the connections were also obtained from the studies. Comparisons of the experimental results gave an estimation of the moment capacity provided by the AC. The culmination of the analytical and laboratory results formed the basis for the recommendations presented for the enhancement of the present AC design.

7.2 Recommendations with regard to the ATLSS Connector

The performance of the ATLSS Connector in moment connections reflected the well thought out and implemented research plan of the previous studies. The ability to carry shear was well proven, and consistently demonstrated throughout these tests. The ease of erection was also demonstrated. Some difficulties were experienced during testing, however, they were mainly due to the high carbon composition of certain castings as discussed previously.

The material properties of the A27 cast connectors exhibited good strength and

weldability. The A148 material used to replace the A27 exhibited increased yield strength. However, this additional strength could not be realized due to welding problems resulting from the material composition. The experimental HSLA castings showed good weldability as well as increased strength.

The bevel located around the perimeter of the mortise should be removed. The additional weld throat it provides was not needed to carry the specified loads. The bevels were not cast with a uniform 45° angle, making insertion of the welding rod difficult. A fillet weld with the same design strength could be applied with more ease and provide the required strength. Also, the overall approach to the welding of the mortise to the column should be simplified. In the laboratory, the mortise took approximately three hours to weld in place. This was due in part to the bevel and also the geometry of the connector perimeter. The flutes located on either side arm of mortise created a difficult situation for the welder to push the slag ahead of the weld. The weld pass must be stopped and the weld cleaned. The bead must be resumed again and stopped when the bead was forced to be cleaned again. Casting of a square back plate to the present AC geometry is a possible solution. This would make the welding easier, but will increase the weight of the connection. A geometry which combined the pair of flutes into a single flute per side would enable continuous passes for the welder and speed the welding process.

The finite element analysis results from the upper bound models suggest that the maximum restraint that can be achieved in a web attached connector is between 9 and 22%. The experimental value of 16% is consistent with the analytical findings. However, the rotation at which the ATLSS Connector begins to develop moment

resistance is much less for the analytical models. Therefore, to increase the percentage of moment carried by the AC in the elastic range, the rotation value at which the moment resistance begins would need to be lowered. This could possibly be attained by improvements on the quality of the contact surfaces between the tenon and the mortise.

7.3 Overall Conclusions

The tests performed on the full moment Type A connections showed that they relied heavily on the AC to carry shear throughout the test. The AC moment capacity was realized during the post-yielding response when larger rotations were experienced. The Type C moment connection configuration displayed very promising results for economical construction because the single connector carried the shear and also developed positive bending moment. The following conclusions can be made regarding the ATLSS Connections studied:

1. The Type A connection configuration achieved 1.11 M_P in negative bending and 1.12 M_P in positive bending.

2. The Type B connection configuration achieved 1.05 M_P in negative bending and 0.80 M_P in positive bending.

3. The Type C connection configuration achieved 0.97 M_P in negative bending and 0.59 M_P in positive bending.

4. ATLSS Connector contributes up to 16% of the moment capacity in a full moment connection, while acting as a mid-web shear attachment.

5. Finite element models for the detailed connection offer analytical predictions of Δ_Y, P_Y, and initial stiffness, which are comparable to those obtained from the tests.

6. The spring model for the ATLSS Connector can be used as an initial approximation for predicting its effect on a connection.

7. The Type C connection has shown the feasibility of employing a shear

connector which can also resist substantial positive bending moment and simplify beam-to-column erection.

8. The material composition of the experimental HSLA provides good strength and weldability.

9. Improvements on the moment resistance of the AC should be in reduction of the rotation required to develop its maximum response.

10. The AC design improvements should eliminate the bevel and also create a simpler weld pattern around the perimeter of the mortise.

7.4 Future Research

The following recommendations on future research in the area of moment connections utilizing the ATLSS Connector anticipate the aforementioned design improvements on the AC.

The results from TAR-5 warrant further investigation of the connection within a frame configuration. Before implementation of a frame test, additional studies on the Type C connection should be performed. Cantilever cyclic tests, to study connection energy dissipation and cruciform tests, to assess the behavior of interior beam-to-column connections are recommended.

Finite element models for assessing the contribution of the AC should be developed to a greater degree, possibly a comprehensive study to determine the parameters for creation of a 'super element'. This super element would comprise the necessary stress-strain behavior and necessary degrees of freedom for the AC. It would be attached between the beam web and column face much like a spring element. The ANSYS program has the capability for performing this type of analysis.

REFERENCES

AISC, LOAD AND RESISTANCE FACTOR DESIGN MANUAL, (1986). First Edition, American Institute of Steel Construction, Chicago, Illinois.

AISC, MANUAL OF STEEL CONSTRUCTION VOLUME II CONNECTIONS, (1992). American Institute of Steel Construction, Chicago, Illinois.

ASCE, (1988). STANDARD MINIMUM DESIGN LOADS FOR BUILDINGS AND OTHER STRUCTURES, American Society of Civil Engineers, New York, New York.

ATLSS, (1990). SIXTH YEAR RENEWAL PROPOSAL TO THE NATIONAL SCIENCE FOUNDATION, Volume 1: Programs, Plans, and Budgets, Center For Advanced Technology for Large Structural Systems, Lehigh University., Bethlehem PA.

ATLSS, (1990). SIXTH YEAR RENEWAL PROPOSAL TO THE NATIONAL SCIENCE FOUNDATION, Volume 2: Projects, Publications, and Biosketches, Center For Advanced Technology for Large Structural Systems, Lehigh University., Bethlehem PA.

AWS, STRUCTURAL WELDING CODE, (1990). D1.1 American Welding Society, Appendix XI, p. 282.

Blodgett, O.W., (1991). DESIGN OF WELDED STRUCTURES,The James F. Lincoln Arc Welding Foundation, Section 5.1.

BOCA, NATIONAL BUILDING CODE (1990). Eleventh Edition, Building Officials & Code Administration International, Inc.

Davis, H.E., Troxell, G.E., and Hauck G.F.W., (1986). THE TESTING OF ENGINEERING MATERIALS. Fourth Edition, McGraw Hill Inc.

DeSalvo, G.J., and Gorman, R.W., (1989). ANSYS ENGINEERING ANALYSIS SYSTEM USER'S MANUAL (Version 4.4), Volume I and II, Swanson Analysis Systems, Inc.

Fleischman, R.B., Viscomi, B.V., and Lu, L.W., (1991). ATLSS CONNECTIONS: CONCEPT, DEVELOPMENT, AND EXPERIMENTAL INVESTIGATION. Proceedings of the Ninth Structures Congress, ASCE, Indianapolis, IN, pp. 426-429.

Fleischman, R.B., Viscomi, B.V., and Lu, L.W., (1993). DEVELOPMENT, ANALYSIS, EXPERIMENTATION, AND IMPLEMENTATION OF ATLSS CONNECTIONS FOR AUTOMATED CONSTRUCTION. 1993 National Steel Construction Conference, AISC, Orlando, Fl., pp. 16-1 - 16-20.

Kaczinski, M.R., Viscomi, B.V., Lu, L.W., and Fleischman, R.B., (1992). AN APPROACH TO INTEGRATED BUILDING SYSTEMS. Proceedings of the Tenth Structures Congress, ASCE, San Antonio, TX, pp. 709-712.

NEHRP, (1991). RECOMMENDED PROVISIONS FOR THE DEVELOPMENT OF SEISMIC REGULATIONS FOR NEW BUILDINGS, Building Seismic Safety Council, Washington, D.C.

Plumier, I.A., (1983). RECOMMENDED TESTING PROCEDURE FOR EVALUATING EARTHQUAKE RESISTANCE OF STRUCTURAL ELEMENTS. European Convention for Construction Steelwork, Technical Committee 13, Brussels, Belgium.

Popov, E.P., and Pinkney, R.B., (1967). BEHAVIOR OF STEEL BUILDING CONNECTIONS SUBJECTED TO REPEATED INELASTIC STRAIN REVERSAL. SESM 67-30, University of California, Berkeley. Report to AISI Earthquake Performance of Steel Members and Connections.

Popov, E.P., and Pinkney, R.B., (1967). BEHAVIOR OF STEEL BUILDING CONNECTIONS SUBJECTED TO REPEATED INELASTIC STRAIN REVERSAL - EXPERIMENTAL DATA. SESM 67-31, University of California, Berkeley. Report to AISI Earthquake Performance of Steel Members and Connections.

Rosa, A.M., (1993). DESIGN, ANALYSIS, AND EXPERIMENTATION OF A SEMI-RIGID COMPOSITE JOINT USING THE ATLSS SHEAR CONNECTION, Masters Thesis, Lehigh University.

Wakabayashi, M., (1986). DESIGN OF EARTHQUAKE RESISTANT BUILDINGS. McGraw Hill Inc.

TABLES

Table 1.1 - AISC Connection Categories (Blodgett, 91)

AISC Connection	Restraint (R)*	Connection Alias
Type 1	above approx. 90%	Rigid
Type 2	below approx. 20%	Simple
Type 3	approx. 20% to 90%	Semi-Rigid

* Restraint (R) is the ratio of moment capacity developed at a connection to plastic moment of the adjoining beam section.

Table 3.1 - LVDT Location Descriptions

LVDT	REFERENCE	DISPLACEMENT
1	Floor	Beam end at load point
2	Floor	Bottom beam end near connection
3	Beam	Bolt slip
4	Beam	Total plate elongation
5	Column	Mortise arm opening
6	Column	Tenon longitudinal
7	Column	Tenon vertical
8	Column	Tee stub bolt elongation
9	Column	Tee stub bending
10	Beam	Tee stub total elongation
11	Column	Top beam end near connection

Table 3.2 - Rolled Section Material Properties

MATERIAL	LOCATION	% ELONG.	YIELD STRESS (ksi)	TENSILE STRENGTH (ksi)
W12X22	Flange	21.8	52.8	75.7
Test #'s 1 thru 4	Web	21.9	55.7	77.5
W12X22	Flange	27.5	48.6	75.4
Test #5	Web	24.5	52.9	77.4
W30X99	Flange	29.9	51.4	69.5
Used for Tee stub	Web	20.4	55.1	72.3
PLATE	Longitudinal	36.9	49.5	73.1

Table 3.3 - ATLSS Connector Material Properties

TEST	CONNECTION MATERIAL ASTM Spec.	YIELD STRESS (ksi)	TENSILE STRENGTH (ksi)	% ELONG.	C_{eq}* (%)
#1	A27 Gr.70-36	38.9	76.8	32.3	.59
#2	A148 Gr.80-50	61.9	93.9	25.5	.67
#4	A148 Gr. 80-50	61.9	93.9	25.5	.67
#5	Exp. HSLA**	53.6	88	13.9	.32

*Carbon Equivalent from $C_{eq} = C + Mn/6 + (Cr+Mo+V)/5 + (Ni+Cu)/15$

**Based on preliminary castings, subsequent castings showed much improved ductility.

Table 3.4 - Experimental Program Summary

TEST NAME	DATE	JOINT TYPE	LOADING
TPA-1	8-19-92	A	Large Amplitude
TPA-CY2	9-3-92	A	Cyclic
TP-3	12-01-92	B	Large Amplitude
TA-4	12-08-92	C	Large Amplitude
TAR-5	03-11-93	C	Large Amplitude

Table 4.1 - Elastic Beam Force Distribution - Simplified Models

FEM RUN ID	MOMENT		SHEAR		Restraint
	Flange	Web	Flange	Web	(R)
FTOT	84%	16%	24%	76%	91%
FFMW	95	5	53	47	85
FF	100	0	100	0	73
FTFBW	63	37	36	64	38

Table 4.2 - Plastic Beam Force Distribution at Four Times Yield Deflection - Simplified Models

FEM RUN ID	MOMENT		SHEAR		Restraint (R)
	Flange	Web	Flange	Web	
FTOT	78%	22%	32%	68%	115%
FFMW	91	9	57	43	105
FF	100	0	100	0	94
FTFBW	50	50	48	52	67

Table 4.3 - Elastic Deformation Behavior - Finite Element Models

FEM RUN ID	Yield Displ. (in.)	Load at Yield (kip)	Initial Stiffness (kip/in)
FTOT	0.29	47.0	162
FFMW	0.26	41.7	160
FF	0.24	37.8	158
FTFBW	0.21	24.0	114
ATP	0.18	27.0	150
ATPA	0.23	39.0	169

Table 5.1 - TPA-1 Connection Response Characteristics

REFERENCE (load direction)	**Displacement (in.)**	**Load (kip)**	**% M_P**	**Rotation (radians)**
Yield (-)	0.207	34.0	0.77	-
1st Reversal (-)	0.979	44.2	0.99	0.0184
2nd Reversal (+)	0.961	49.6	1.11	0.0209
Maximum (-)	1.482	52.2	1.17	0.0340
Failure (-)	1.711	47.4	1.07	0.0413
Maximum (+)	-	53.1	1.19	-
Failure (+)	-	46.2	1.04	-

NOTES: (-) Negative Bending (+) Positive bending

Table 5.2 - Experimental Energy and Ductility Values

TEST	W_E (in-kip)	E (in-kip / in-kip)	Cumul. W_E (in-kip)	Δ (in)	π_d (in/in)	μ or μ_C * (in/in)
#1	91.2	25.9	-	1.39	6.71	8.3
#2 cycle 1	0.16	0.045	0.16	0.009	0.043	-
2	0.15	0.043	0.31	0.007	0.034	-
3	0.18	0.051	0.49	0.013	0.060	-
4	0.50	0.142	0.99	0.021	0.101	-
5	0.38	0.108	1.37	0.017	0.082	-
6	0.42	0.119	1.79	0.020	0.097	-
7	2.54	0.722	4.33	0.067	0.324	-
8	2.44	0.693	6.77	0.065	0.314	-
9	2.54	0.722	9.31	0.069	0.333	-
10	6.72	1.90	16.0	0.164	0.792	-
11	6.93	1.97	23.0	0.164	0.792	-
12	7.10	2.02	30.1	0.167	0.807	-
13	32.19	9.15	62.3	0.603	2.91	-
14	27.50	7.81	89.8	0.575	2.78	-
15	26.95	7.66	117	0.575	2.78	-
16	61.77	17.6	178	1.09	5.27	-
17	57.75	16.4	236	1.10	5.30	-
18	99.64	28.3	336	1.73	8.35	-
19	91.06	25.9	427	1.73	8.35	82.2
#3	65.1	22.8	-	1.10	6.06	12.7
#5	44.5	14.7	-	1.26	5.6	8.9

*Tests #1, 3, and 5, μ is defined by Eq. 5.2. Test #2 μ_C is defined by Eq. 5.3.

Table 5.3 - TP-3 Connection Response Characteristics

REFERENCE (load direction)	**Displacement (in.)**	**Load (kip)**	**% M_P**	**Rotation (radians)**
Yield (-)	0.181	31.5	0.71	-
1st Reversal (-)	0.798	39.9	0.90	0.0167
2nd Reversal (+)	0.791	40.0	0.90	0.0194
Maximum (-)	1.944	46.4	1.05	0.0393
Failure (-)	2.330	28.9	0.65	0.0522
Maximum (+)	-	35.7	0.80	-
Failure (+)	-	35.7	0.80	-

NOTES: (-) Negative Bending (+) Positive bending

Table 5.4 - TAR-5 Connection Response Characteristics

REFERENCE (load direction)	**Displacement (in.)**	**Load (kip)**	**% M_P**	**Rotation (radians)**
Yield (-)	0.225	27.0	0.65	-
1st Reversal (-)	0.520	29.6	0.71	0.0112
2nd Reversal (+)	0.998	24.6	0.59	0.0250
Maximum (-)	1.625	40.6	0.97	0.0402
Failure (-)	1.995	28.7	0.69	0.0495
Maximum (+)	-	24.6	0.59	-
Failure (+)	-	24.6	0.59	-

NOTES: (-) Negative Bending (+) Positive bending

Table 6.1 - Connection Strength and Failure Mode

	Negative Bending		Positive Bending	
TEST	**FAILURE MODE**	**Maximum M / M_p**	**FAILURE MODE**	**Maximum M / M_p**
#1	Tee Stub	1.17	Plate	1.19
#2	Mortise Weld	1.05	Mortise / Plate	1.05
#3	Tee Stub	1.05	Plate	0.80
#4	Tee Stub	1.06	Mortise Weld	0.34
#5	Tee Stub	0.97	Tenon	0.59

Table 6.2 - Yield Deformation Behavior - Comparison of Finite Element Models with Experimental Results

Connection	FEM / EXP Name	Yield Displ. (in.)	Load at Yield (kip)	Initial Stiffness (kip/in)
Type A	TPA-1	0.21	34.0	170
	FFMW	0.26	41.7	160
	ATPA	0.23	39.0	169
Type B	TP-3	0.18	31.5	171
	FF	0.24	37.8	158
	ATP	0.18	27.0	150
Type C	TAR-5	0.23	27.0	98
	FTFBW	0.21	24.0	114

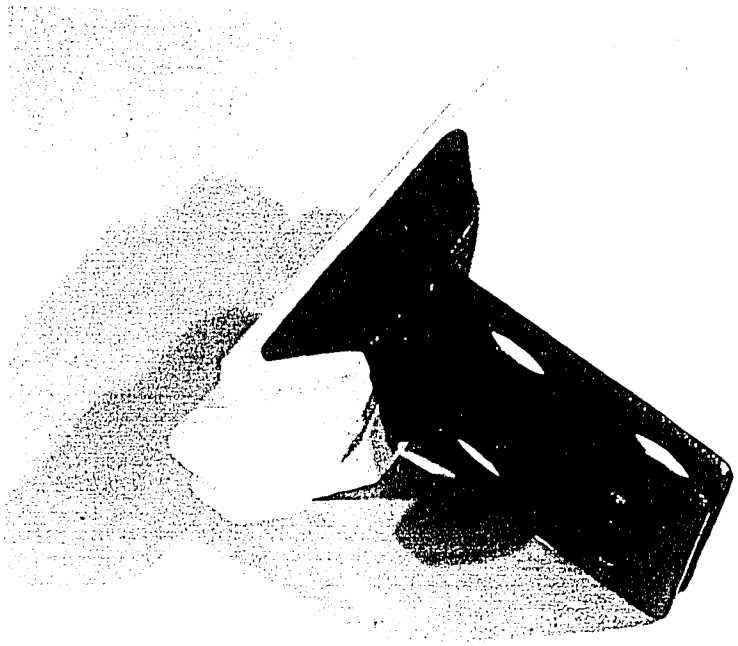

a) Phase II Design

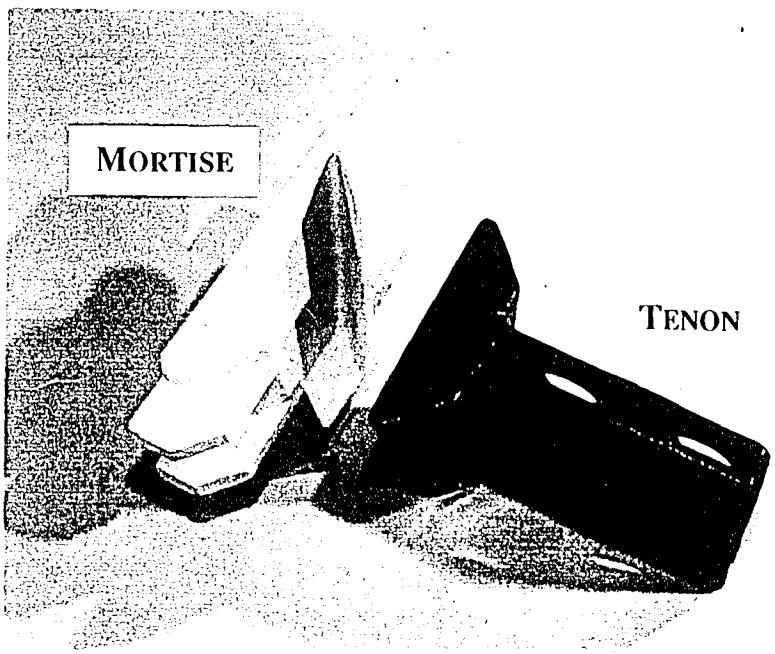

b) AC Components

Figure 1.1 ATLSS Connector

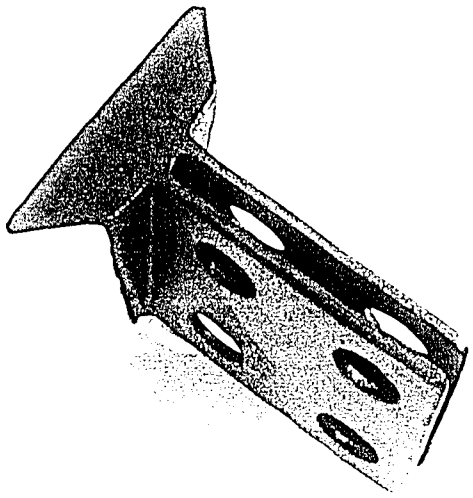

a) Phase II Design

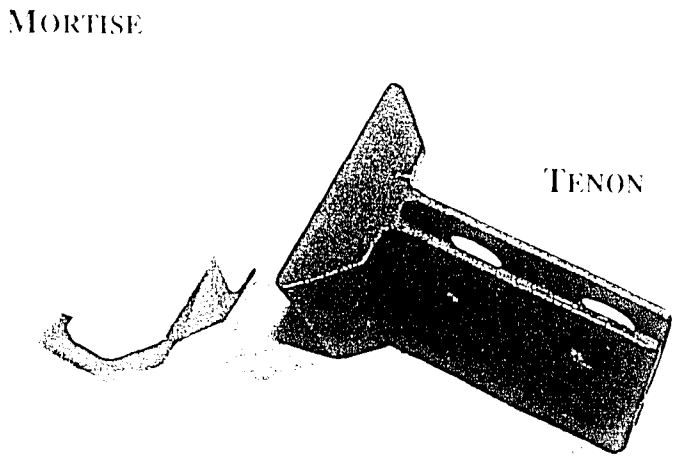

b) AC Component

Figure 1.1 ATLSS Connector

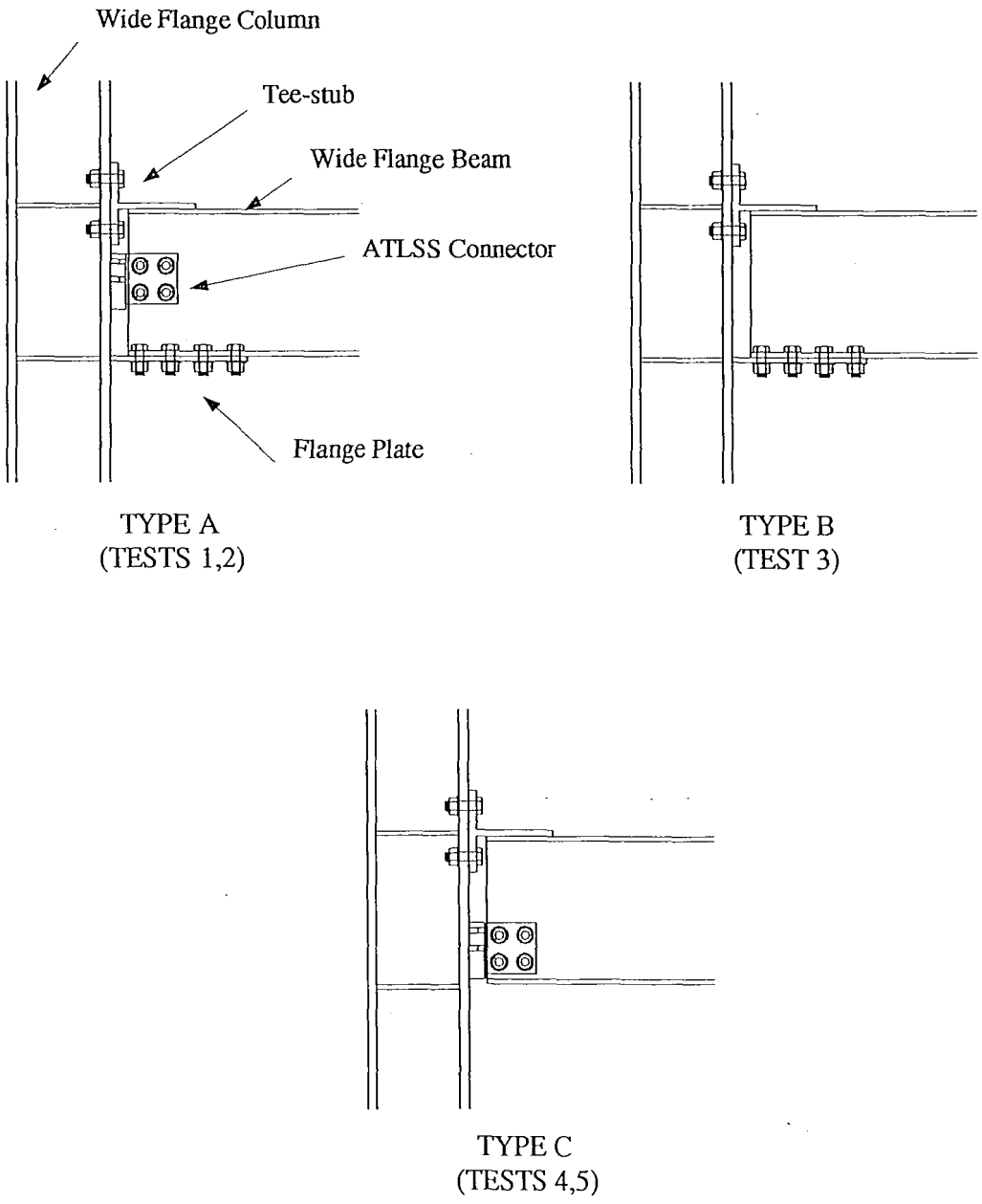

Figure 1.2 Connection Types Studied

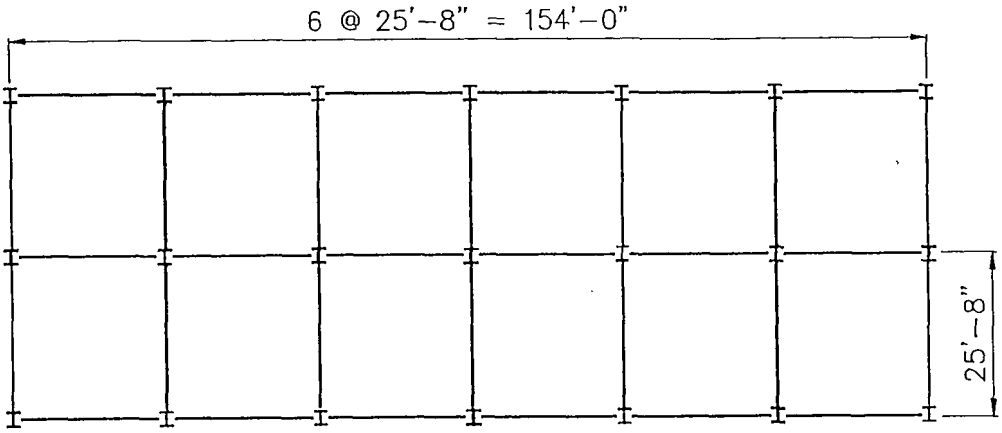

a) Plan View

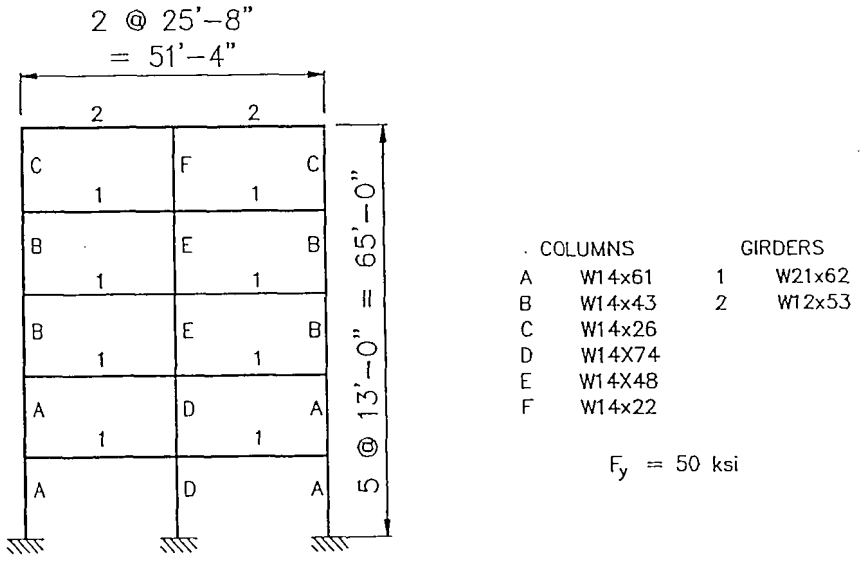

b) Elevation View and Member Schedule

Figure 2.1 Prototype 5-Story Frame

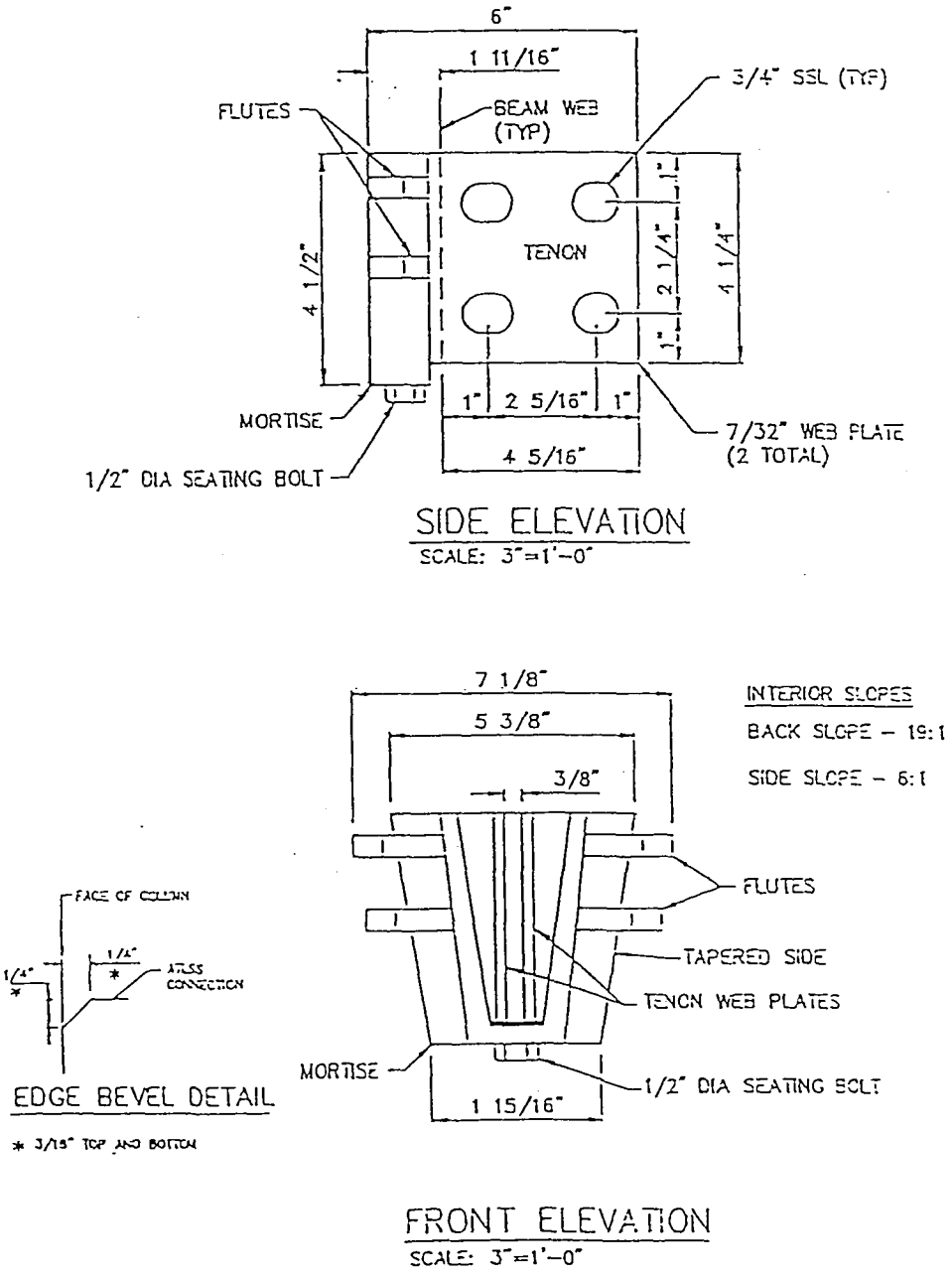

Figure 2.2 ATLSS Connector Detail (Rosa, 93)

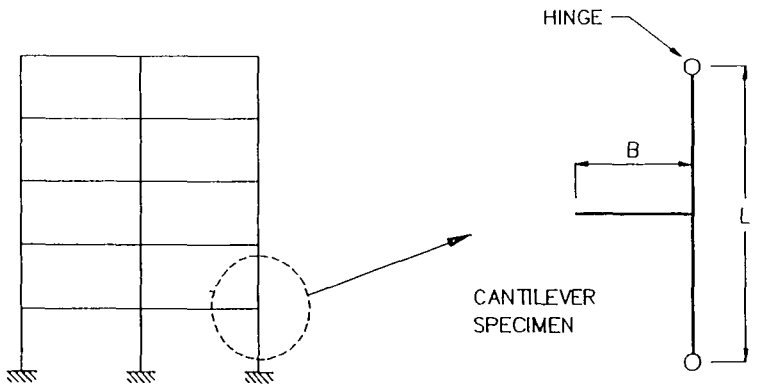

STORY HEIGHT = 13'
BAYS = 2@ 25' -8"
SCALE FACTOR = 0.58

	A	B
PROTOTYPE	156"	65"
SPECIMEN	91.2"	38"

Figure 3.1 Scale Factor of Model

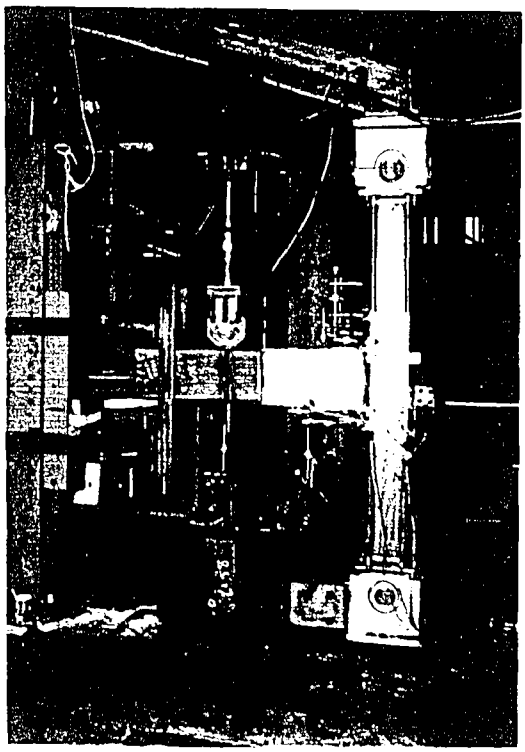

Figure 3.2 Typical Test Specimen

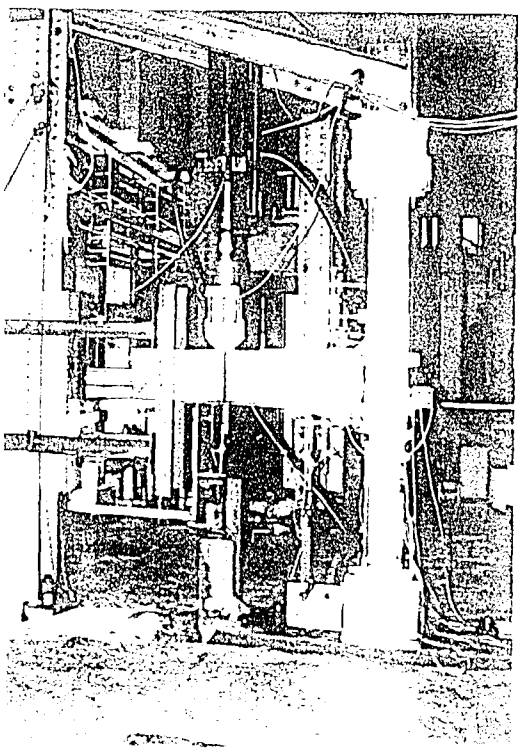

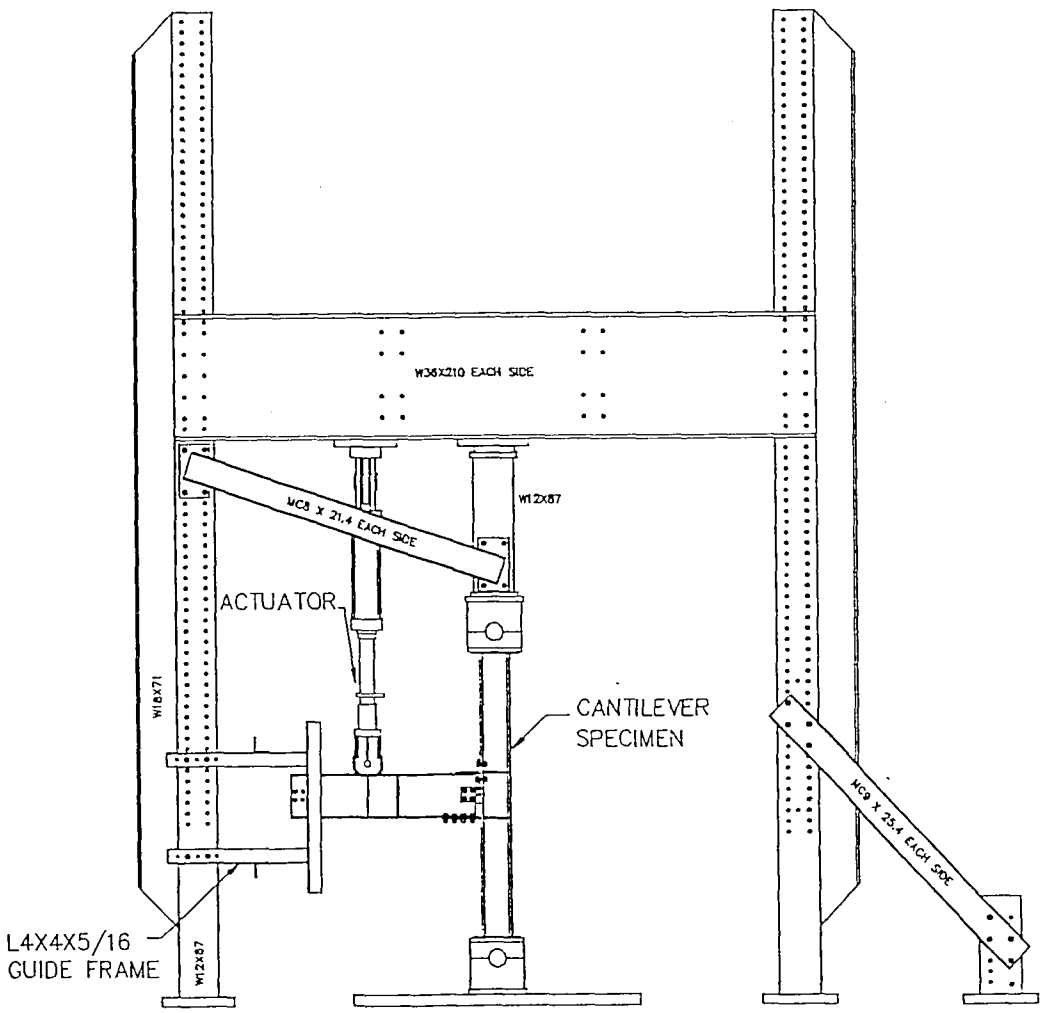

Figure 3.3 Testing Frame & Specimen

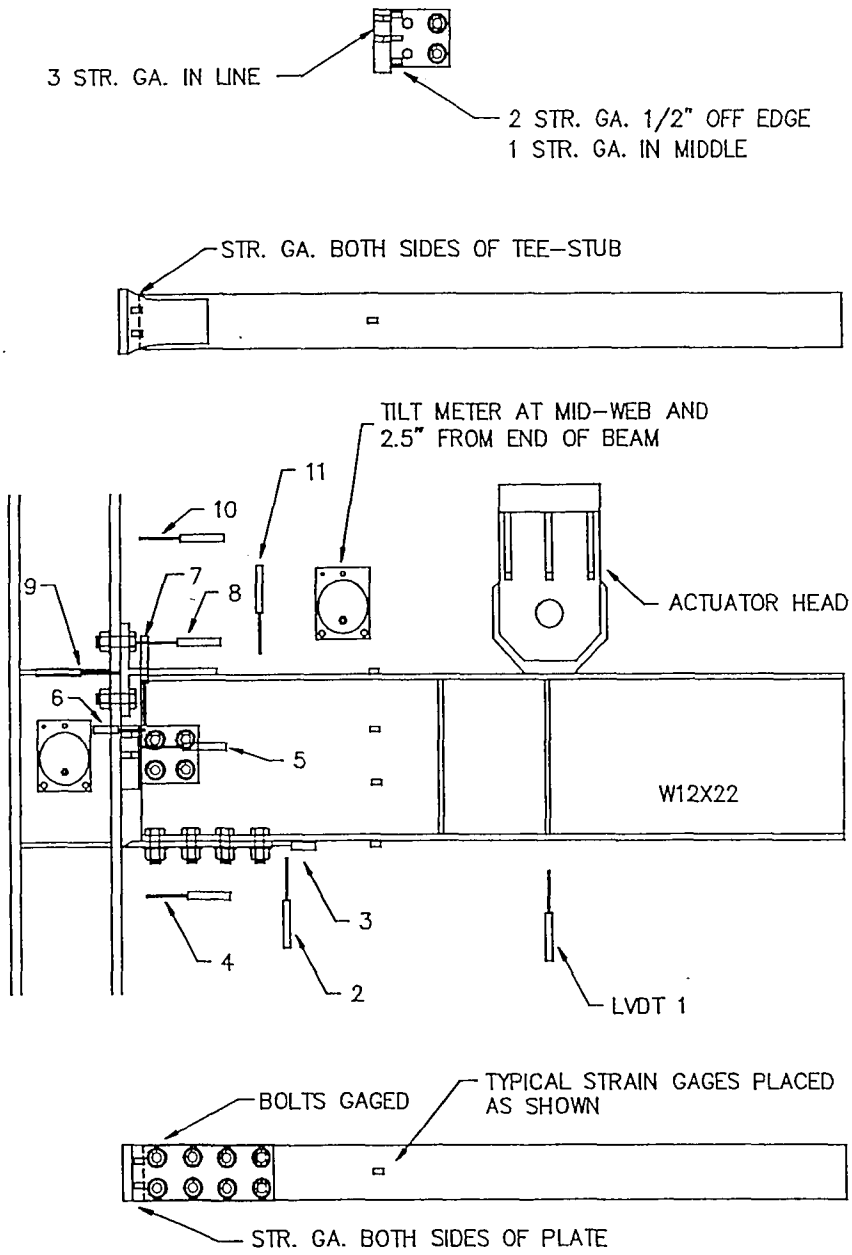

NOTES:
1. TEE–STUB BOLTS ALSO GAGED
2. REFER TO TABLE 3.1 FOR LVDT LOCATION DESCRIPTIONS

Figure 3.4 Typical Instrumentation Detail

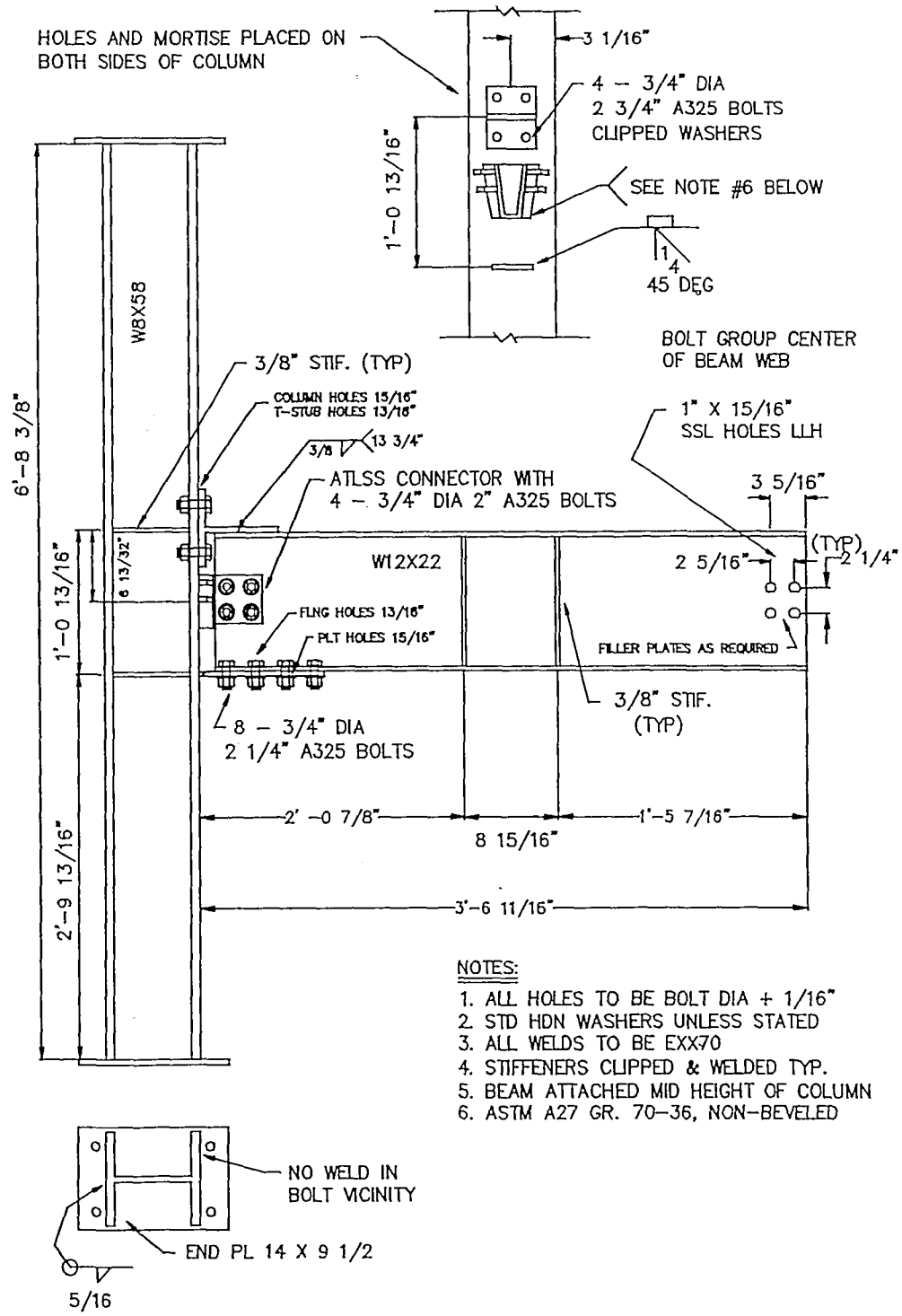

Figure 3.5 Type-A Connection Detail

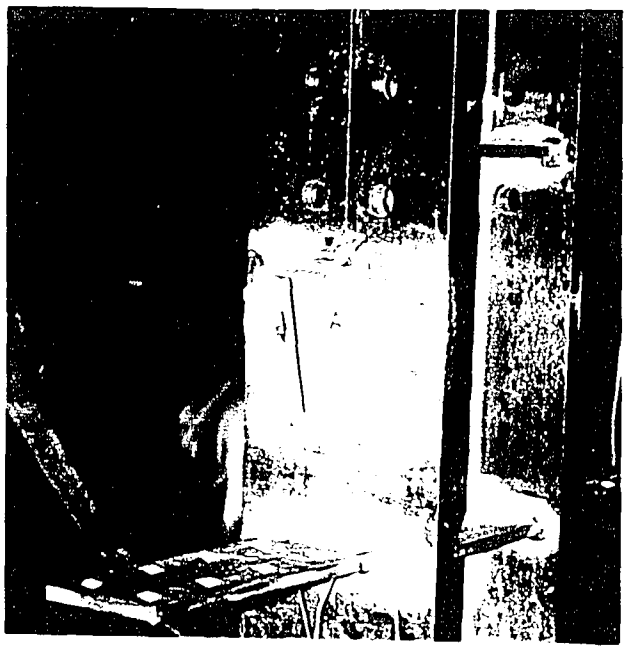

Figure 3.6 ATLSS Connector Mortise and Flange Plate Welded to Column

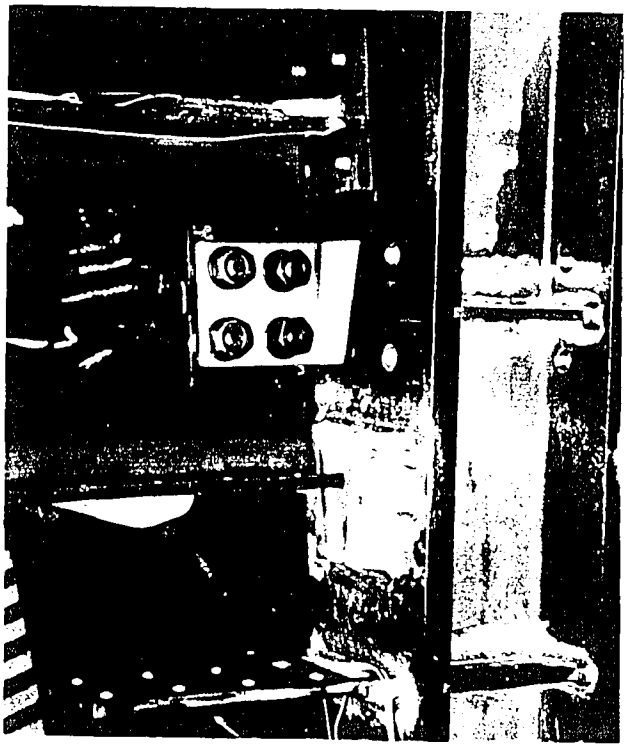

Figure 3.7 ATLSS Connector Tenon and Tee-stub During Erection

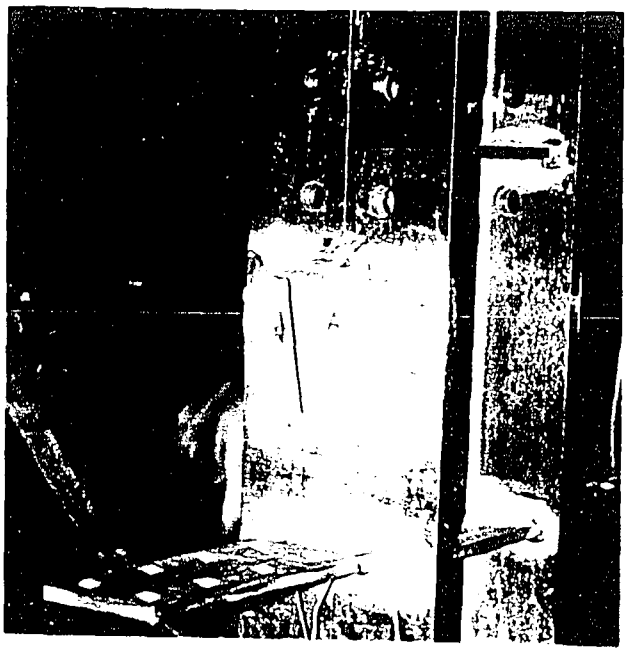

Figure 3.6 ATLSS Connector Mortise and Flange Plate Welded to Column

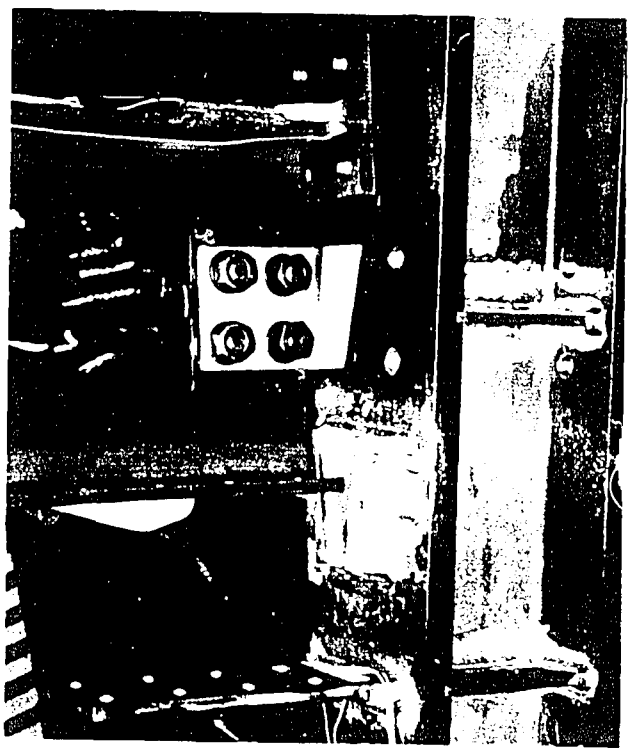

Figure 3.7 ATLSS Connector Tenon and Tee-stub During Erection

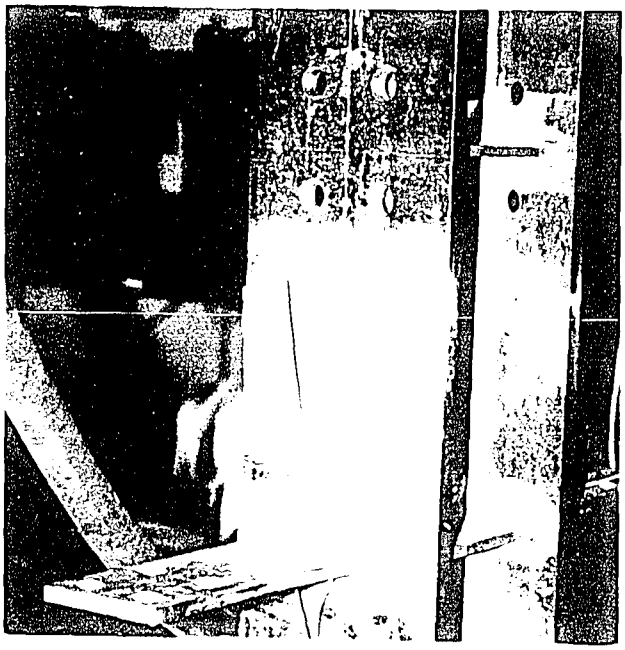

Figure 3.6 ATLSS Connector Mortise and Flange Plate Welded to Column

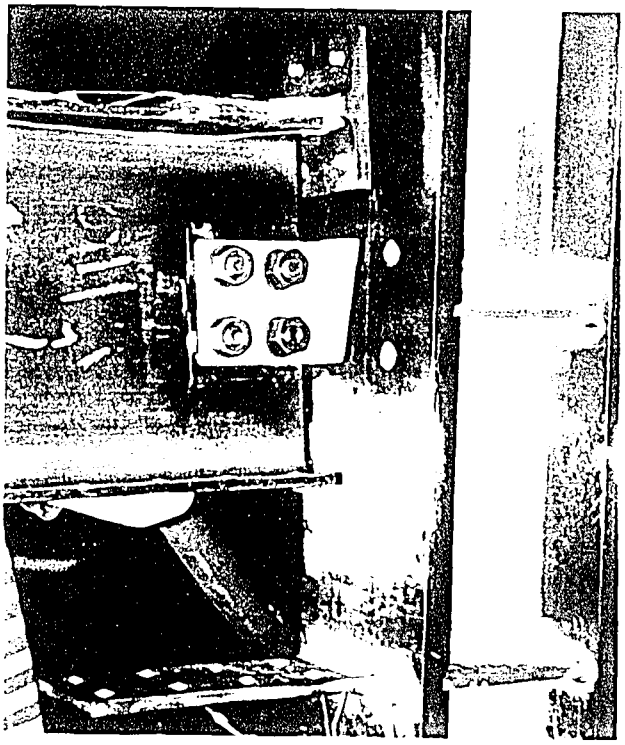

Figure 3.7 ATLSS Connector Tenon and Tee-stub During Erection

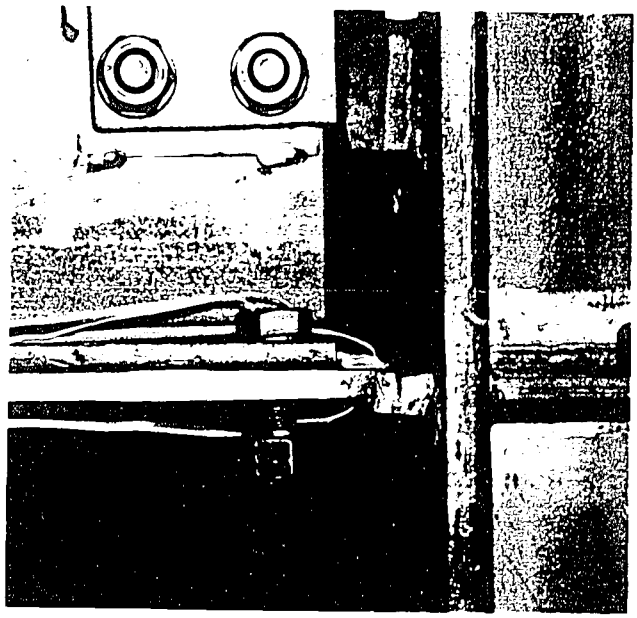

Figure 3.8 Flange Bolts Placed to Seat AC

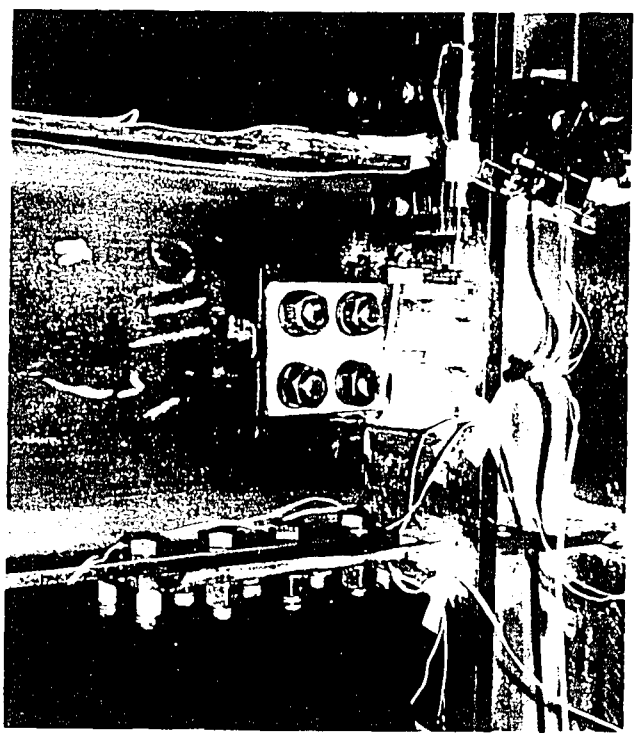

Figure 3.9 Completed Type-A Connection (TPA-1)

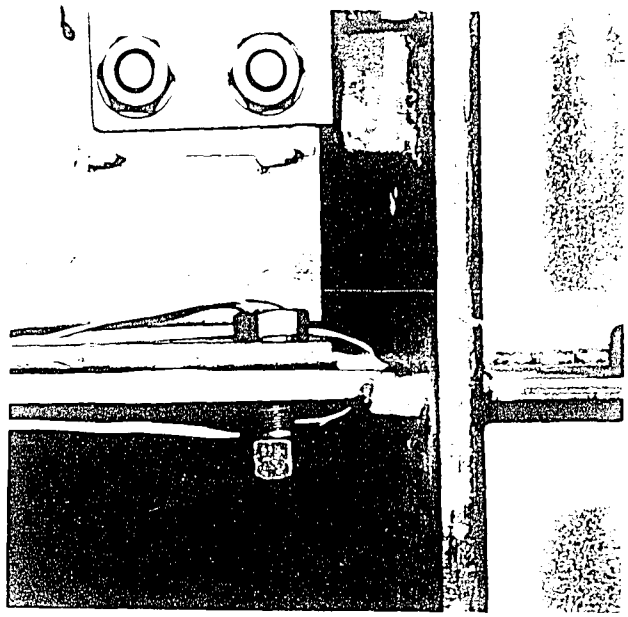

Figure 3.8 Flange Bolts Placed to Seat AC

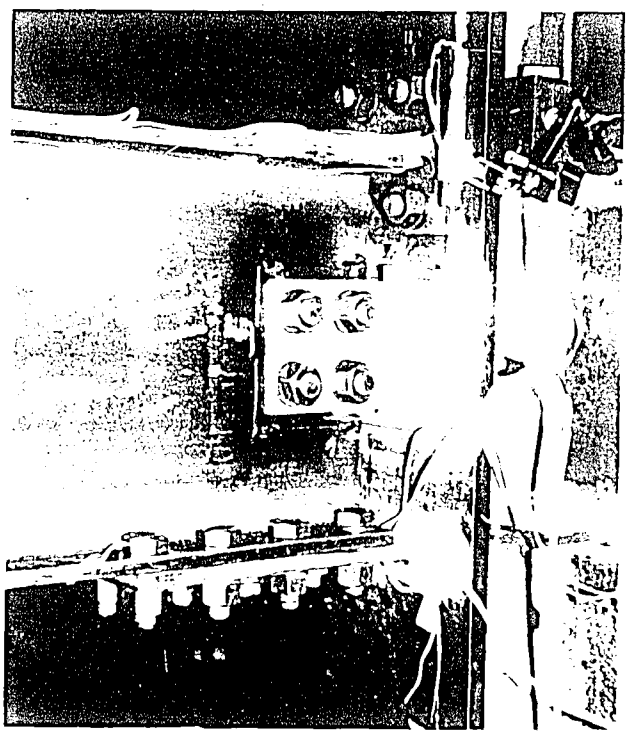

Figure 3.9 Completed Type-A Connection (TPA-1)

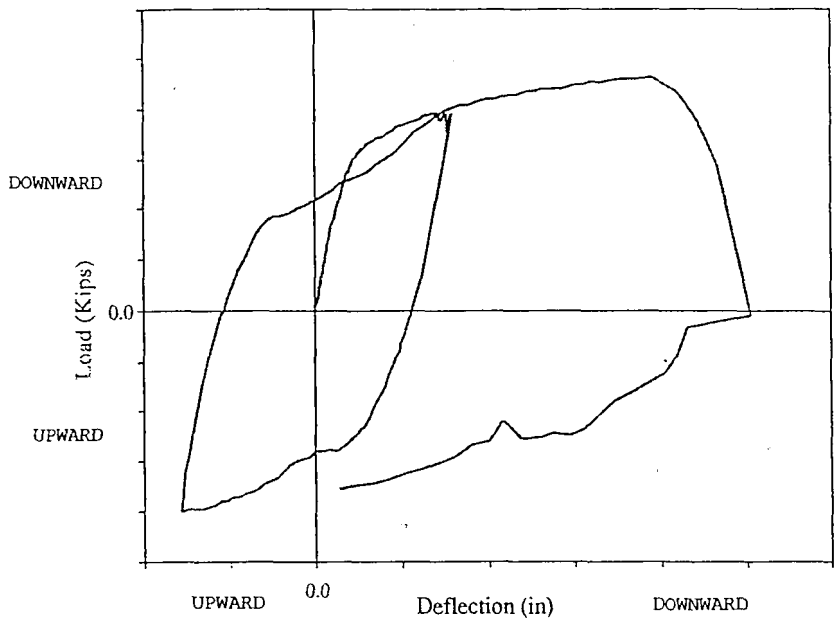

Figure 3.10 Typical Loading Sequence (TP-3)

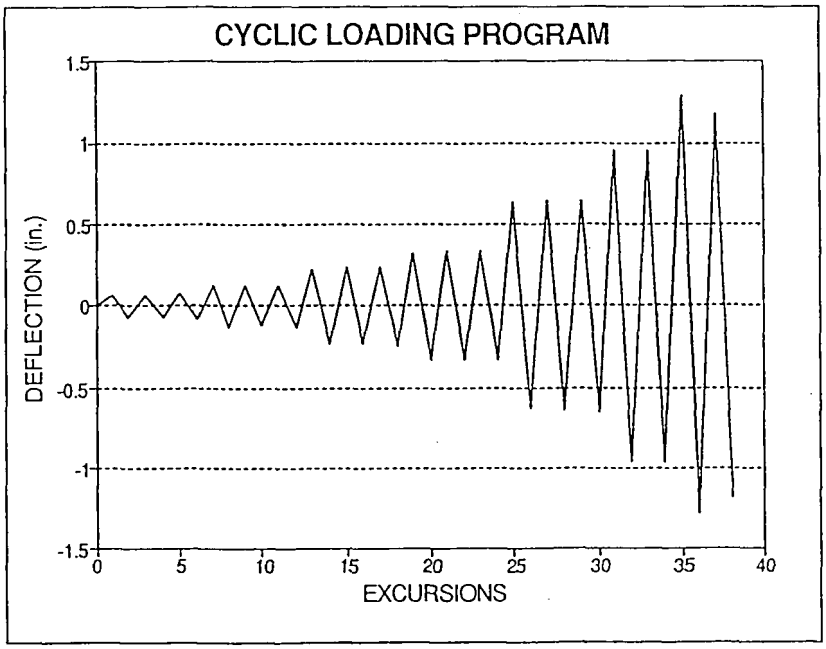

Figure 3.11 Cyclic Loading Program (TPA-CY2)

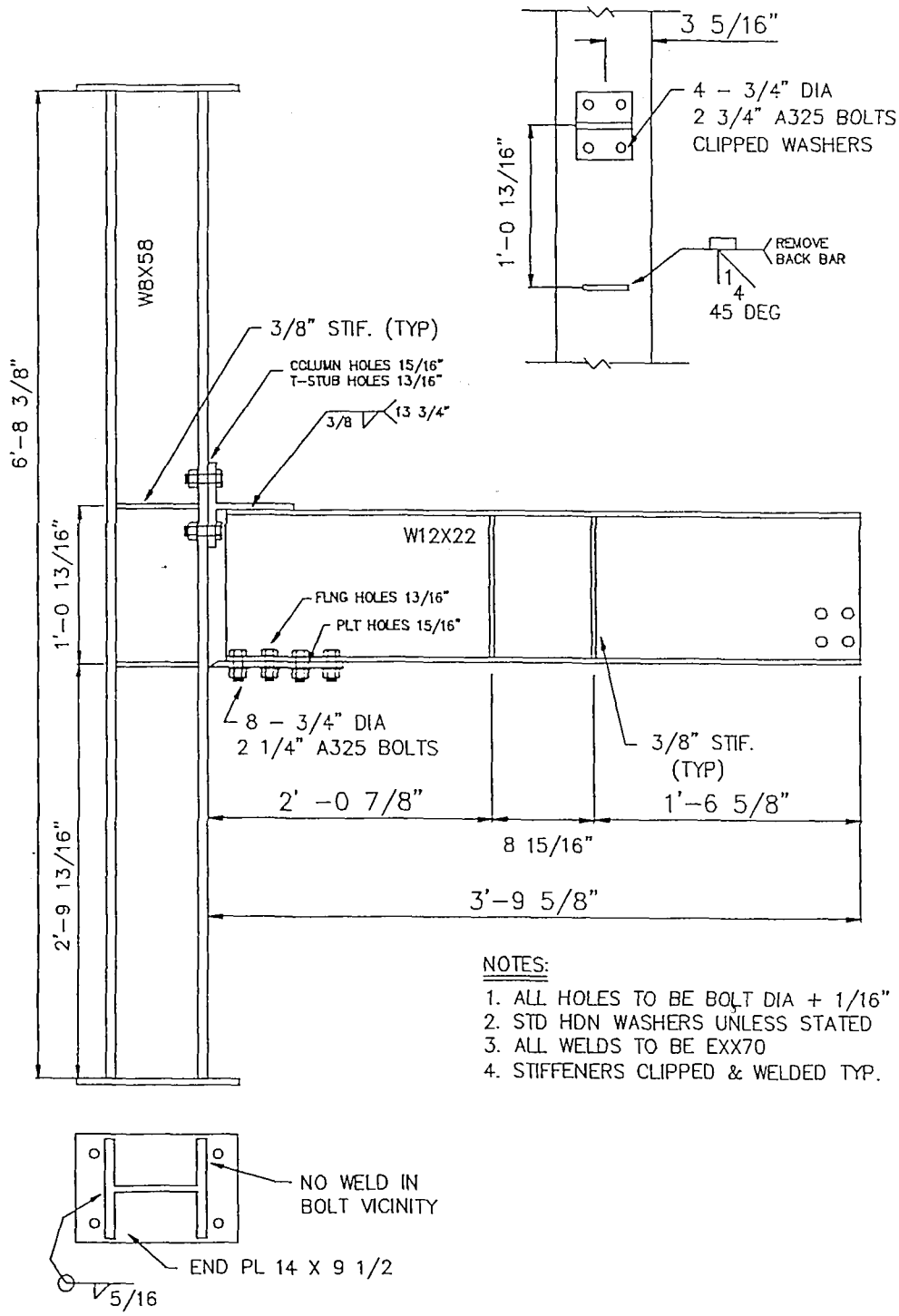

Figure 3.12 Type-B Connection Detail (TP-3)

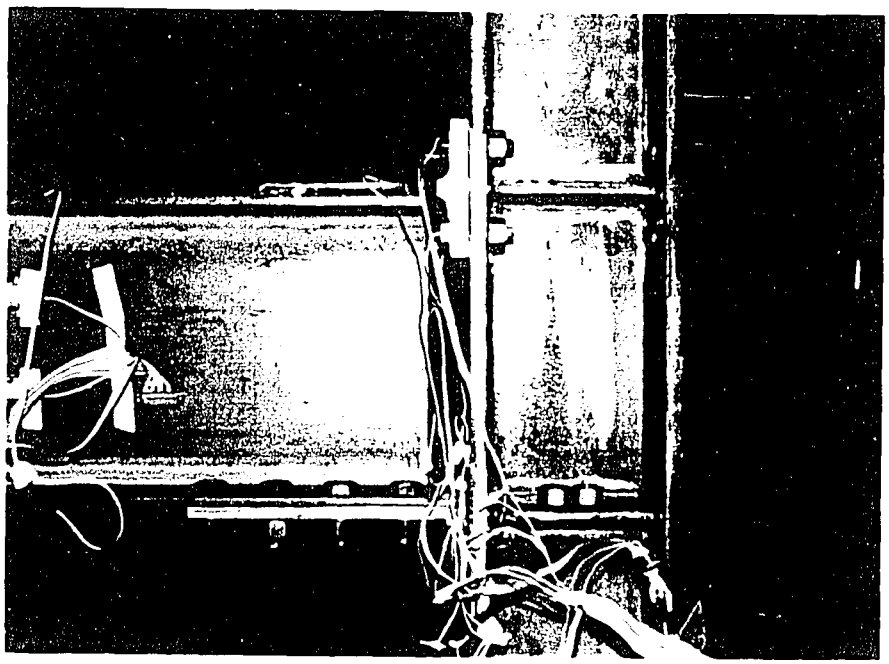

Figure 3.13 Completed Type-B Connection (TP-3)

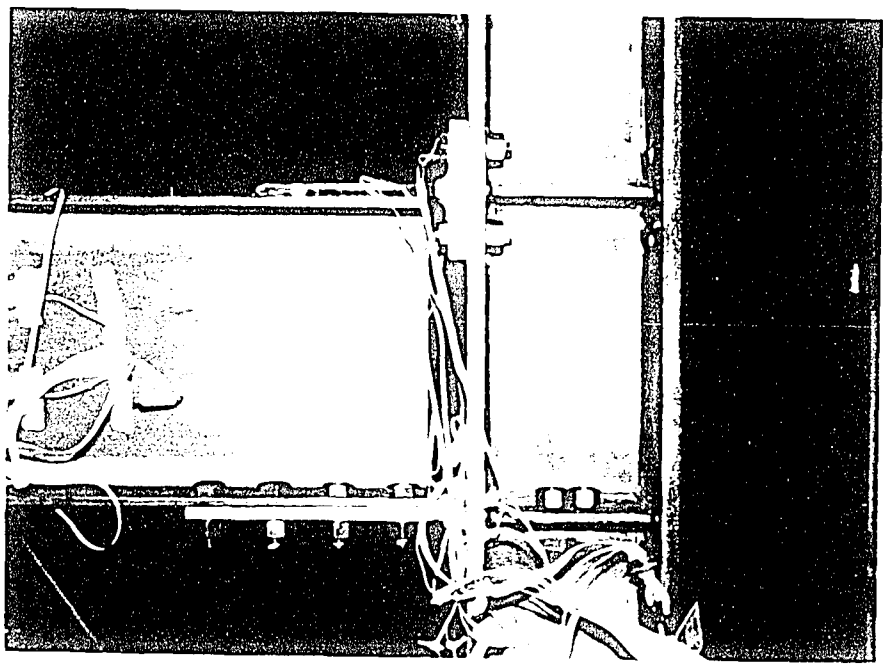

Figure 3.13 Completed Type-B Connection (TP 3)

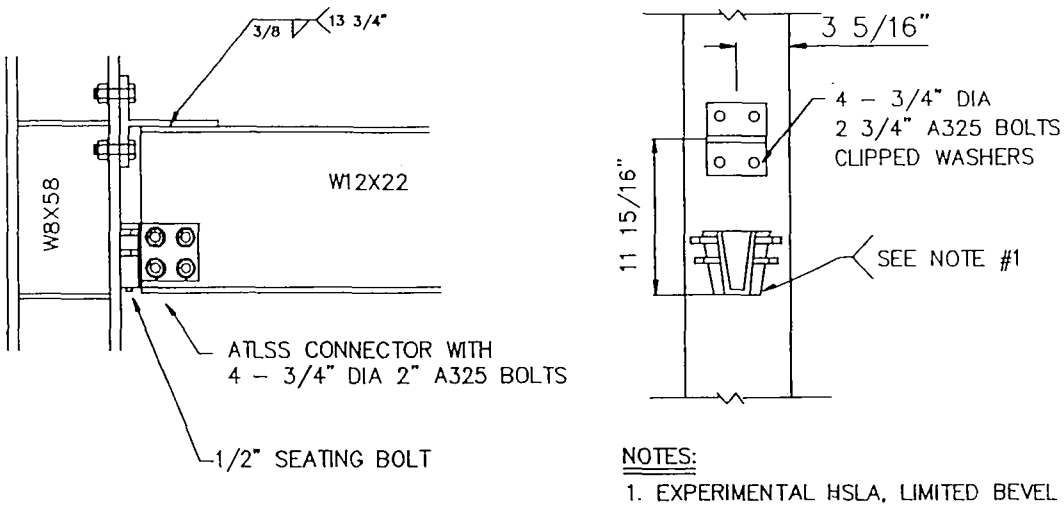

Figure 3.14 Type-C Connection Detail (TAR-5)

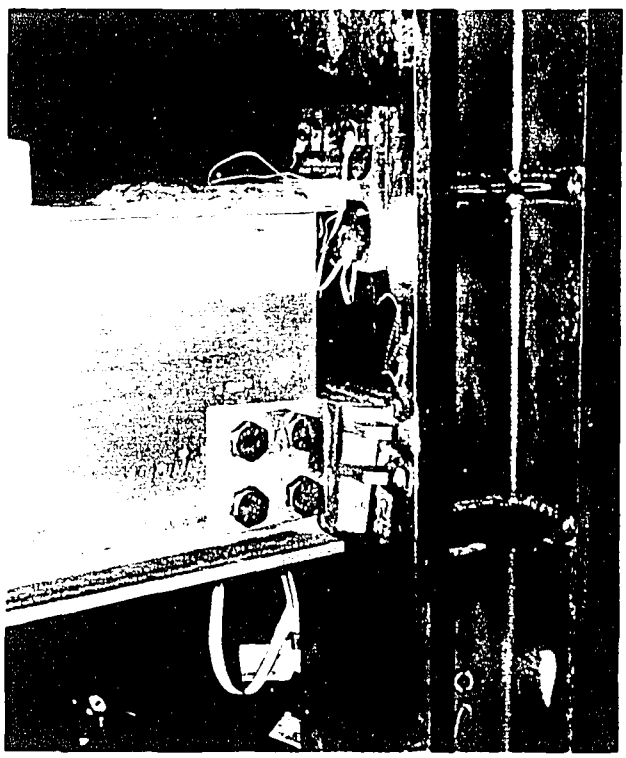

Figure 3.15 Completed Type-C Connection (TAR-5)

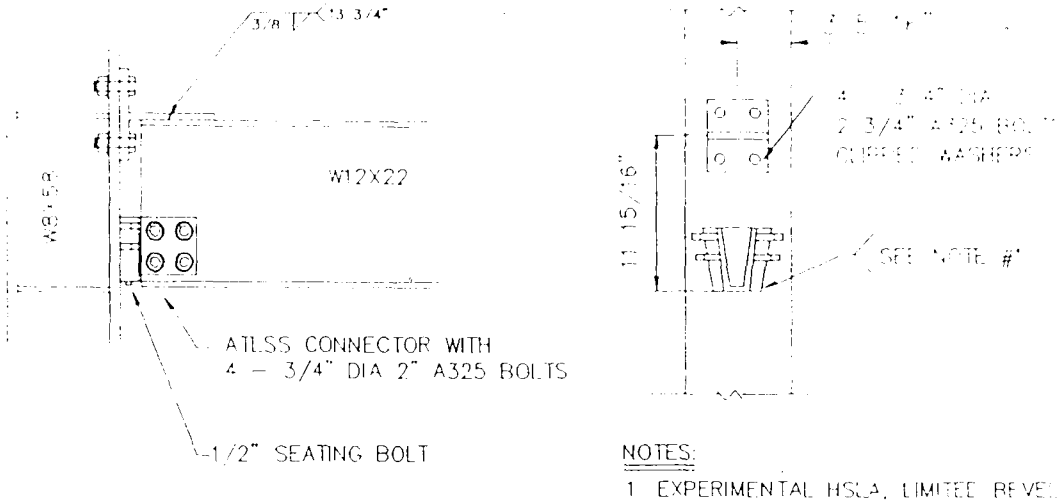

Figure 3.14 Type-C Connection Detail (TAR-5)

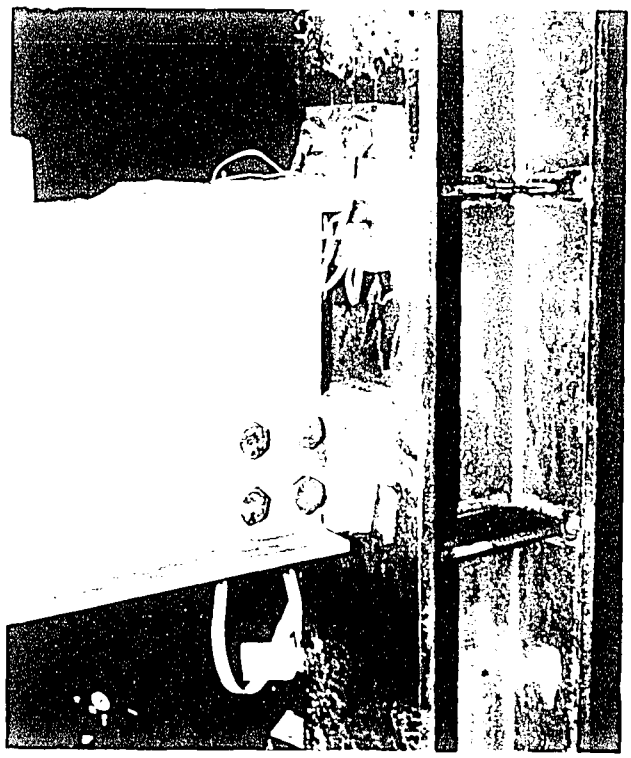

Figure 3.15 Completed Type-C Connection (TAR-5)

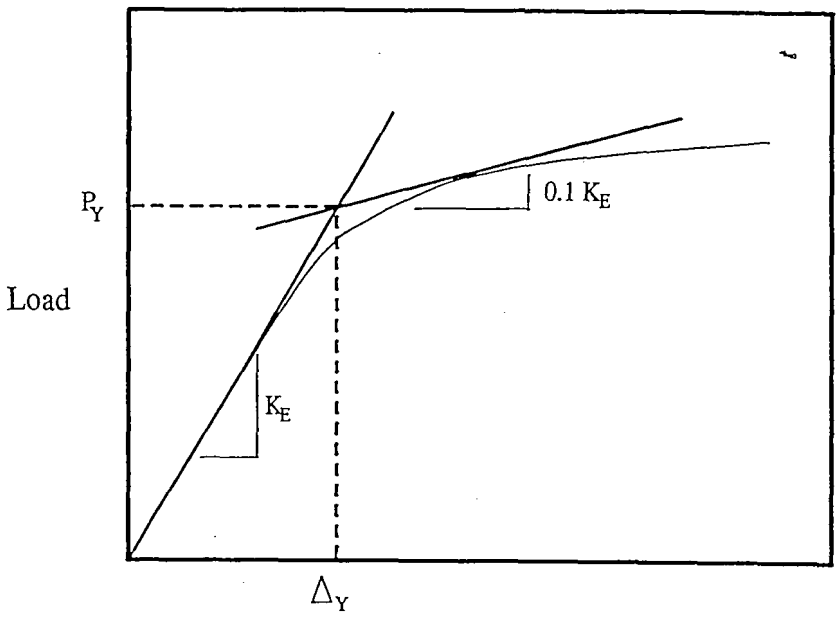

Figure 4.1 Yield Deflection Calculation

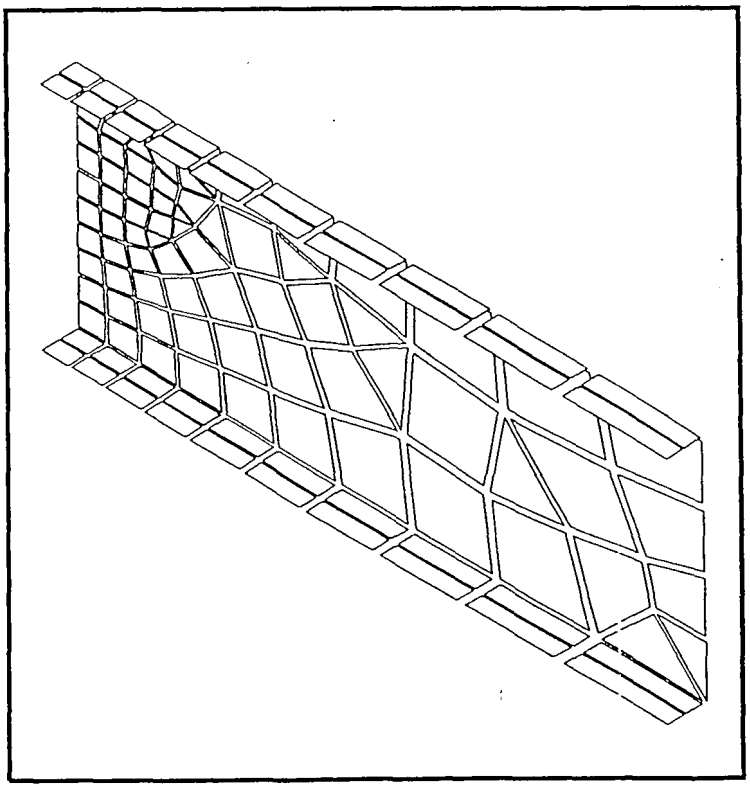

Figure 4.2 Finite Element Model for W12x22 Beam (Simplified Analyses)

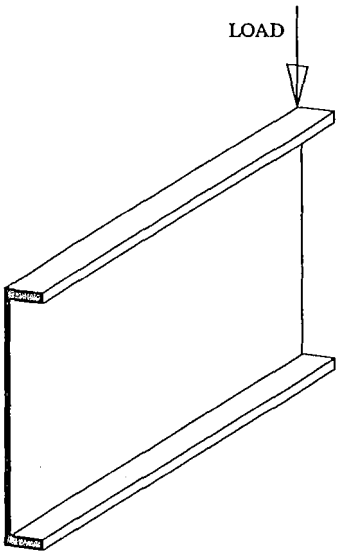

Fixed End (FTOT)

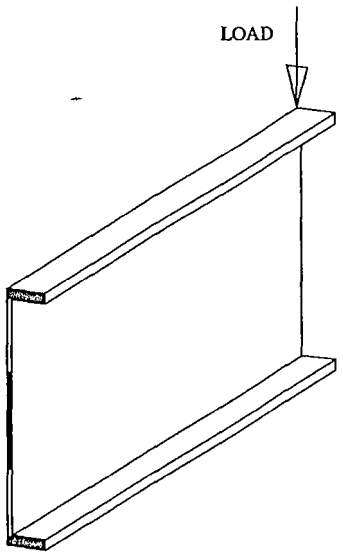

Fixed Flange and Mid-Web (FFMW)

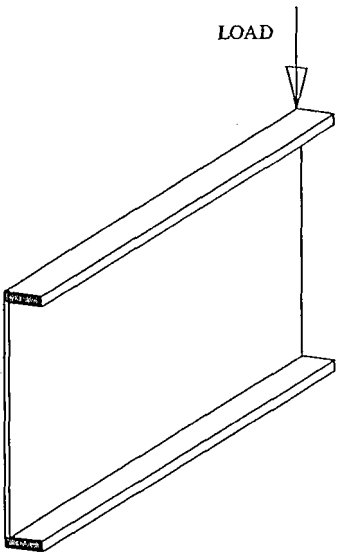

Fixed Flange (FF)

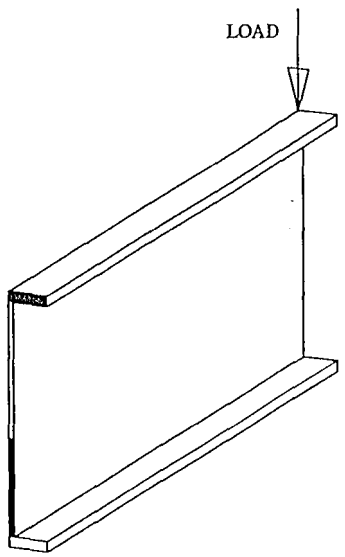

Fixed Top Flange and Bottom of Web (FTFBW)

Figure 4.3 Boundary Conditions for Simplified Models

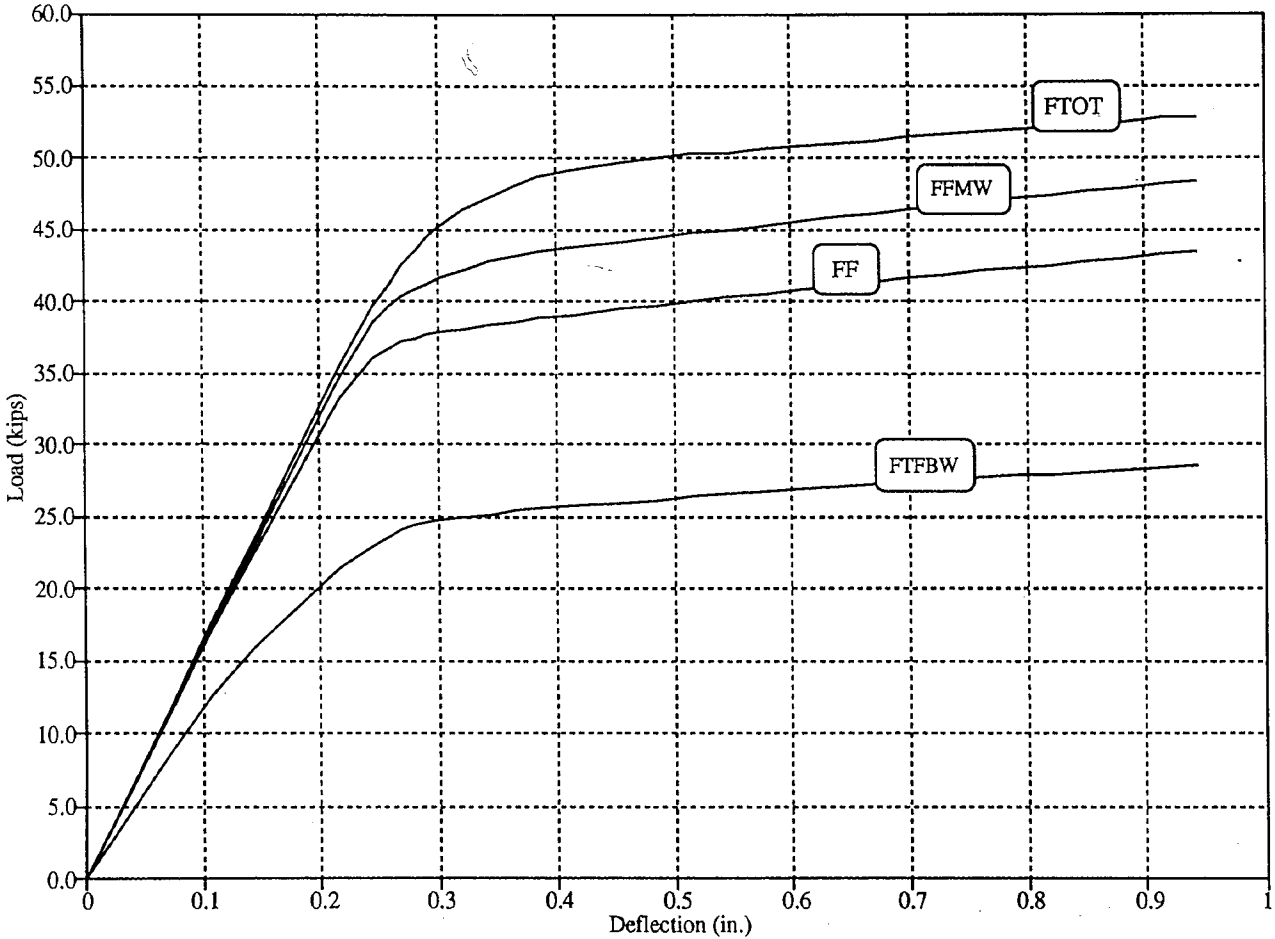

Figure 4.4 Load Deflection Comparisons of Varied End Conditions

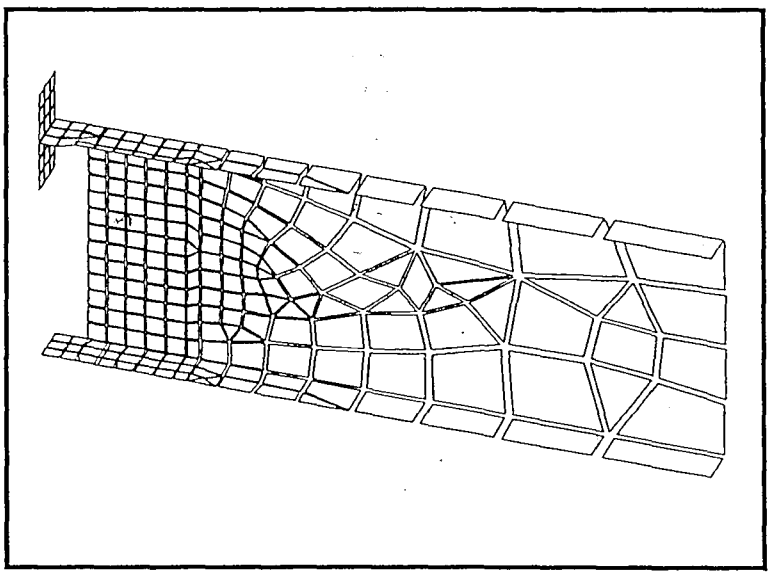

Figure 4.5 Finite Element Model for W12x22 Beam with Tee Stub and Flange Plate (Refined Analyses)

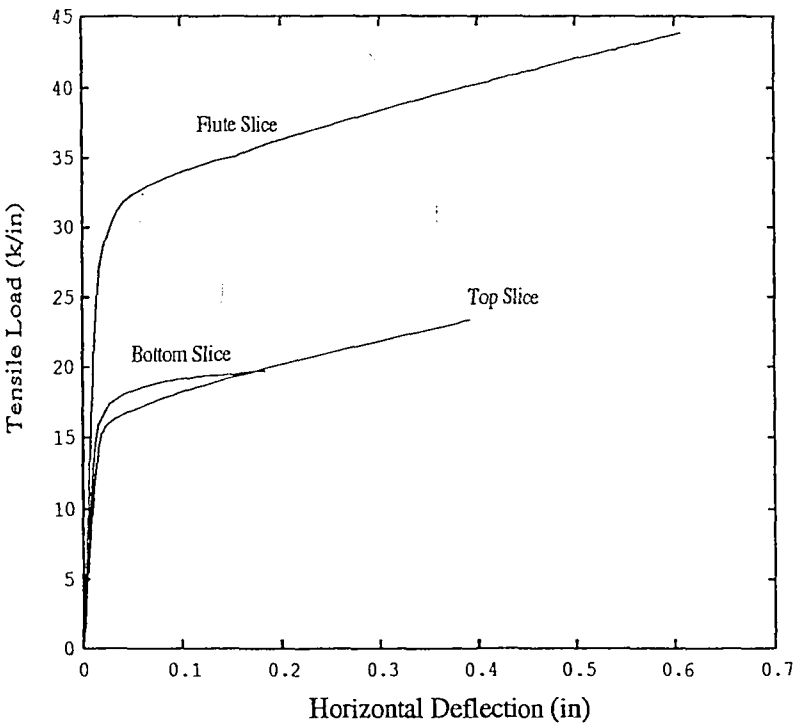

Figure 4.6 AC Slices Spring Stiffness Curves (Fleischman, et al, 93)

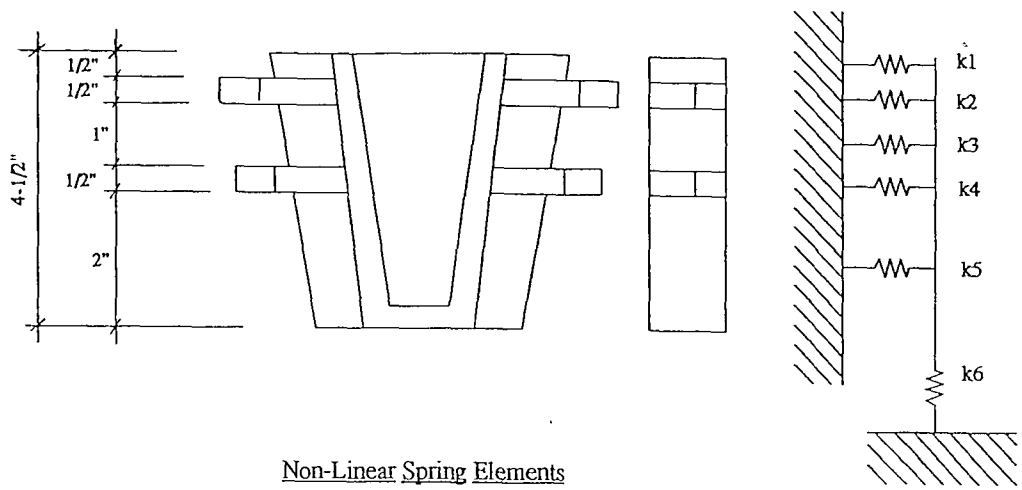

Non-Linear Spring Elements

k1 - Pure Mortise 1/2"
k2 - Flutes 1/2"
k3 - Pure Mortise 1"
k4 - Flutes 1/2"
k5 - Pure Mortise 2"
k6 - Seat

Figure 4.7 Non-Linear Spring Model of ATLSS Connector

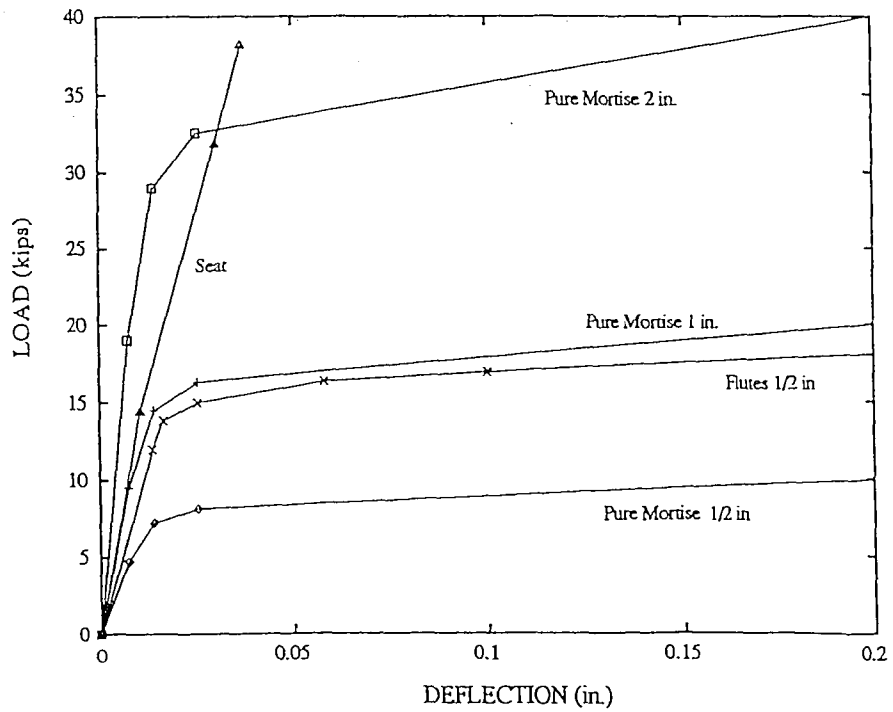

Figure 4.8 Individual AC Non-Linear Spring Stiffness Curves

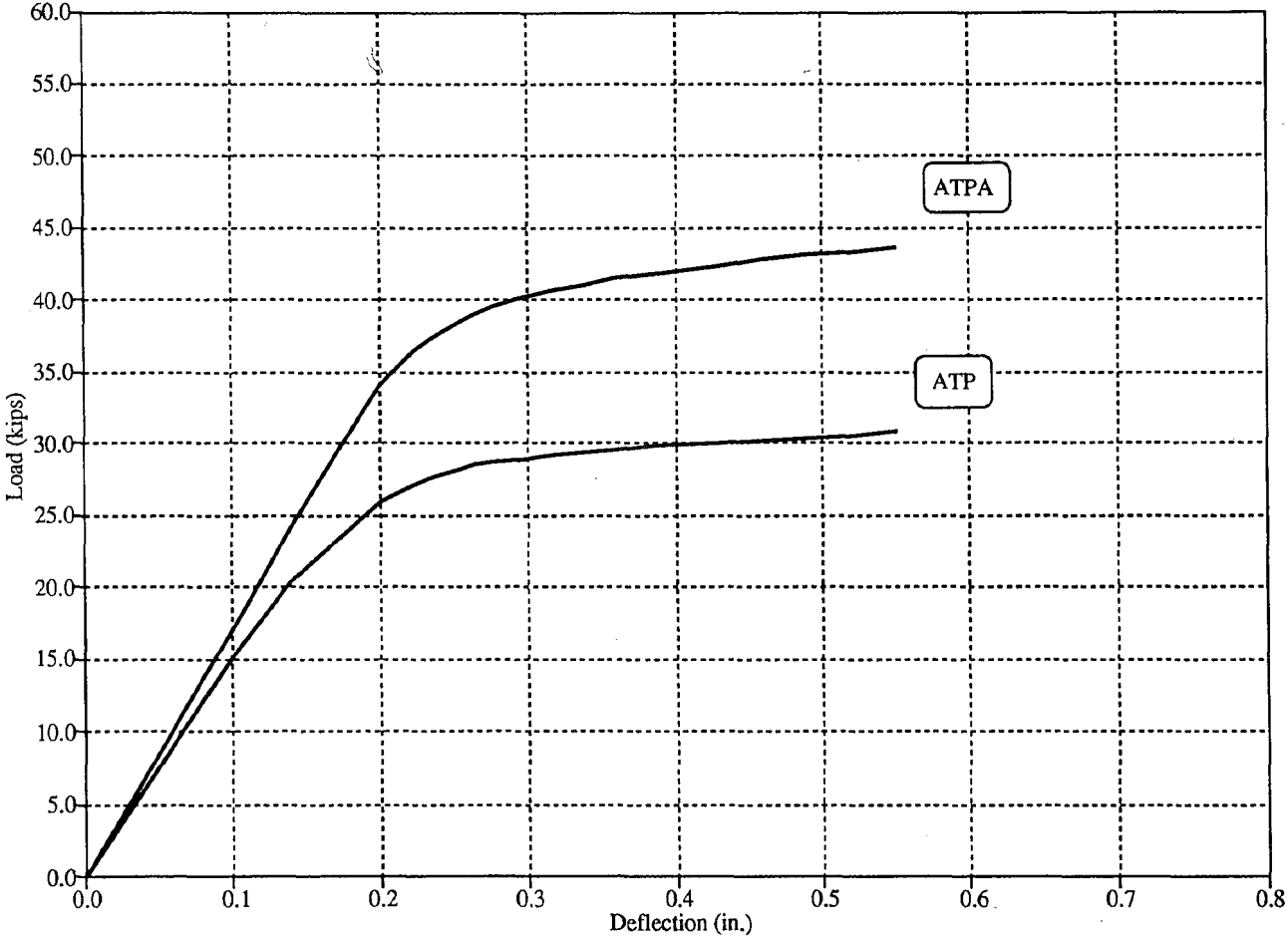

Figure 4.9 Analytical Load-Deflection Comparison of Type A and Type B Connections

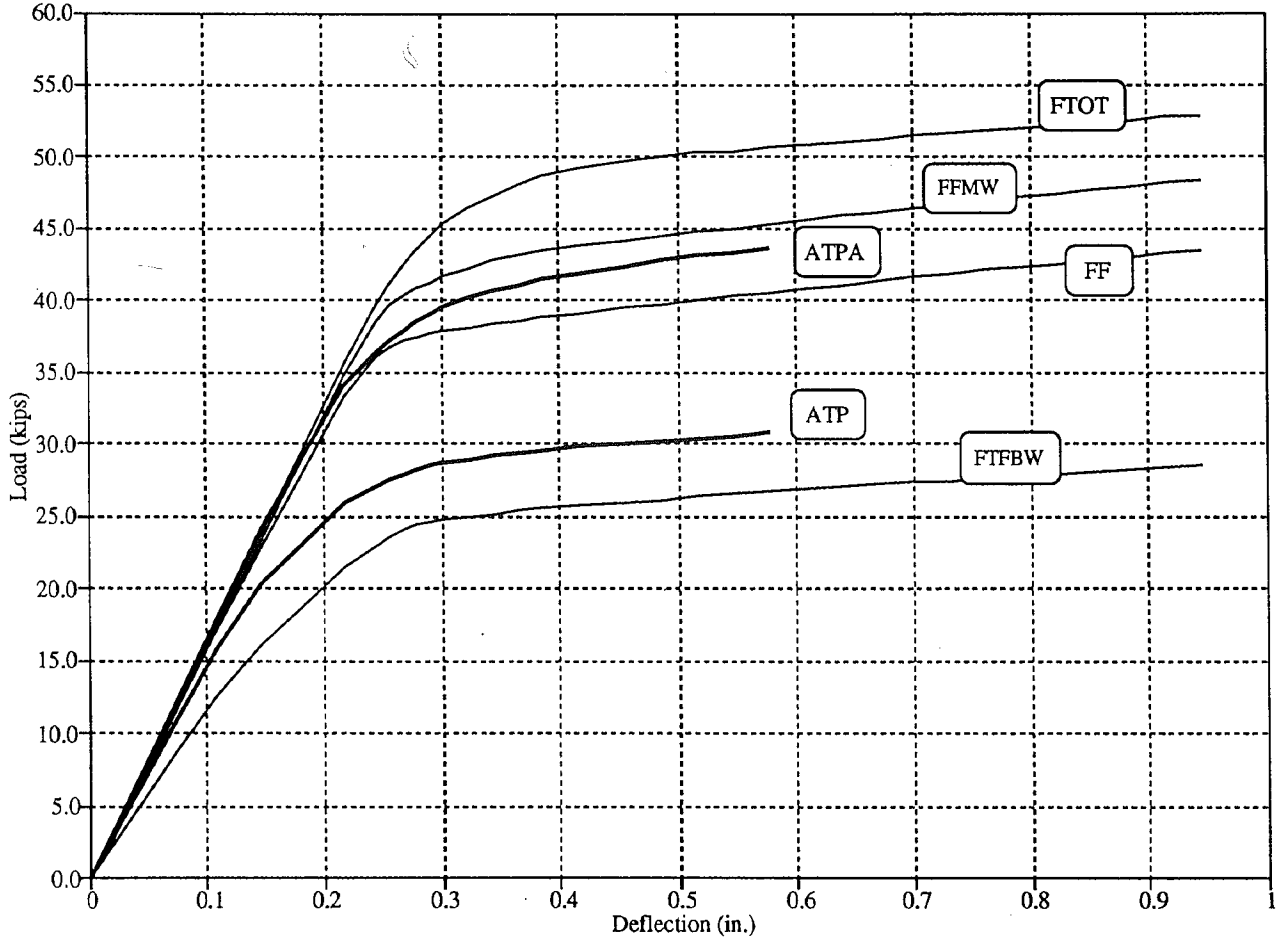

Figure 4.10 Analytical Load-Deflection Comparison for all Finite Element Models

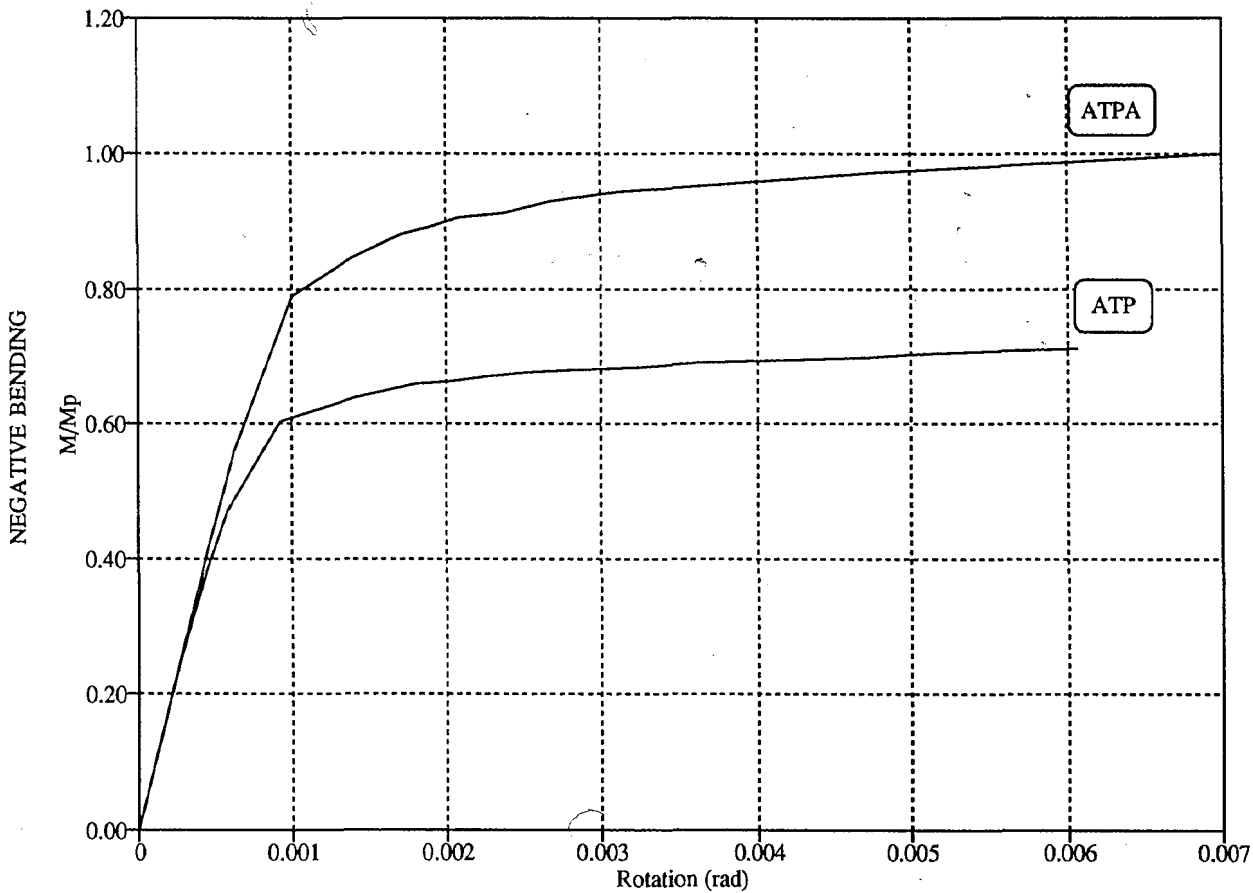

Figure 4.11 Analytical Moment-Rotation Comparison of Type A and Type B Connections

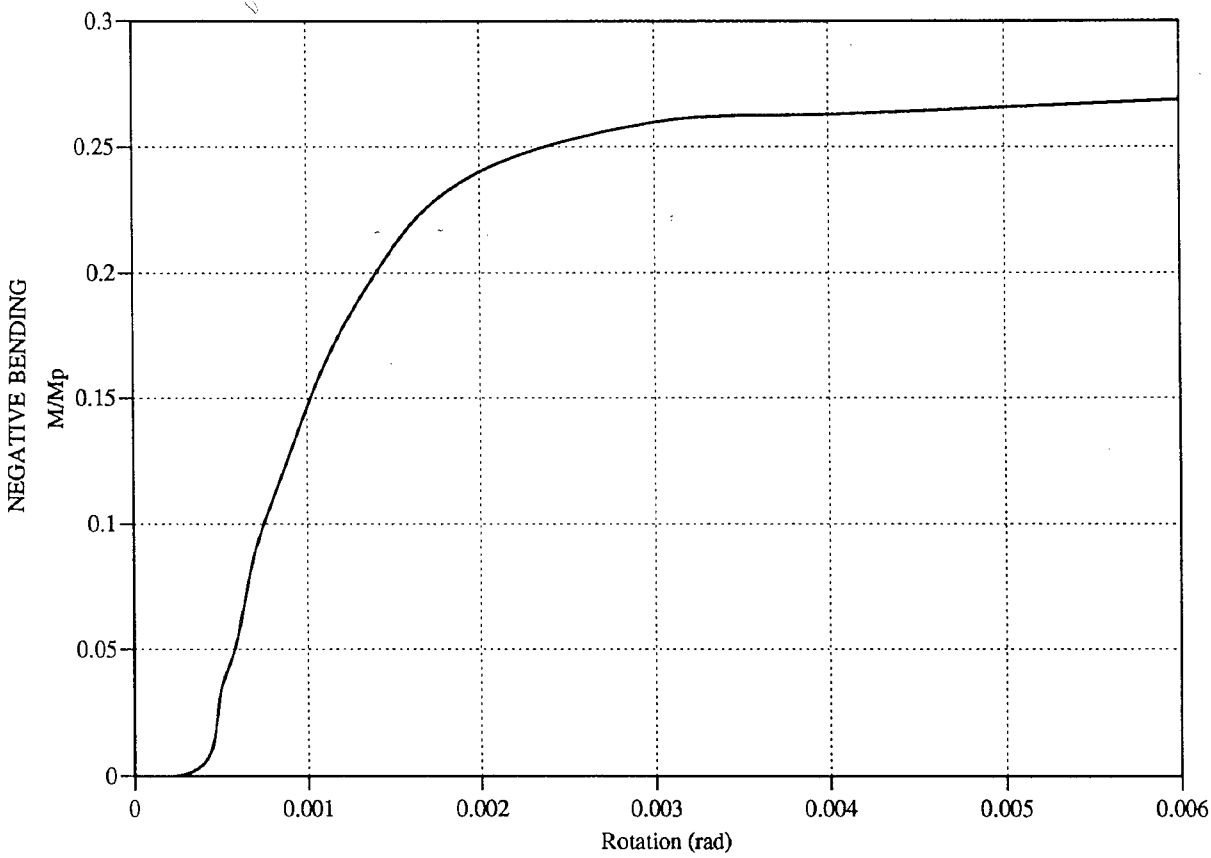

Figure 4.12 Analytical Predicted Moment Contribution of AC in Type A Connection

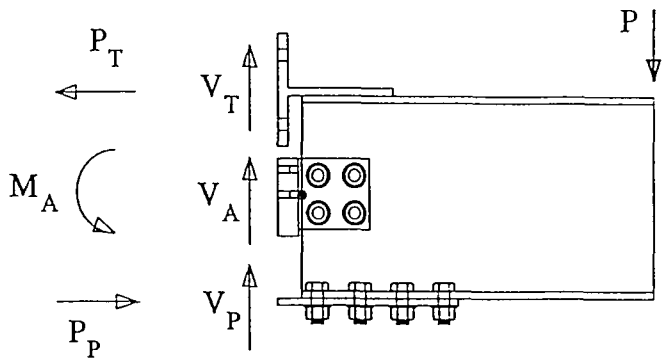

P = Applied load
P_T = Axial load carried by the tee-stub
P_P = Axial load carried by the plate
V_T = Shear force carried by the tee-stub
V_A = Shear force carried by the ATLSS Connector
V_P = Shear force carried by the plate
M_A = Moment carried by the ATLSS Connector

Figure 5.1 Joint Statics

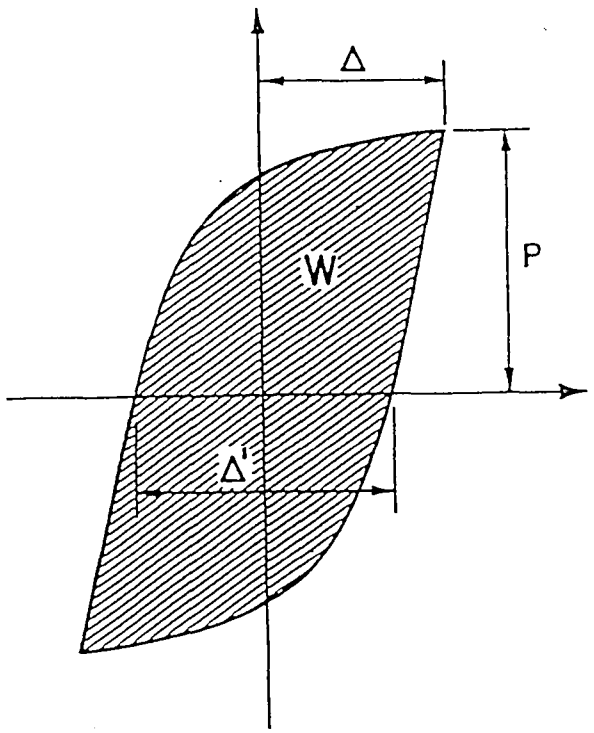

Figure 5.2 Hysterisis Curve Notation (Popov and Pinkney, 67)

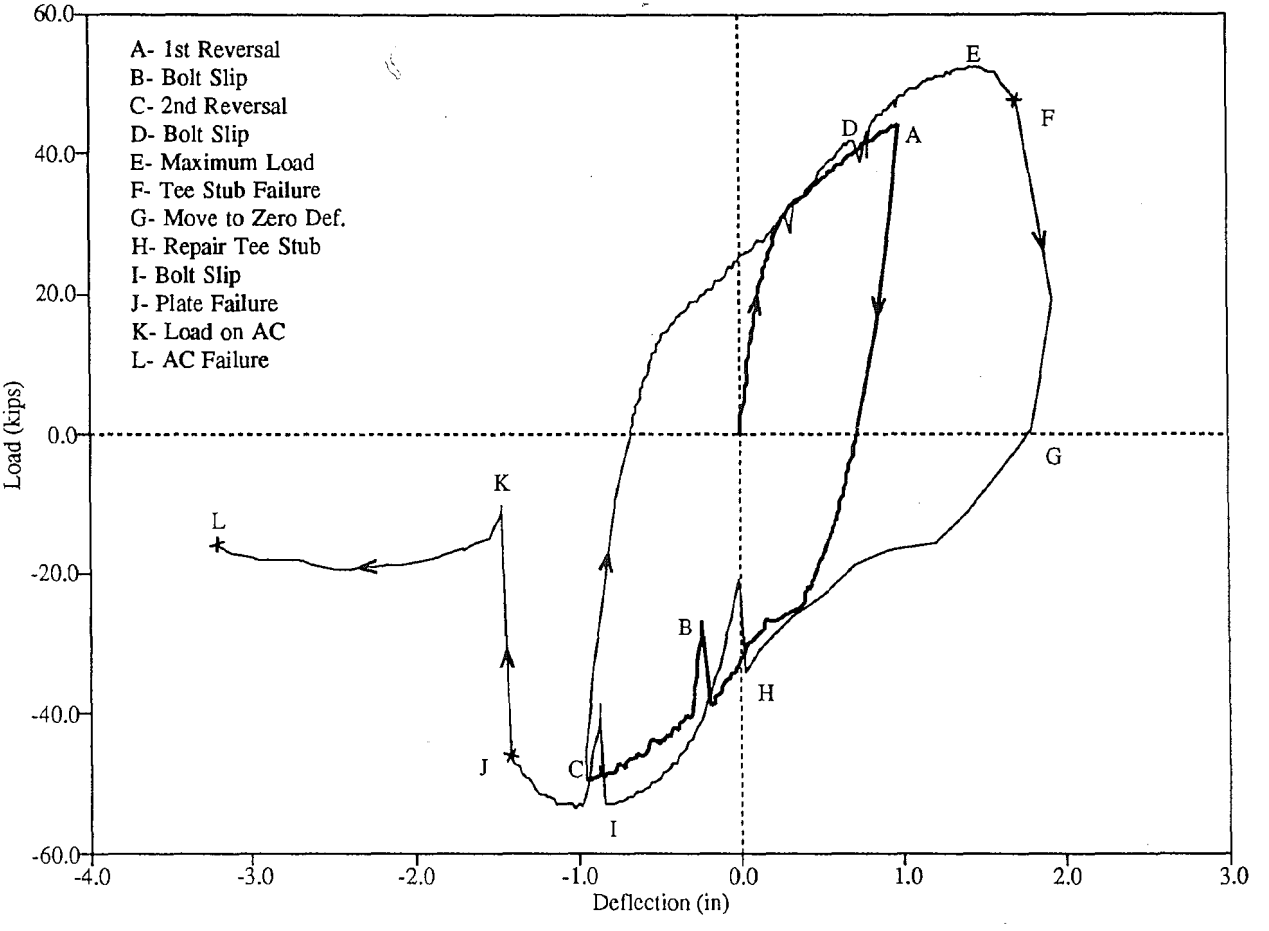

Figure 5.3 Load - Deflection Relationship TPA-1

Figure 5.4 Fracture of Tee Stub in TPA-1 (Negative Bending)

Figure 5.4 Fracture of Tee Stub in TPA-1 (Negative Bending)

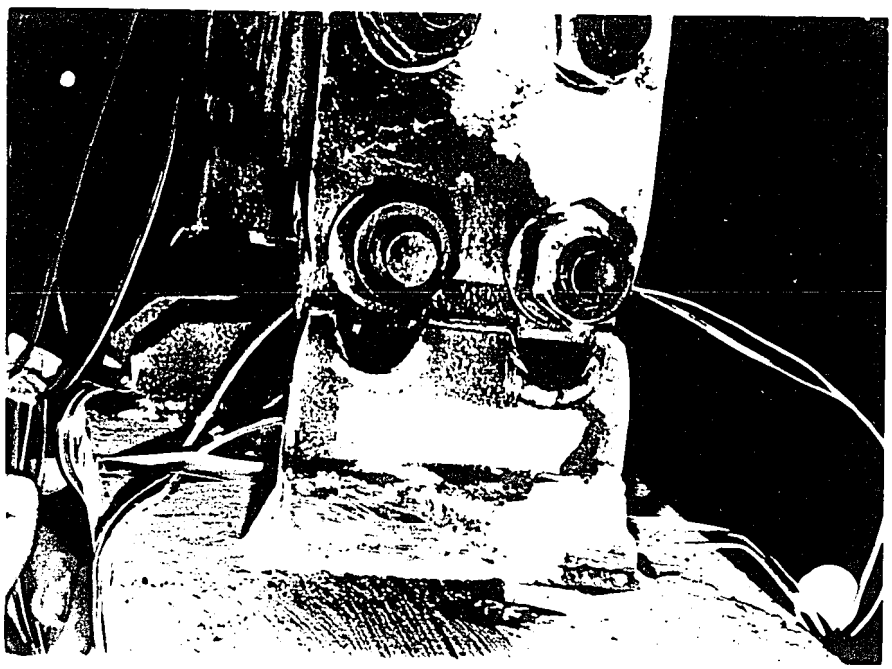

Figure 5.5 Fracture of Flange Plate in TPA-1 (Positive Bending)

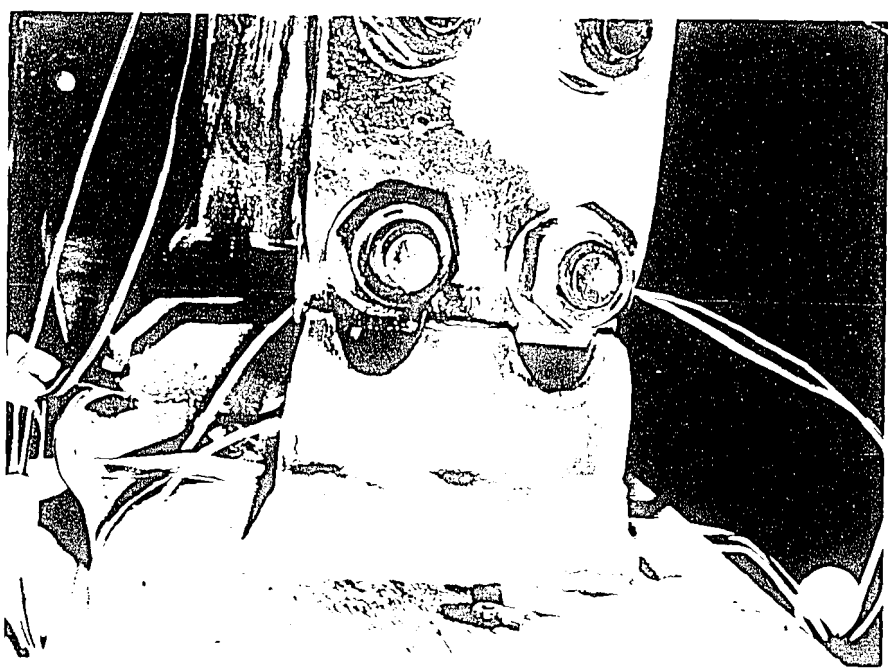

Figure 5.5 Fracture of Flange Plate in TPA 1 (Positive Bending)

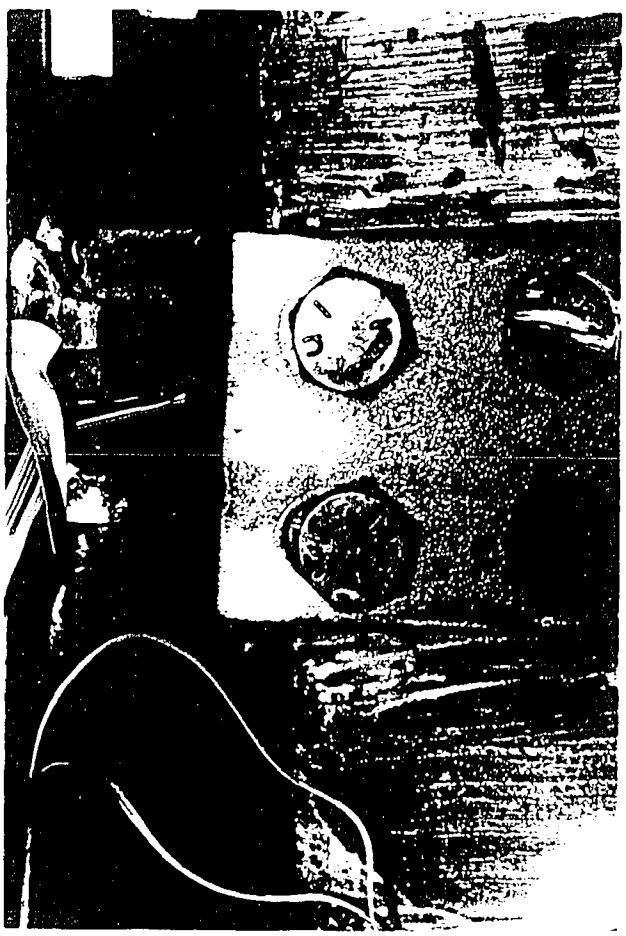

Figure 5.6 Fracture of Tenon Plate in TPA-1 (Positive Bending)

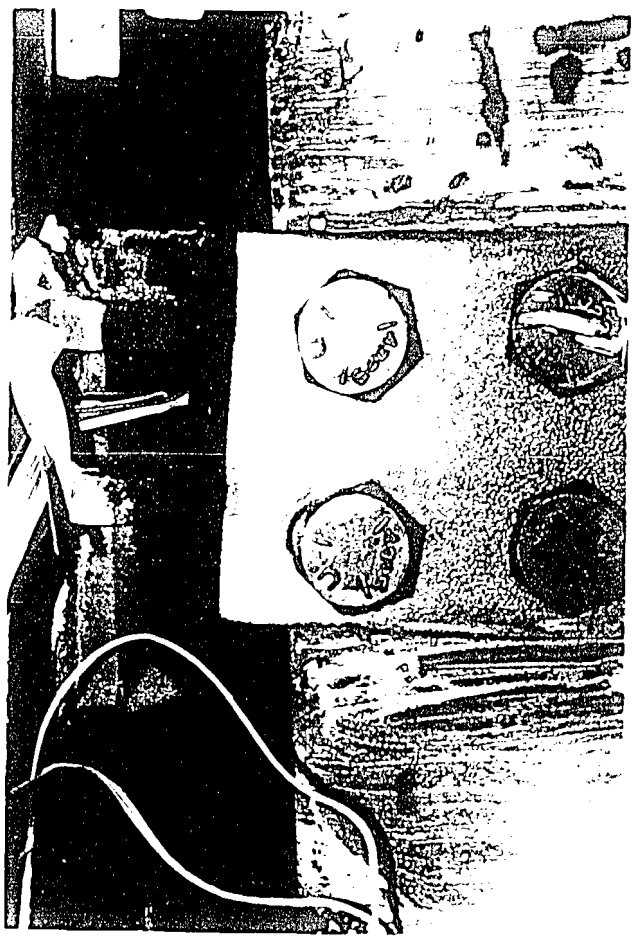

Figure 5.6 Fracture of Tenon Plate in TPA-1 (Positive Bending)

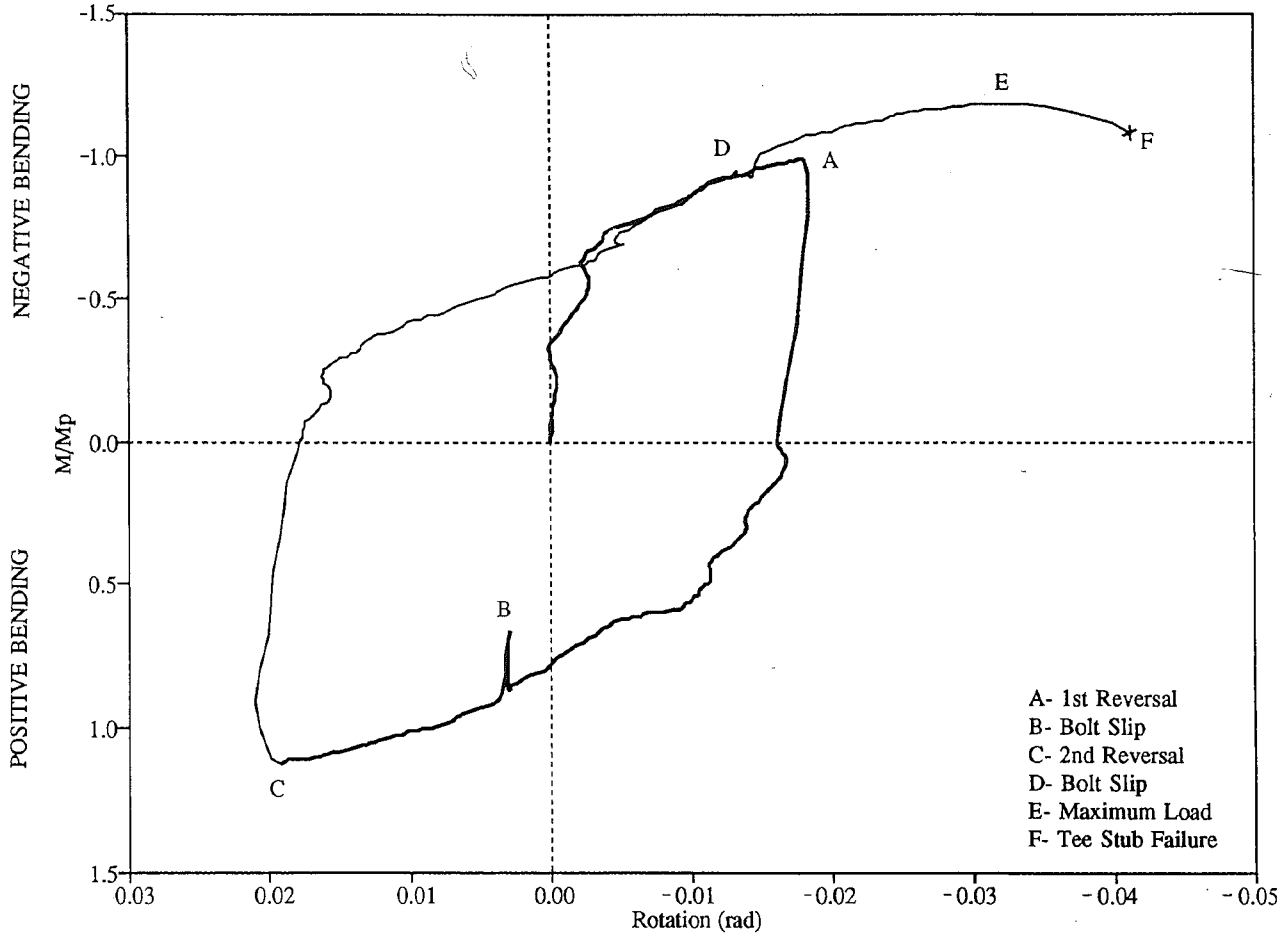

Figure 5.7 Moment - Rotation Relationship of TPA-1

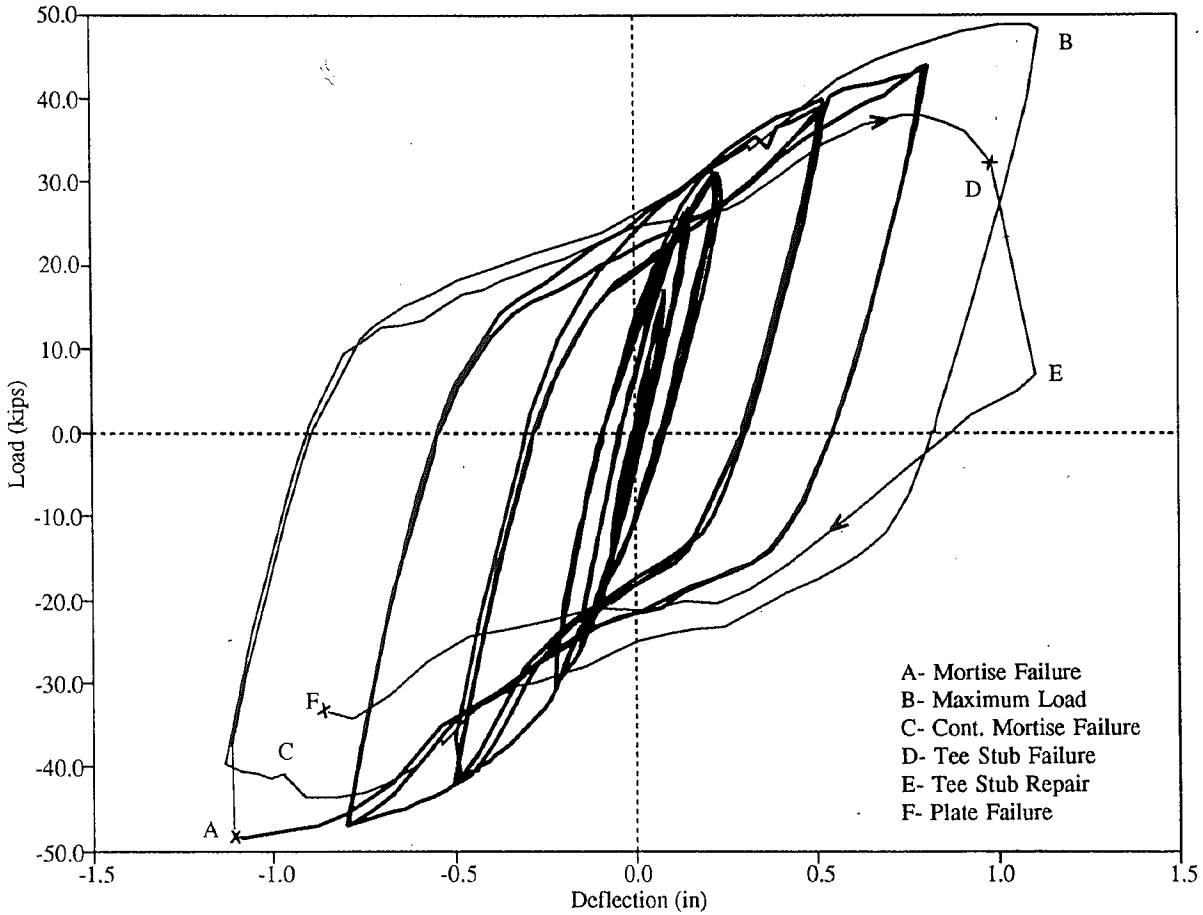

Figure 5.8 Load - Deflection Relationship of TPA-CY2

Figure 5.9 Fracture of Heat Affected Zone of Mortise in TPA-CY2 (Positive Bending)

Figure 5.9 Fracture of Heat Affected Zone of Mortise in TPA CY2 (Positive Bending)

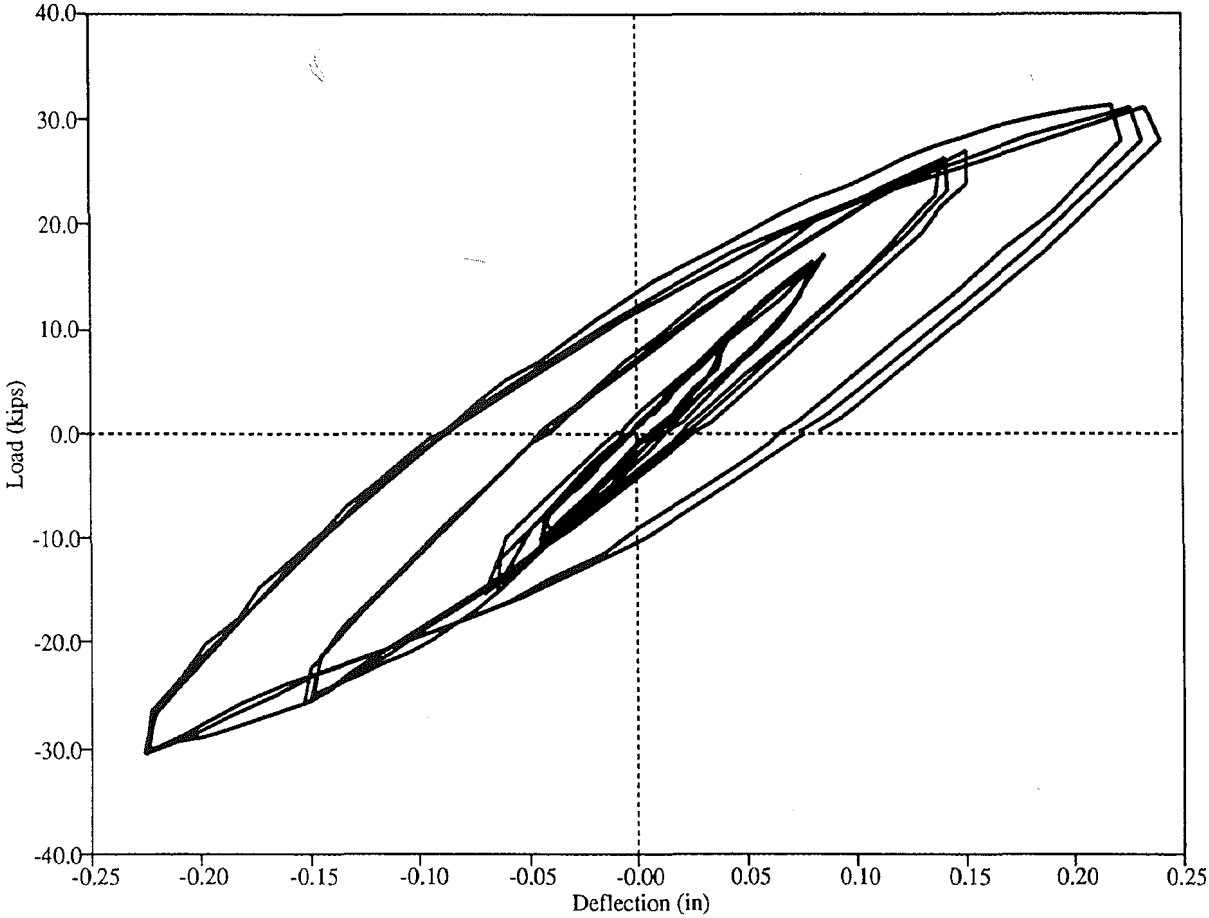

Figure 5.10 Load - Deflection Relationship of TPA-CY2, Cycles 1 Through 12

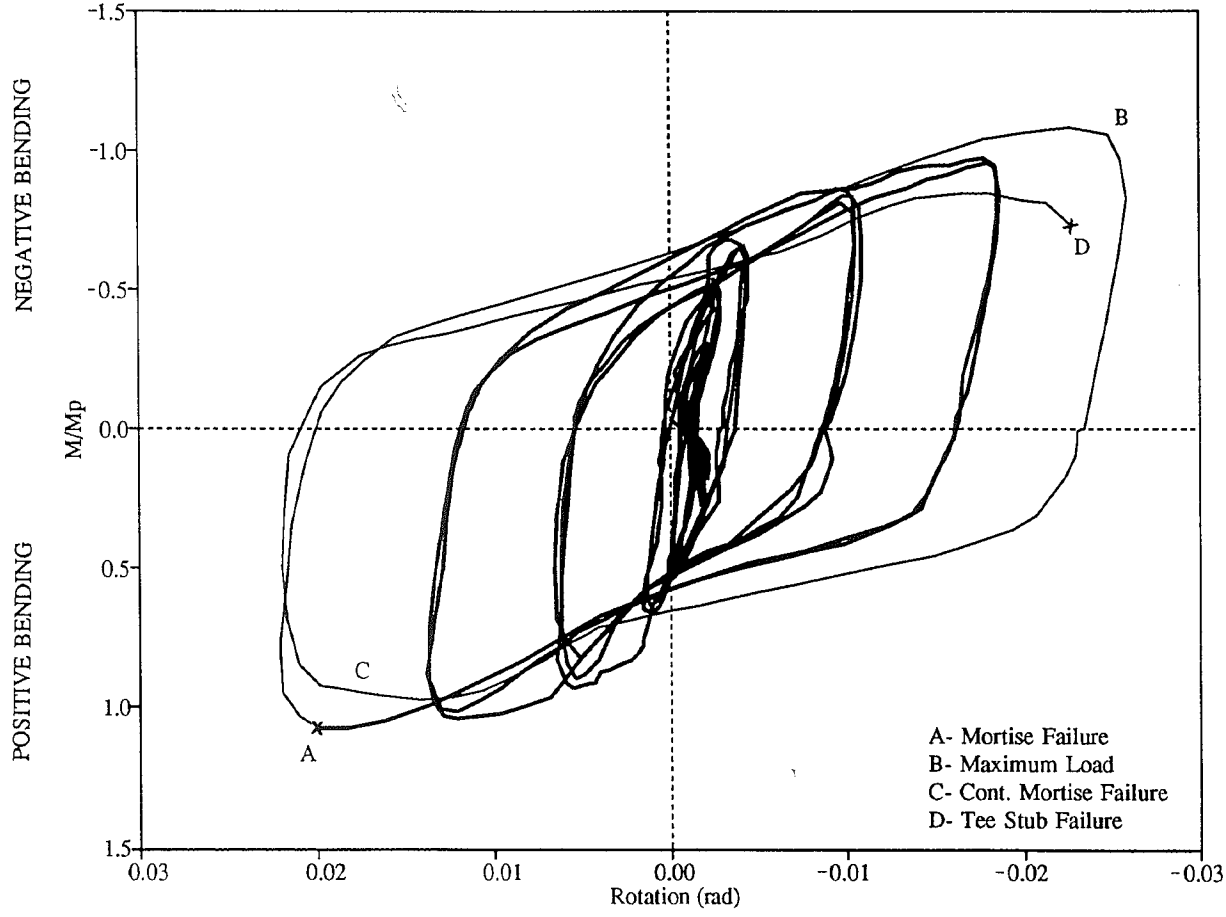

Figure 5.11 Moment - Rotation Relationship of TPA-CY2

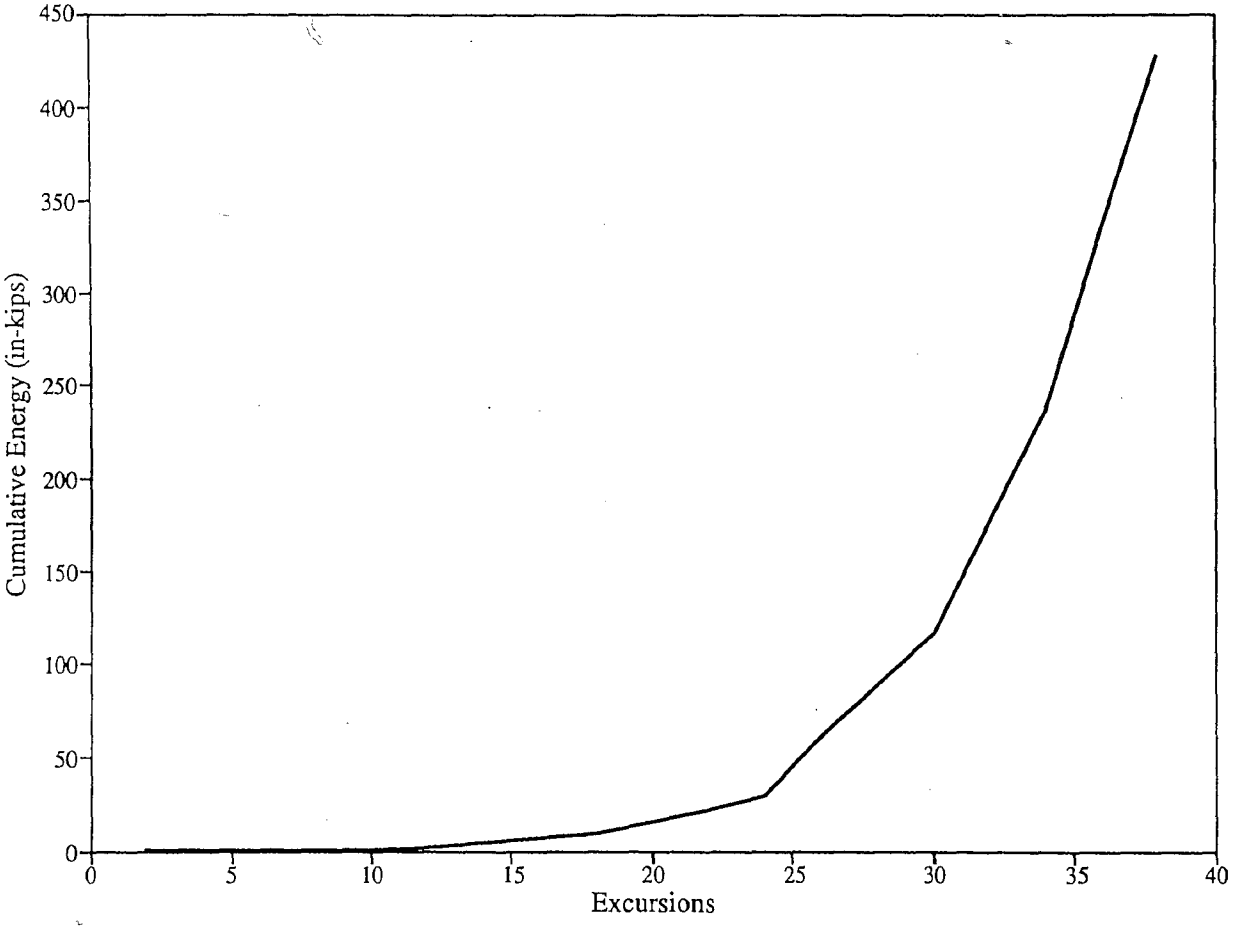

Figure 5.12 Cumulative Energy Dissipation of TPA-CY2

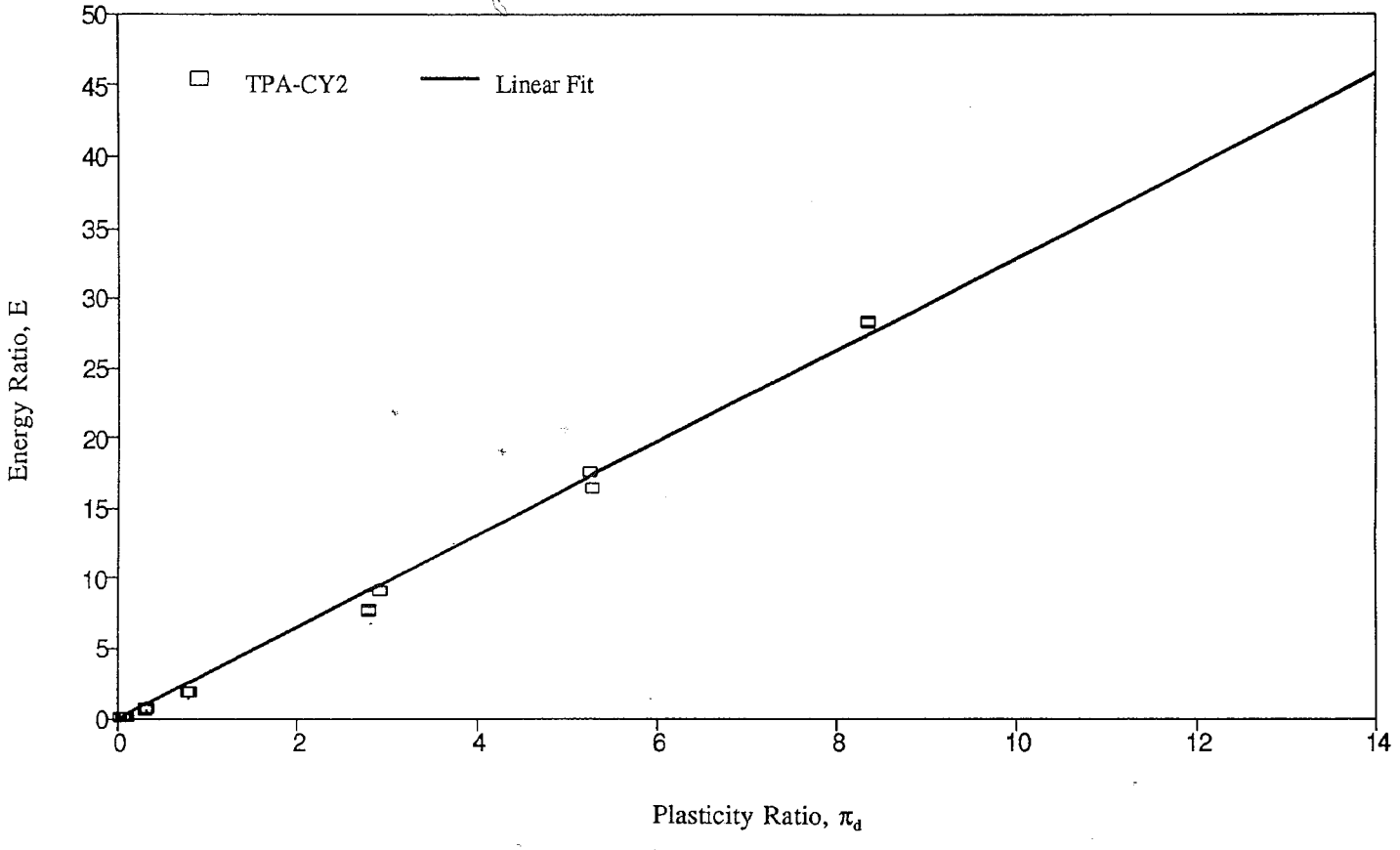

Figure 5.13 Energy Ratio and Plasticity Ratio for TPA-CY2

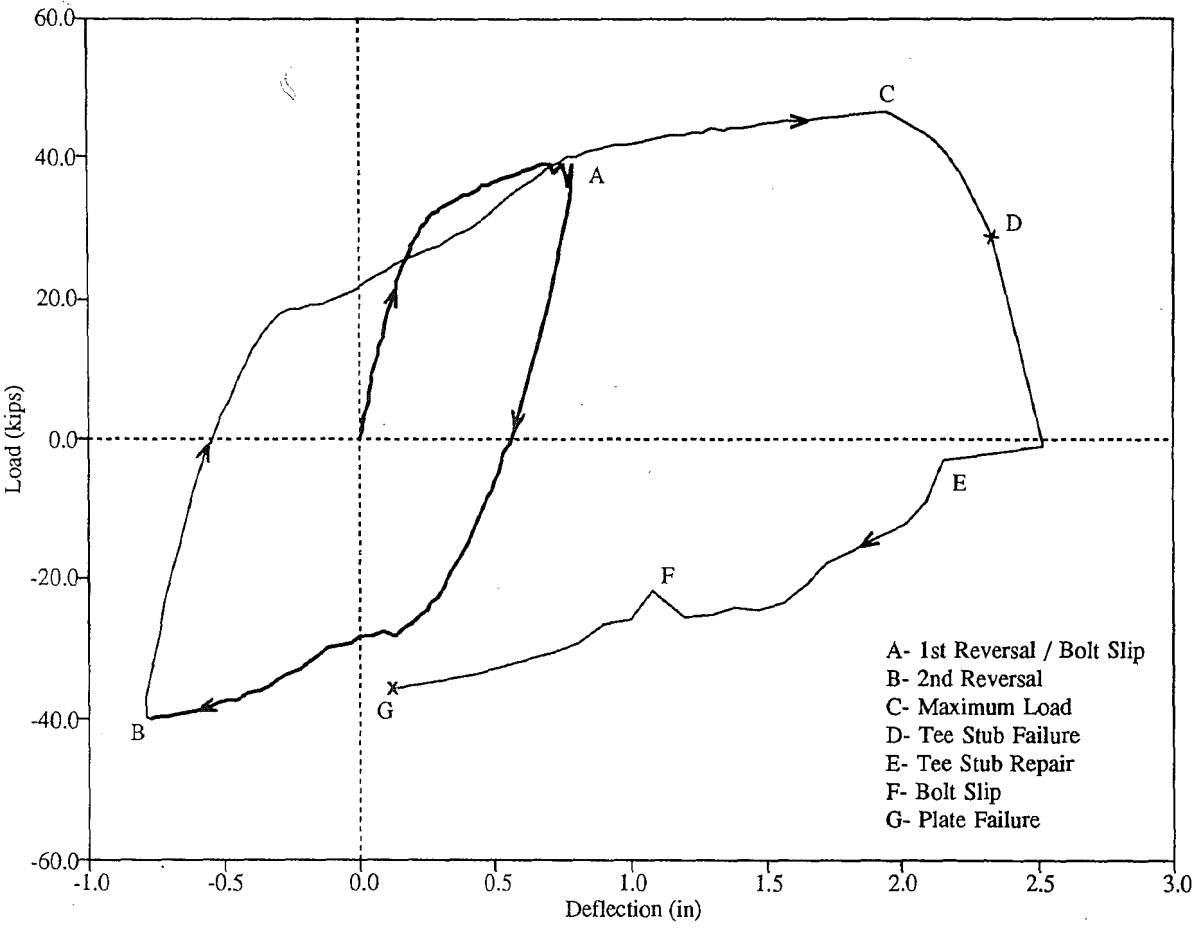

Figure 5.14 Load - Deflection Relationship of TP-3

Figure 5.15 Fracture of Tee Stub in TP-3 (Negative Bending)

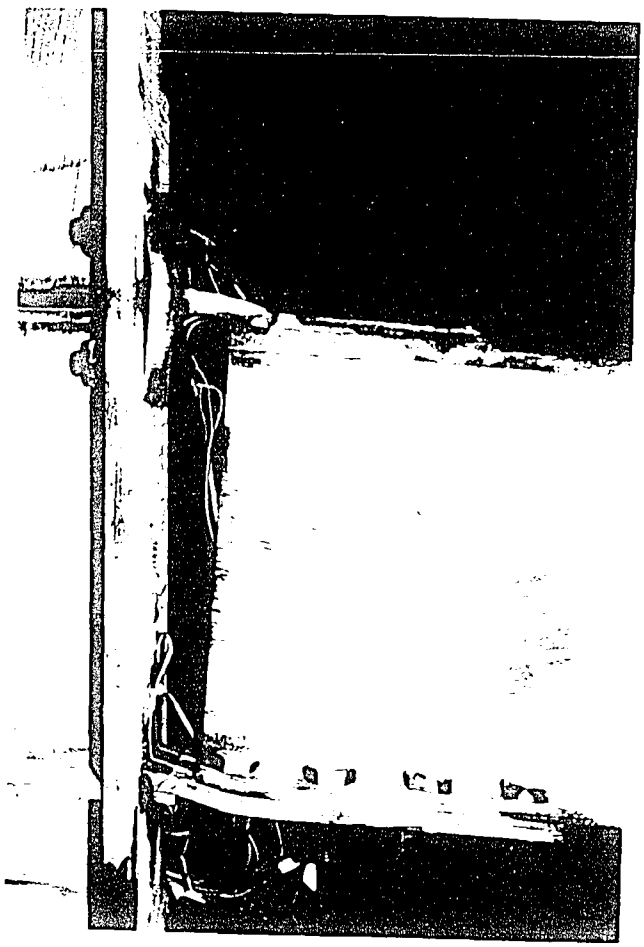

Figure 5.15 Fracture of Tee Stub in TP-3 (Negative Bending)

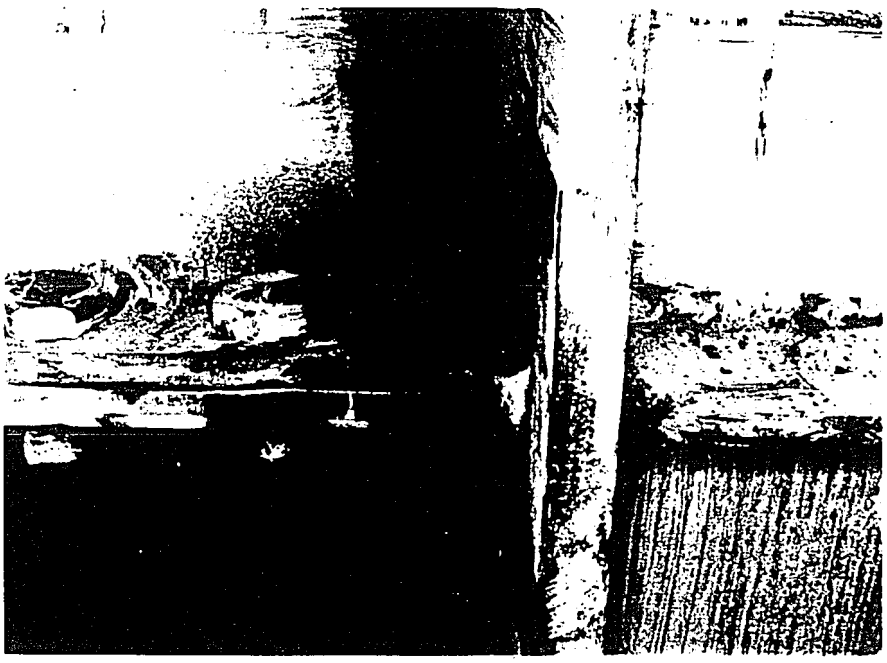

Figure 5.16 Fracture of Flange Plate in TP-3 (Positive Bending)

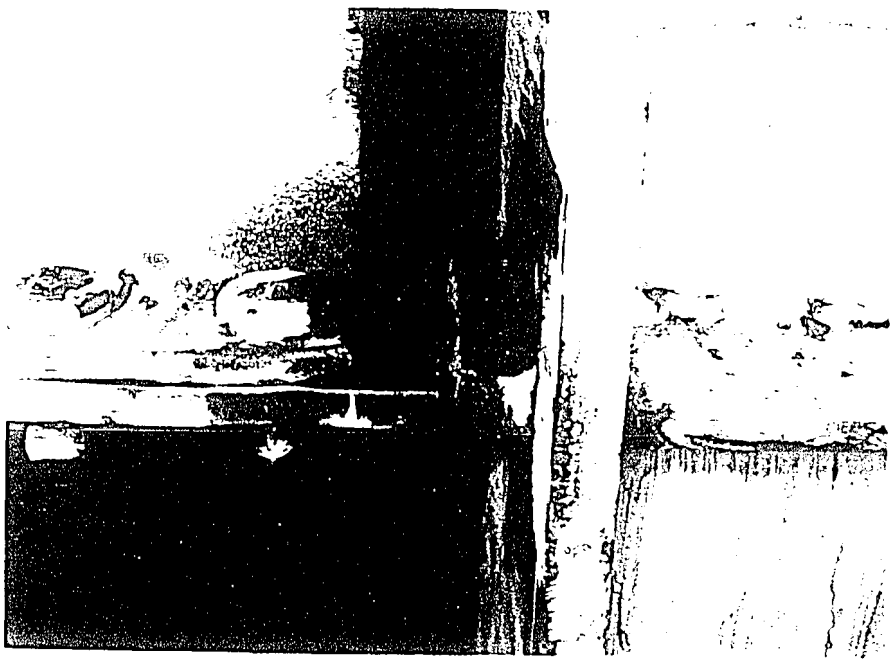

Figure 5.16 Fracture of Flange Plate in TP-3 (Positive Bending)

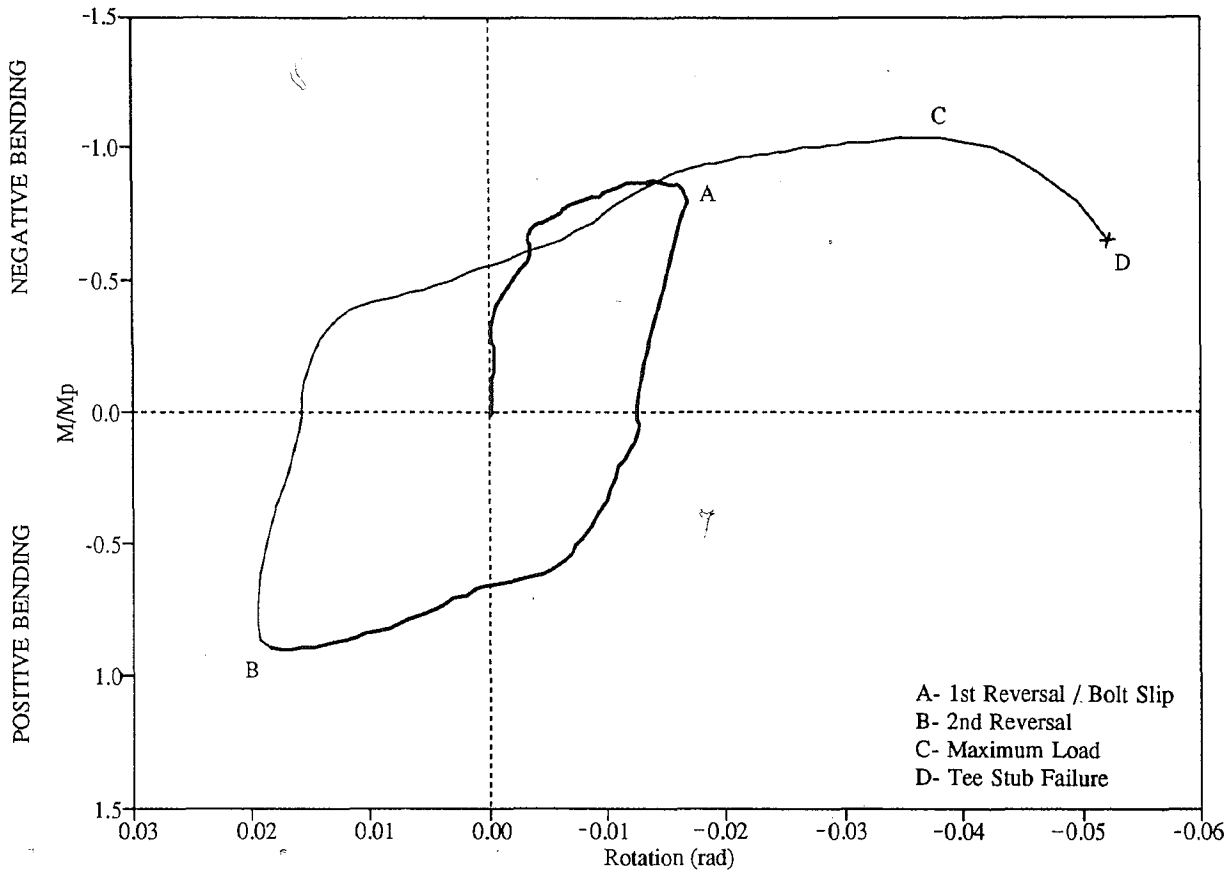

Figure 5.17 Moment - Rotation Relationship of TP-3

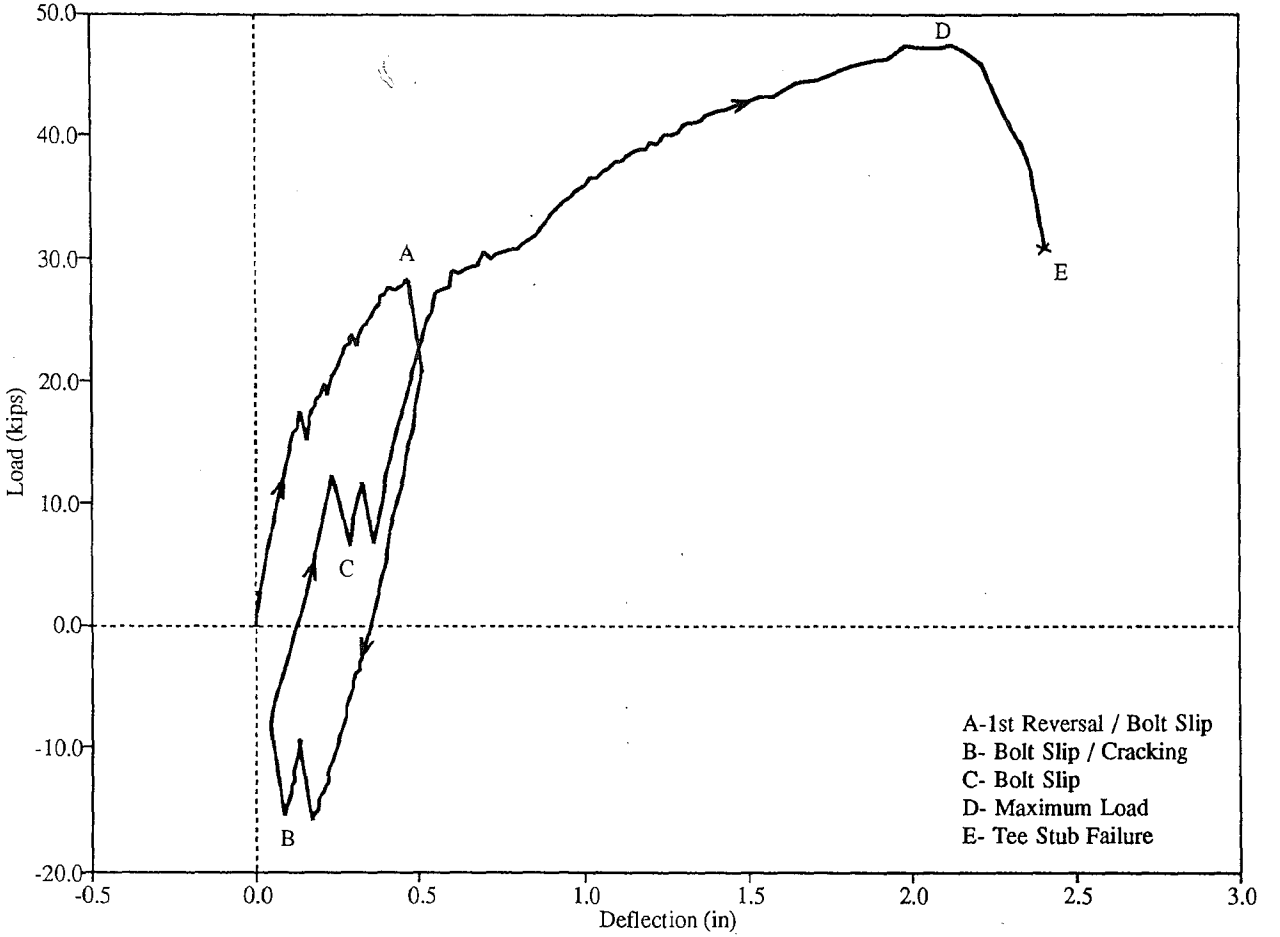

Figure 5.18 Load - Deflection Relationship of TA-4

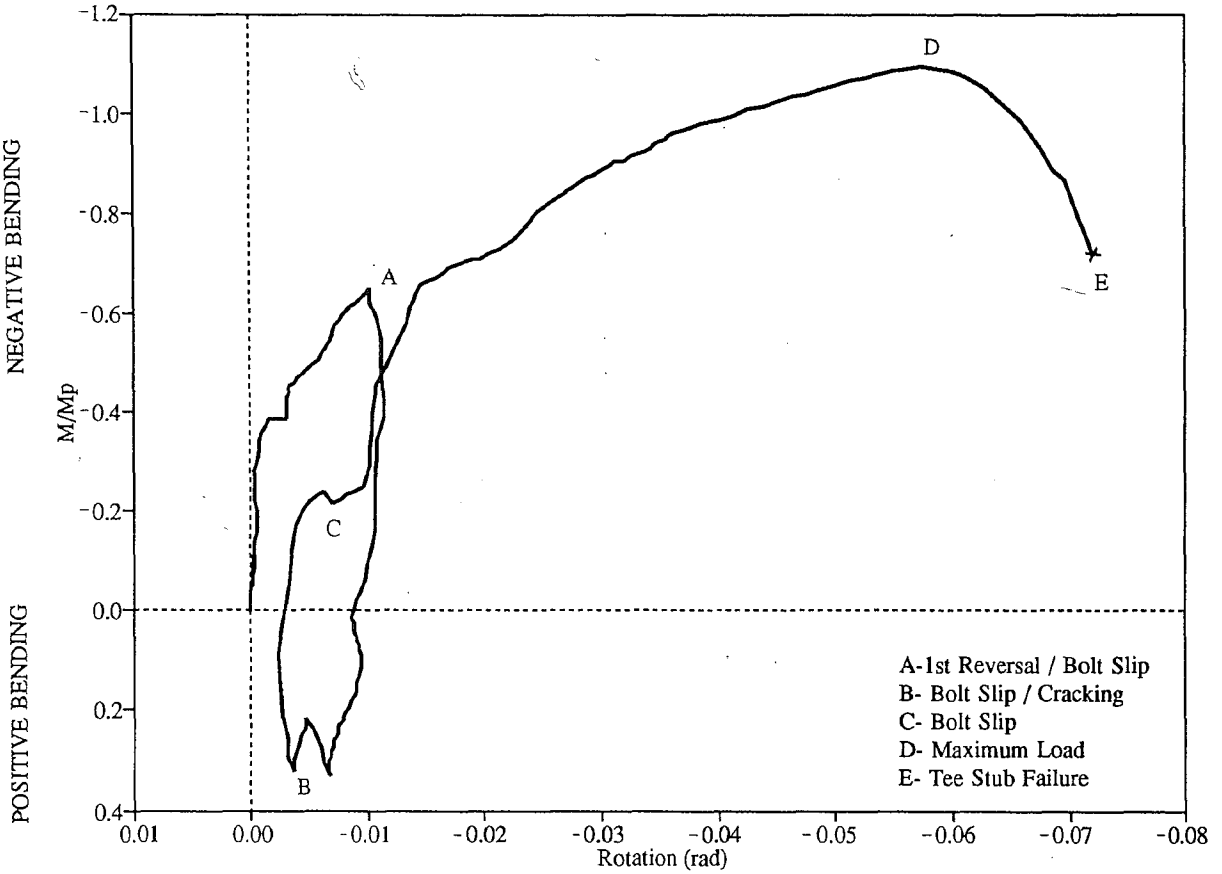

Figure 5.19 Moment - Rotation Relationship of TA-4

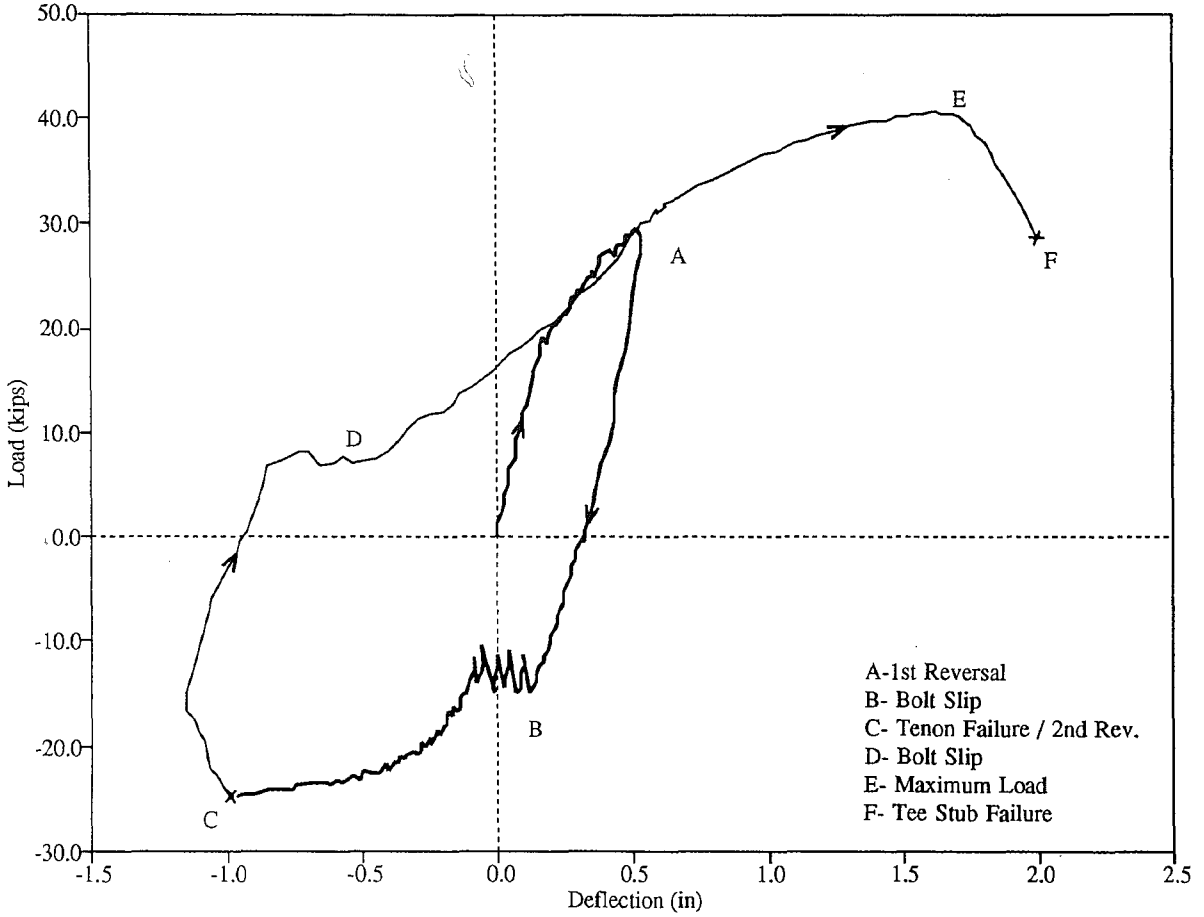

Figure 5.20 Load - Deflection Relationship TAR-5

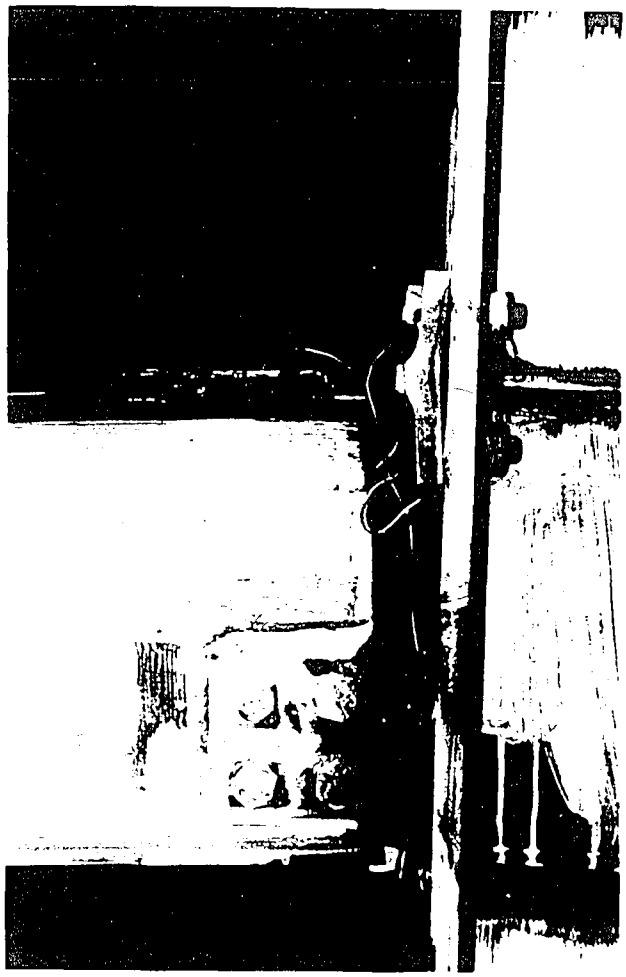

Figure 5.21 Fracture of Tee Stub in TAR-5 (Negative Bending)

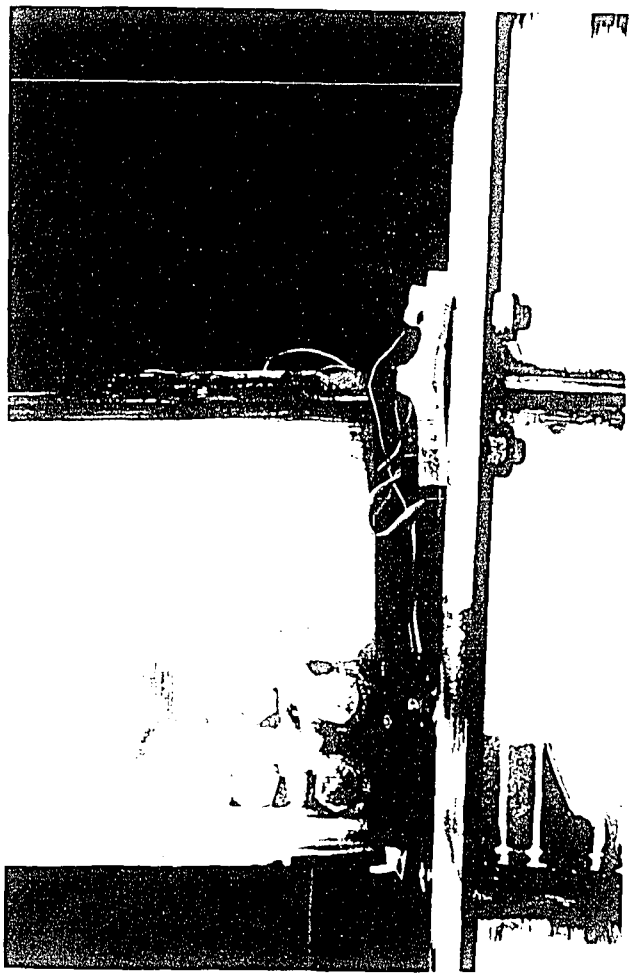

Figure 5.21 Fracture of Tee Stub in TAR-5 (Negative Bending)

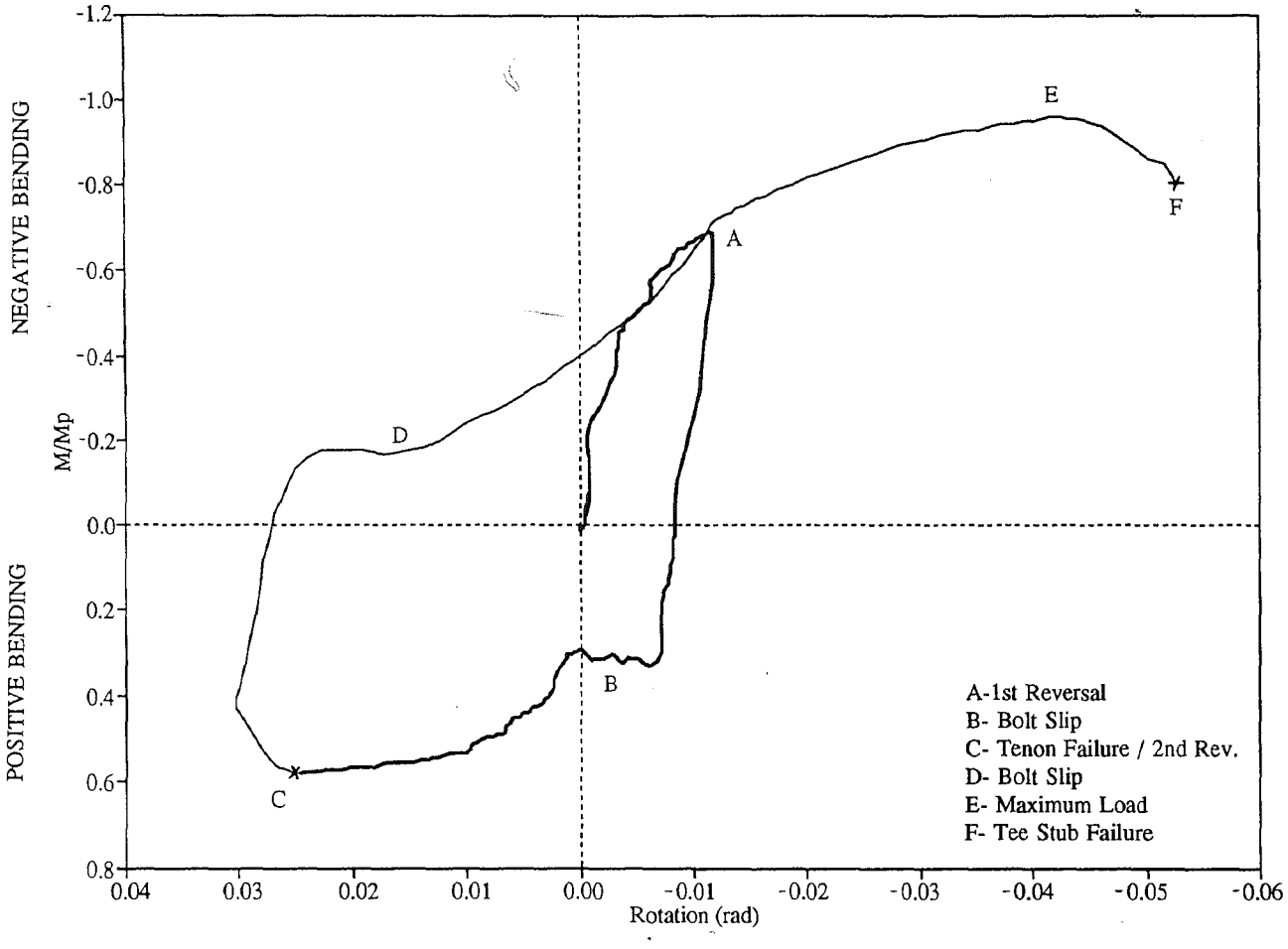

Figure 5.22 Moment - Rotation Relationship of TAR-5

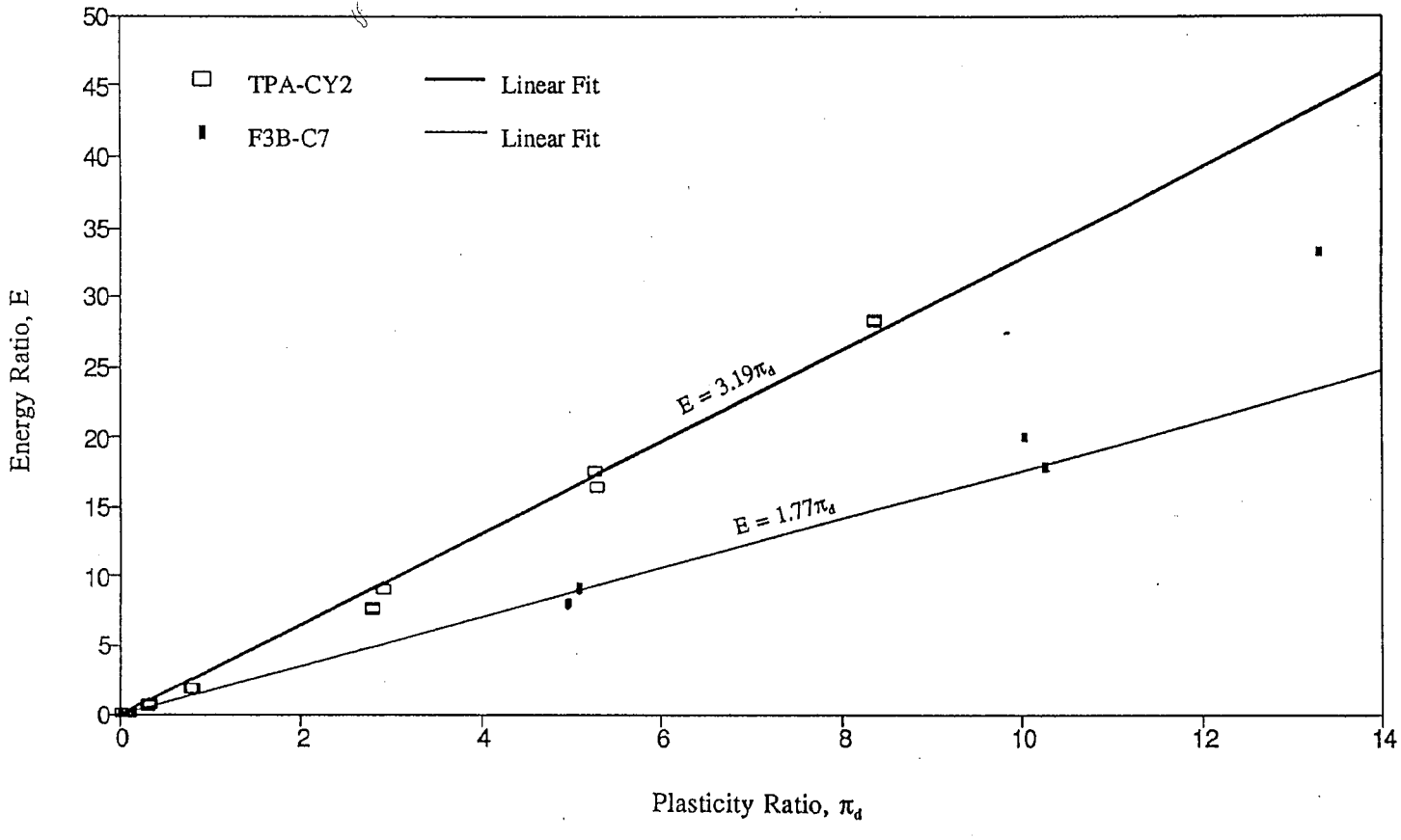

Figure 6.1 Comparison of Energy Dissipation of TPA-CY2 and Popov and Pinkney's F3B-C7

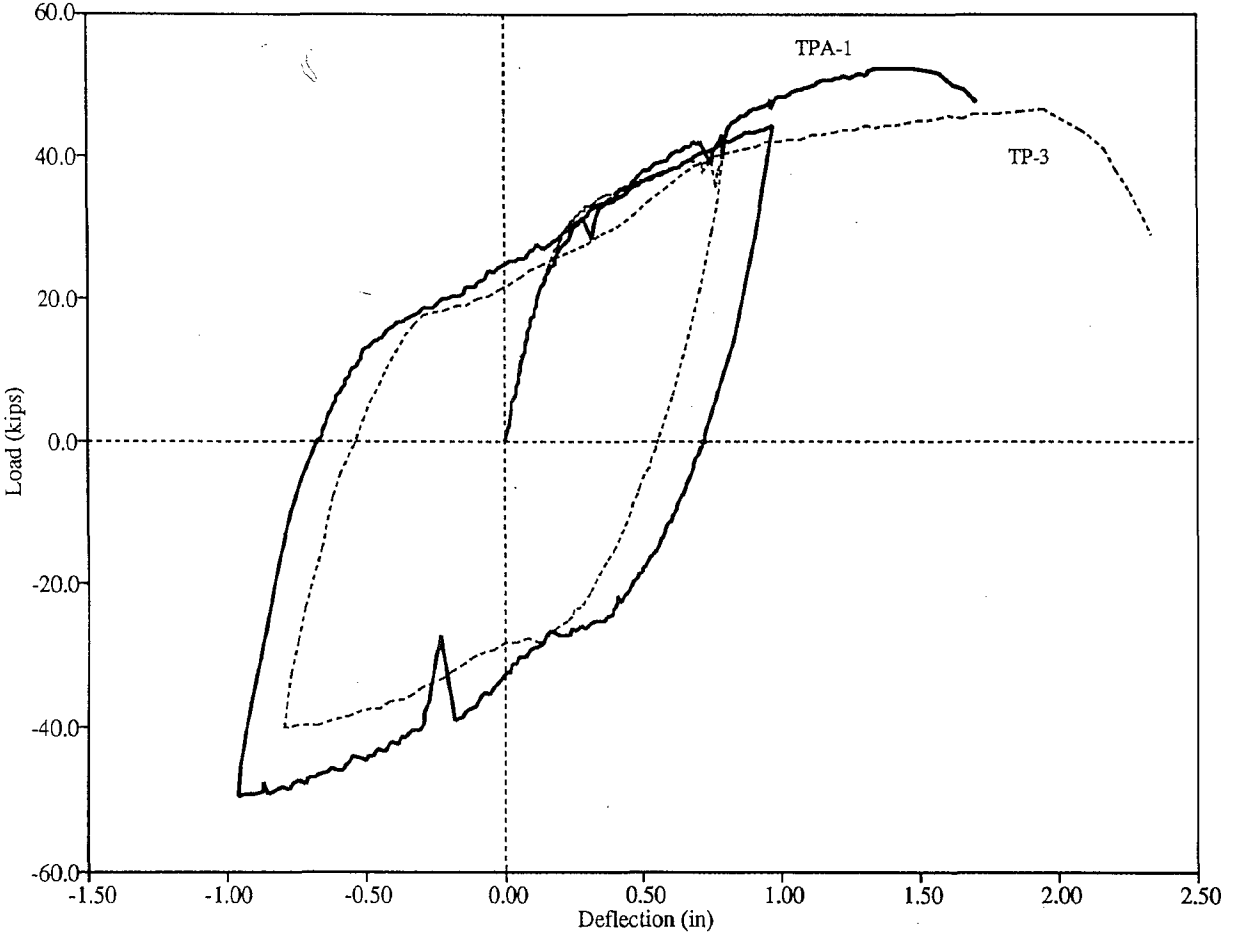

Figure 6.2 Load-Deflection Comparison of TPA-1 and TP-3 (Selected Portions)

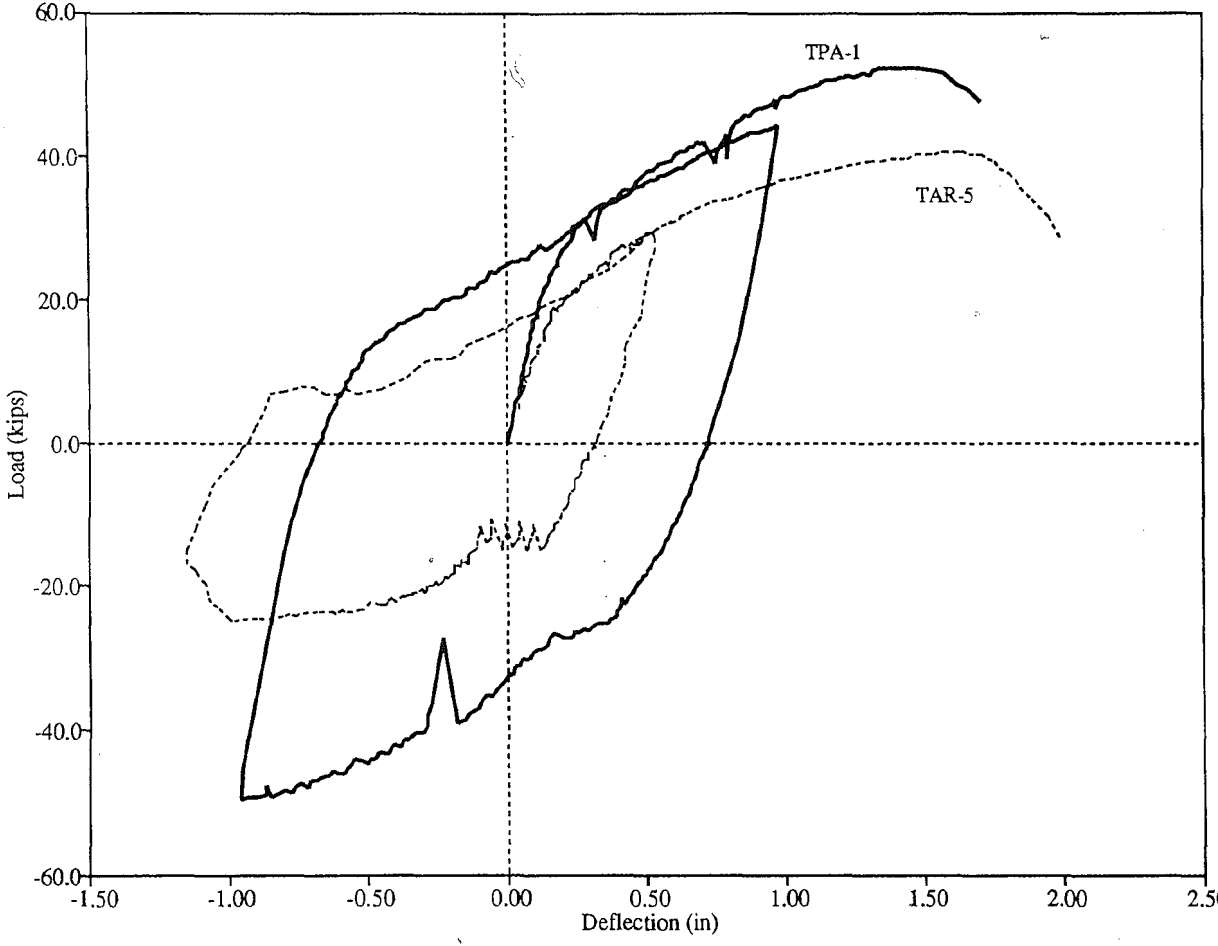

Figure 6.3 Load-Deflection Comparison of TPA-1 and TAR-5 (Selected Portions)

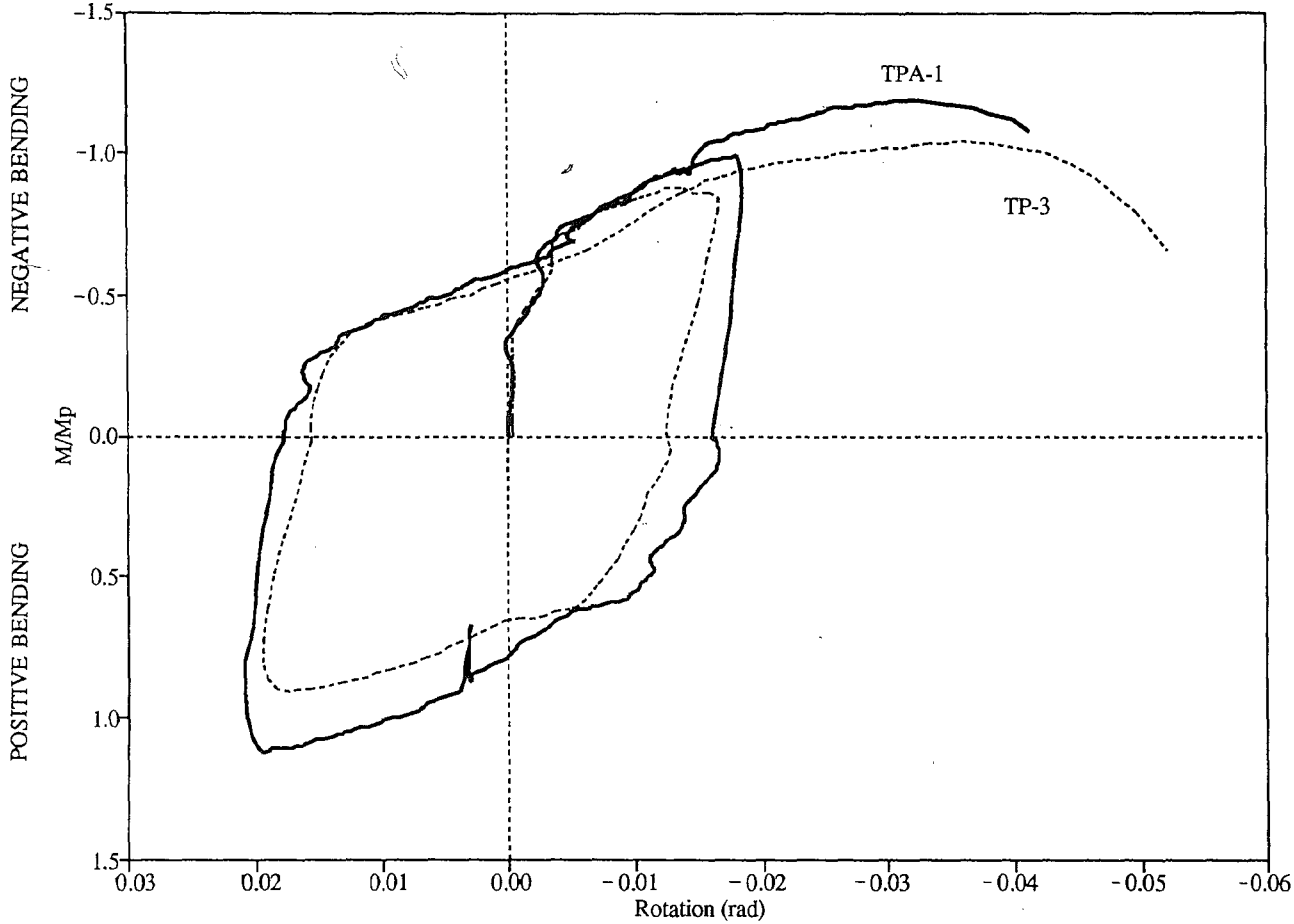

Figure 6.4 Moment-Rotation Comparison of TPA-1 and TP-3 (Selected Portions)

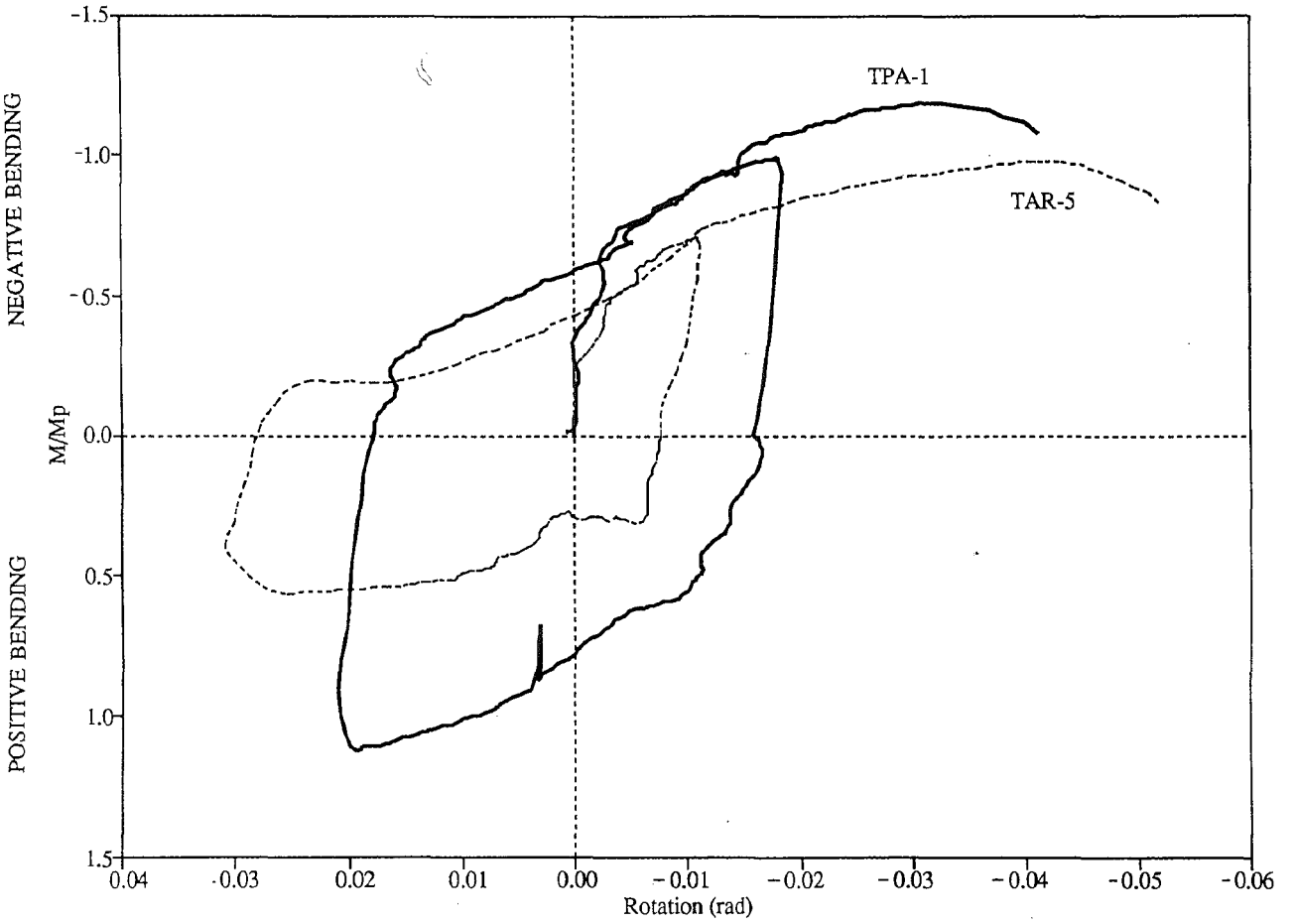

Figure 6.5 Moment-Rotation Comparison of TPA-1 and TAR-5 (Selected Portions)

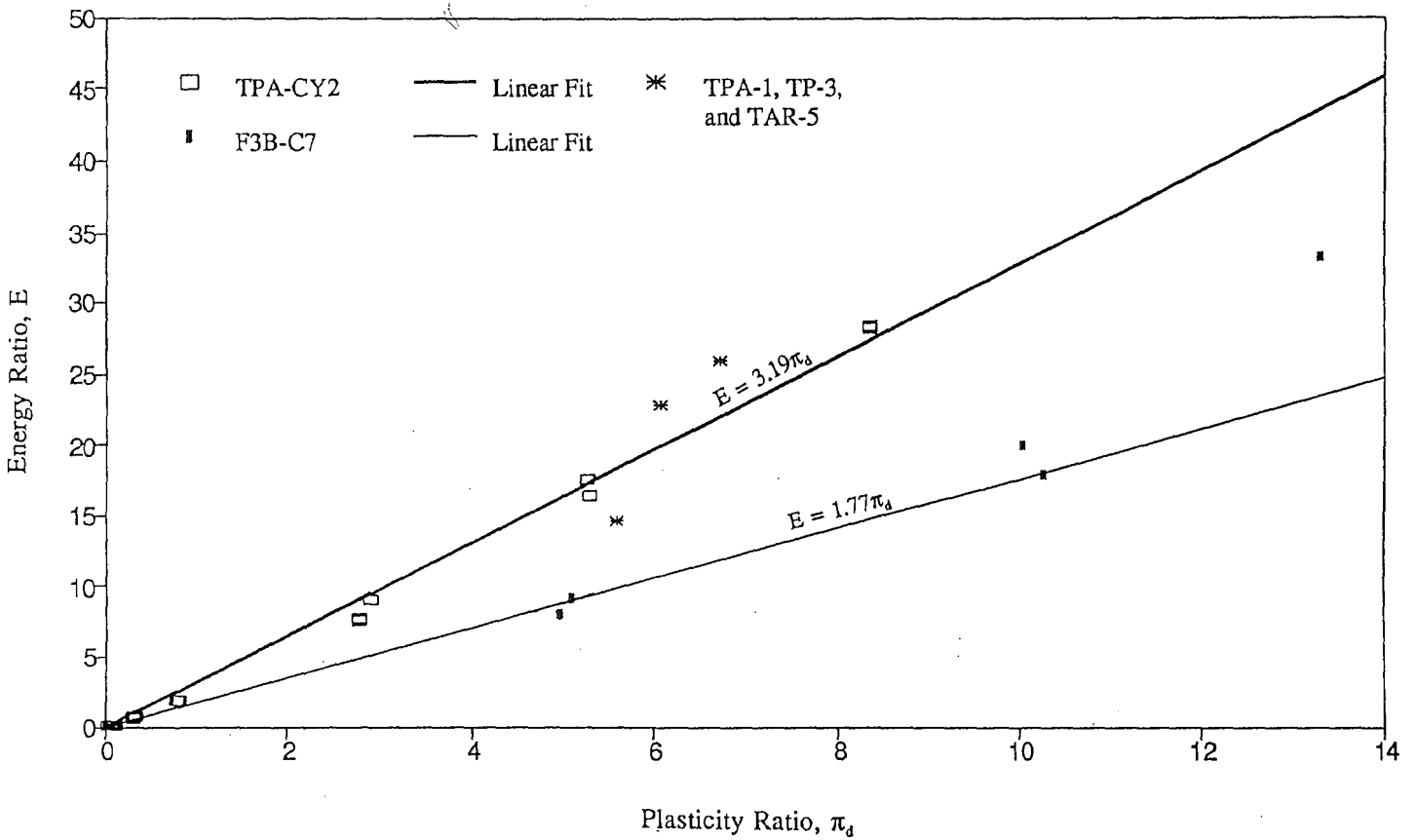

Figure 6.6 Comparison of Energy Dissipation of TPA-1, TPA-CY2, TP-3, TAR-5, and Popov and Pinkney's F3B-C7

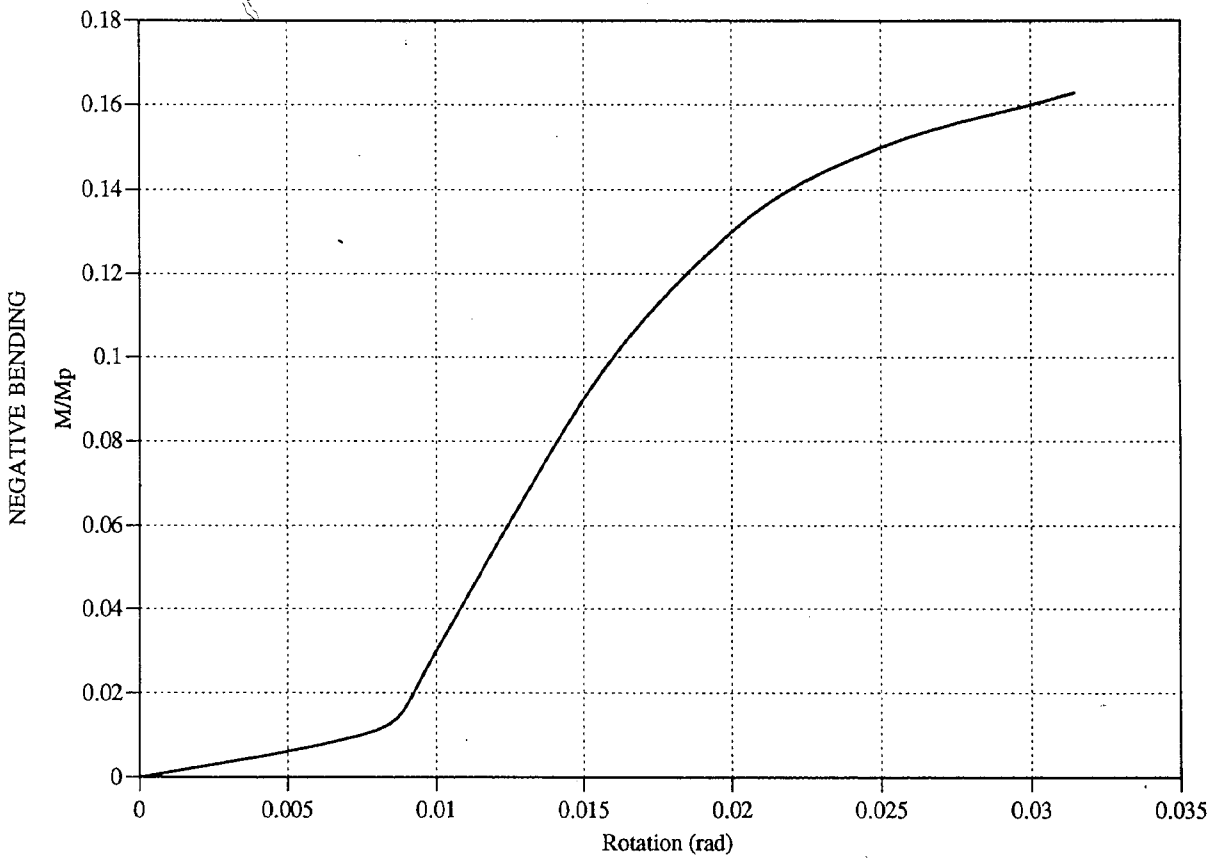

Figure 6.7 Contribution of ATLSS Connector to Moment Capacity

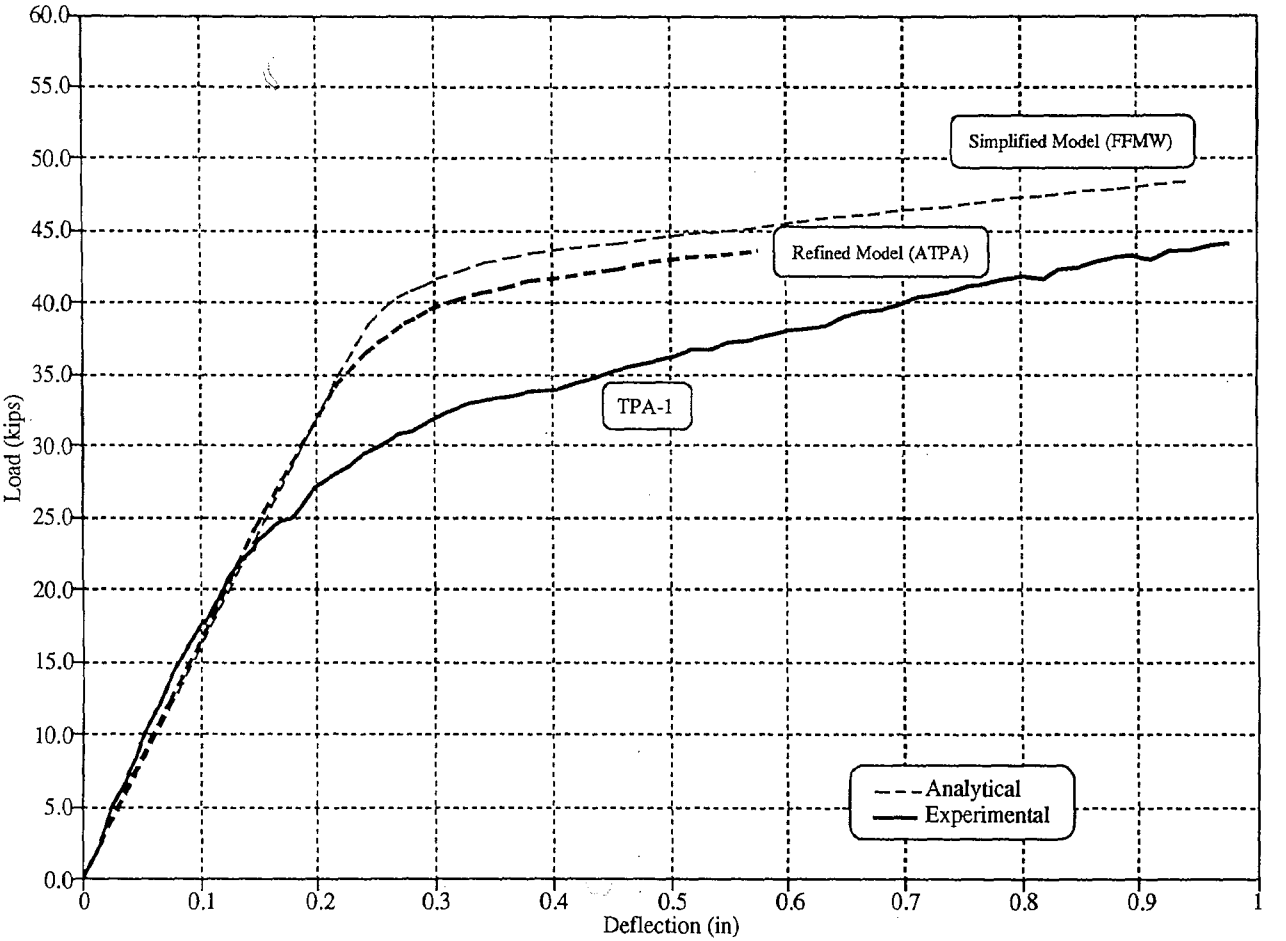

Figure 6.8 Comparison of Analytical and Experimental Load-Deflection Relationships -- Type A Configuration

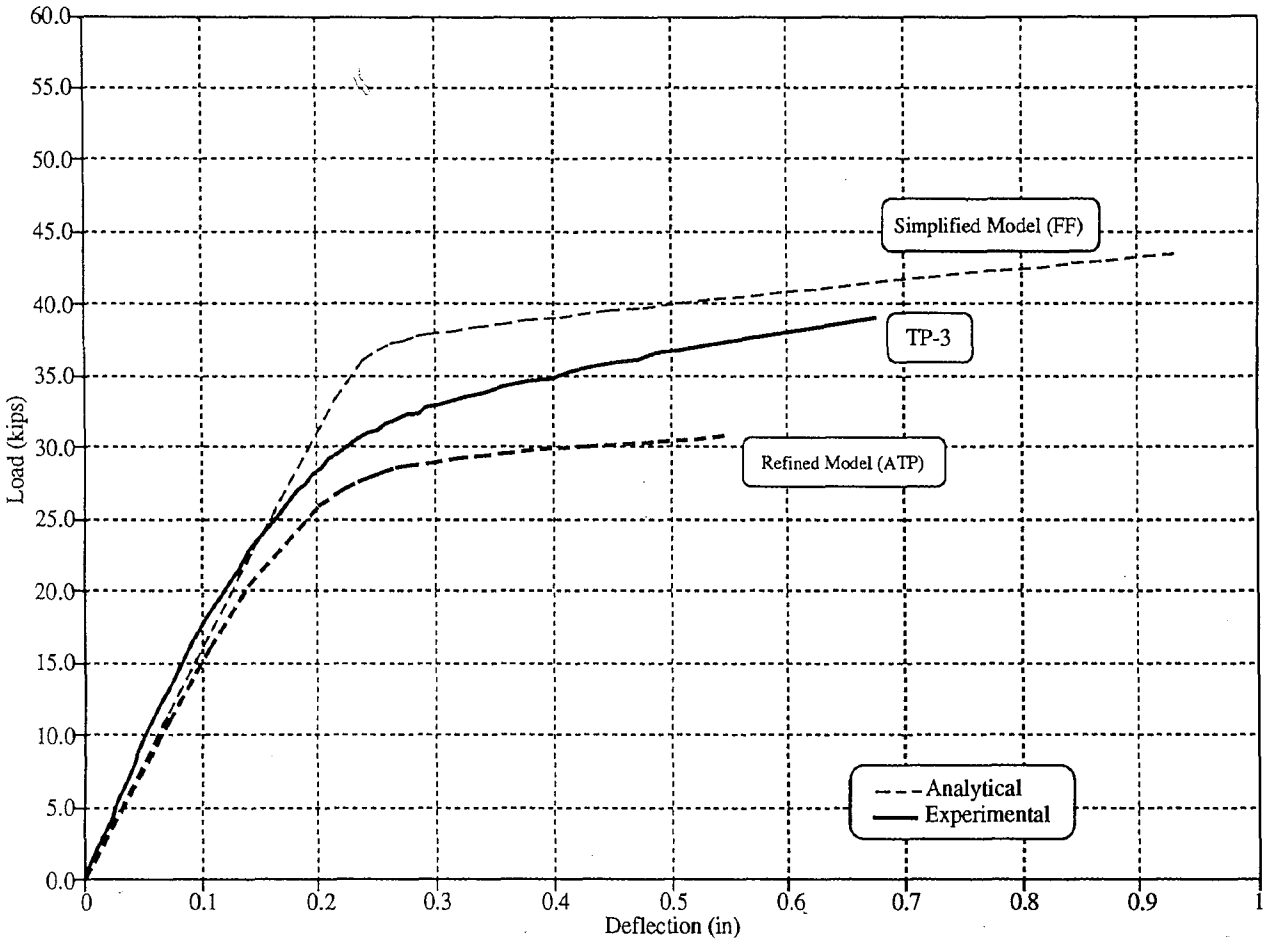

Figure 6.9 Comparison of Analytical and Experimental Load-Deflection Relationships -- Type B Configuration

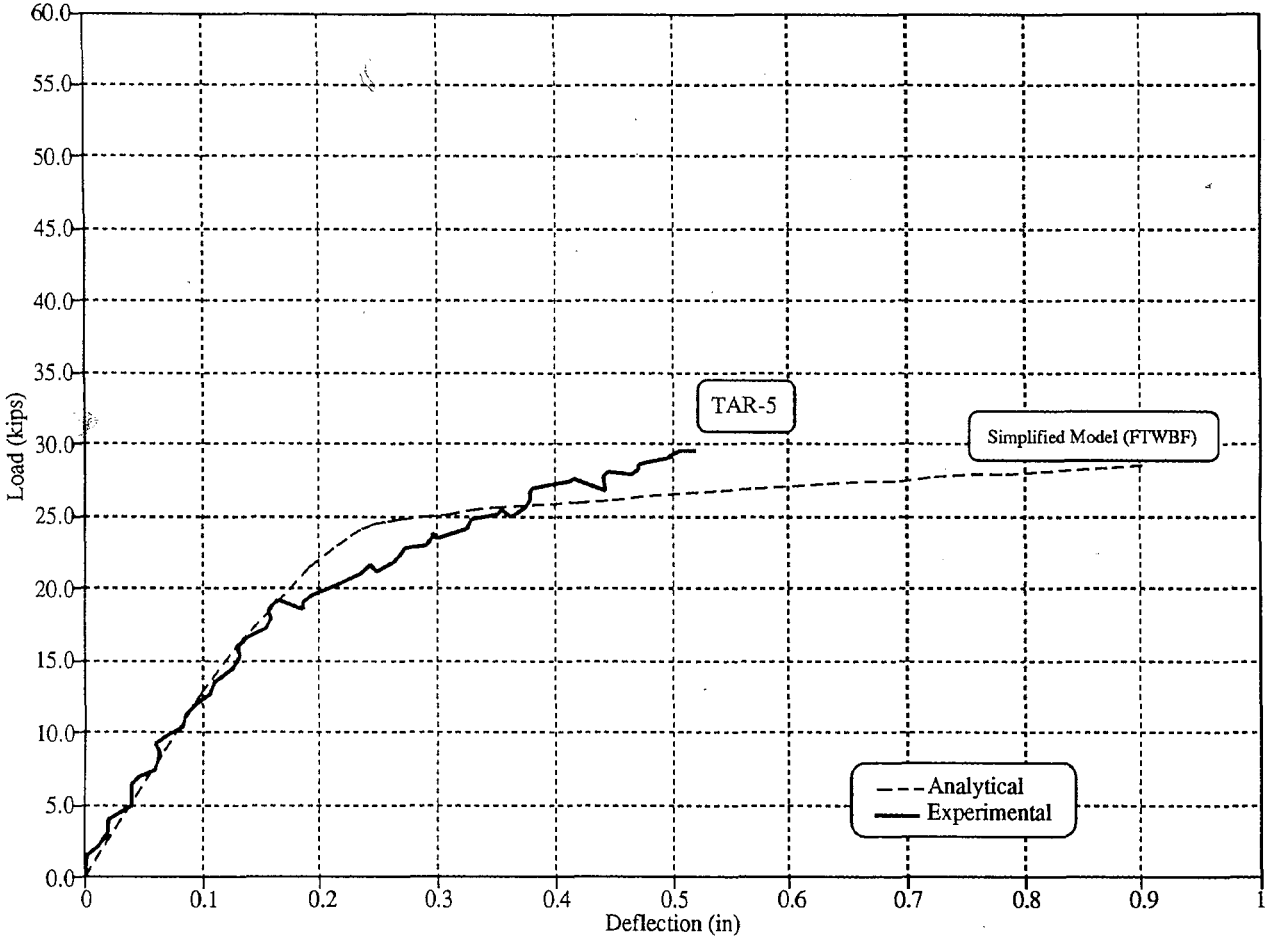

Figure 6.10 Comparison of Analytical and Experimental Load-Deflection Relationships -- Type C Configuration

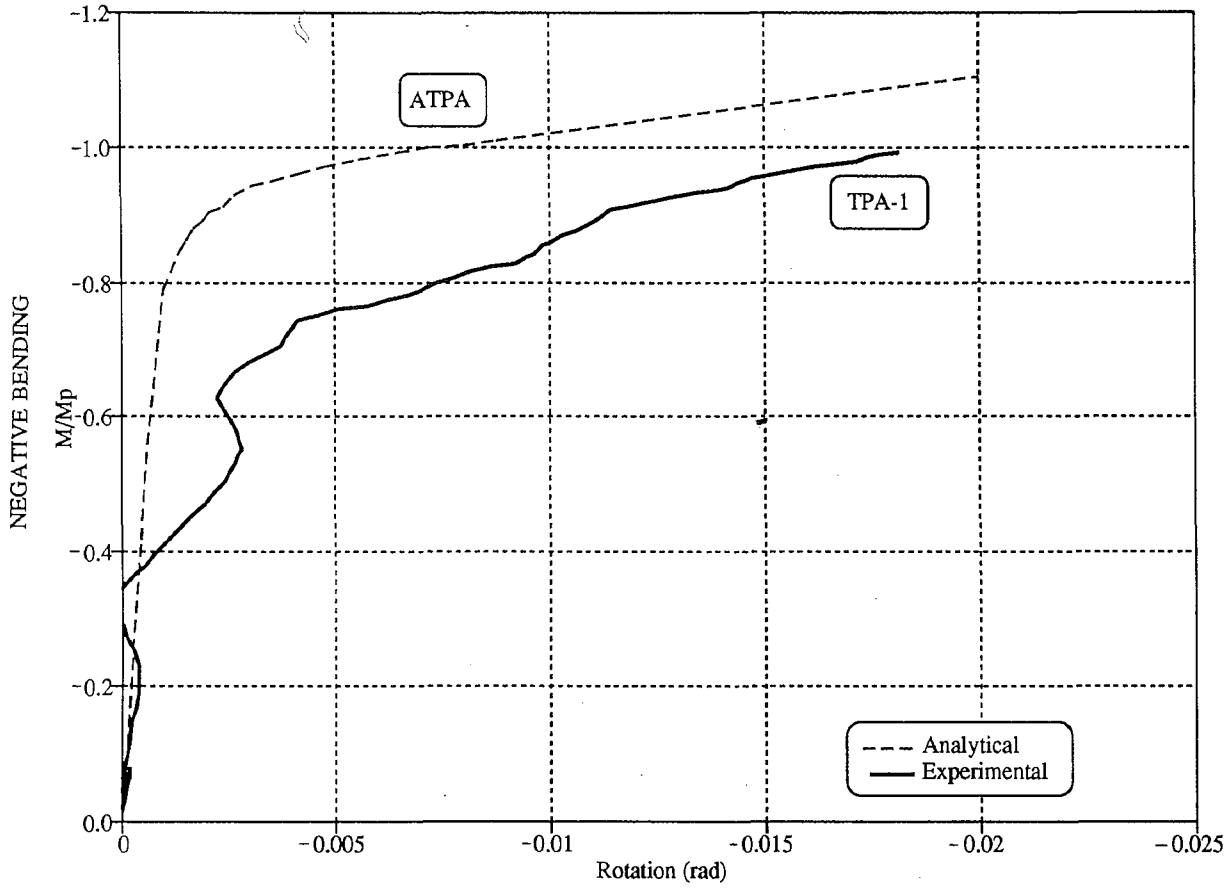

Figure 6.11 Comparison of Analytical and Experimental Moment-Rotation Relationships -- Type A Configuration

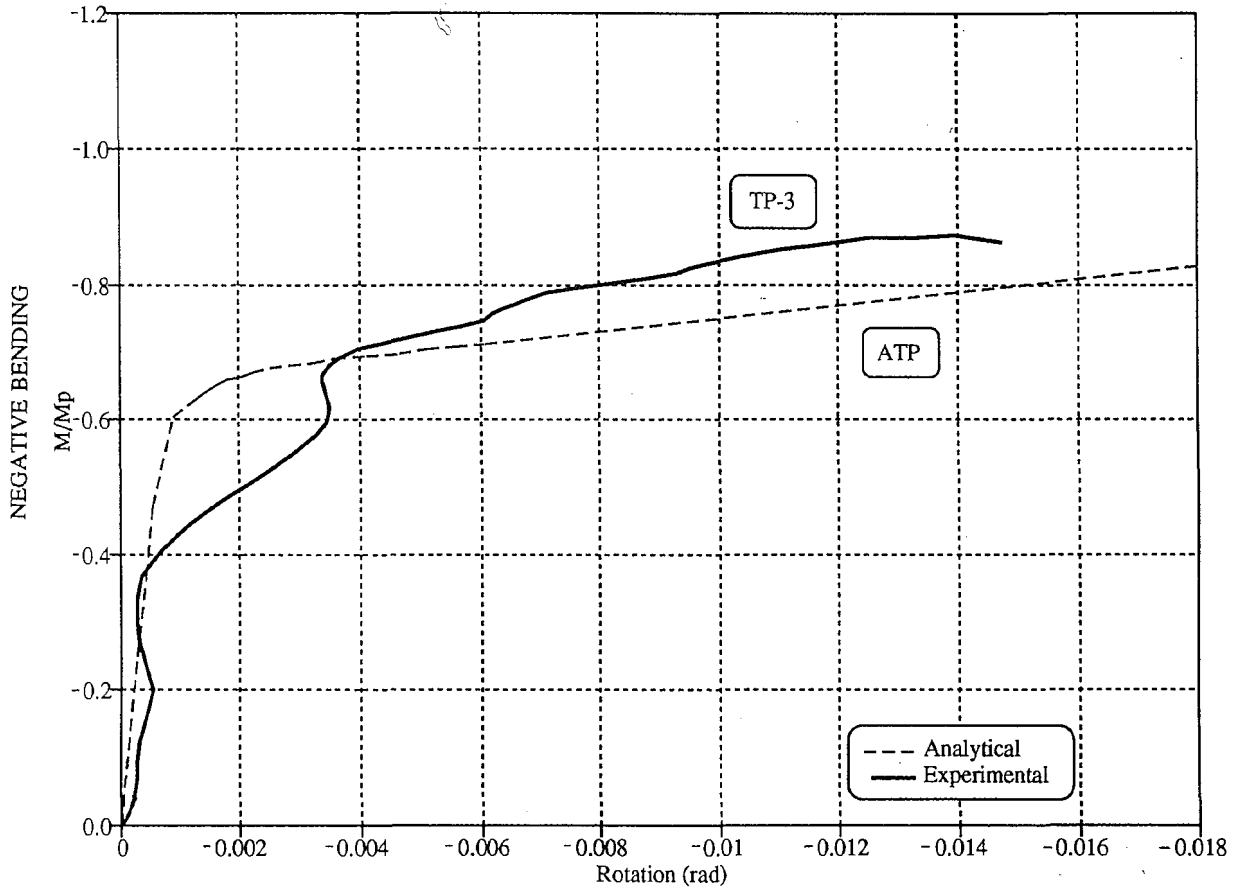

Figure 6.12 Comparison of Analytical and Experimental Moment-Rotation Relationships -- Type B Configuration

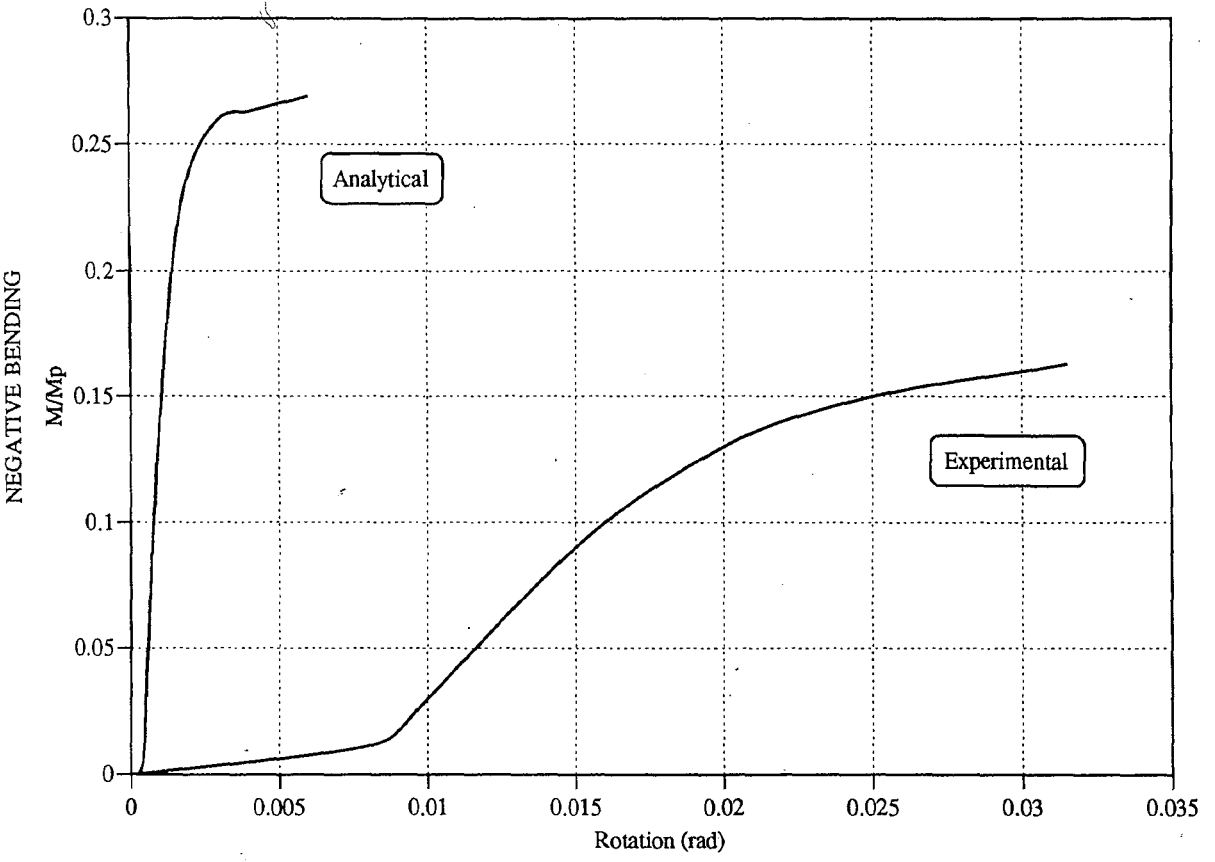

Figure 6.13 Contribution of ATLSS Connector to Moment Capacity -- Comparison Between Experimental Results and Analytical Predictions

VITA

Richard B. Garlock was born in Clifton Springs, New York on March 12, 1968 as the last of three children to Genevieve Francis Bissell and Richard Allen Garlock. After graduating from Wayne Central High School, Ontario, New York, in 1986 he entered Syracuse University, Syracuse, New York. He received his Bachelor of Science Degree of Civil Engineering from Syracuse University in December, 1990.

After graduation, the author remained in Syracuse and worked for the consultant engineering firm of W&M Associates, P.C. In September, 1991, he entered The Graduate School of Lehigh University and worked as a research scholar within the Center for Advanced Technology for Large Structural Systems.

END

OF

TITLE